AD-A033 544 POLYTECHNIC INST OF NEW YORK FARMINGDALE DEPT OF ELE--ETC F/G 9/3
SURFACE RAY METHODS FOR MUTUAL COUPLING IN CONFORMAL ARRAYS ON --ETC(U)
JUL 76 Z W CHANG, L B FELSEN, A HESSEL N00123-76-C-0236
UNCLASSIFIED POLY-EE/EP-76-016 NL

1 OF 2
ADA033544

F.C.

Department of
Electrical Engineering
and Electrophysics

July 1976

Surface Ray Methods For Mutual Coupling In Conformal Arrays On Cylindrical And Conical Surfaces

by Z.W. Chang, L.B. Felsen and A. Hessel

Final Report for Period September 1975 - February 1976
Contract N00123-76-C-0236 POLY-EE/EP-76-016
Prepared for: Naval Regional Procurement Office
Long Beach, California

Polytechnic
Polytechnic Institute of New York
Long Island Center
Farmingdale, New York 11735

UNCLASSIFIED

SECURITY CLASSIFICATION OF THIS PAGE (When Data Entered)

REPORT DOCUMENTATION PAGE	READ INSTRUCTIONS BEFORE COMPLETING FORM
1. REPORT NUMBER	2. GOVT ACCESSION NO. / 3. RECIPIENT'S CATALOG NUMBER
4. TITLE (and Subtitle): Surface Ray Methods For Mutual Coupling In Conformal Arrays On Cylindrical and Conical Surfaces	5. TYPE OF REPORT & PERIOD COVERED: Final Report - Sep 75 - 29 Feb 76
	6. PERFORMING ORG. REPORT NUMBER: POLY-EE/EP-76-016
7. AUTHOR(s): Z. W. Chang, L. B. Felsen, A. Hessel	8. CONTRACT OR GRANT NUMBER(s): N00123-76-C-0236 NEW
9. PERFORMING ORGANIZATION NAME AND ADDRESS: Polytechnic Institute of New York, Route 110, Farmingdale, N. Y. 11735	10. PROGRAM ELEMENT, PROJECT, TASK AREA & WORK UNIT NUMBERS
11. CONTROLLING OFFICE NAME AND ADDRESS: Mr. J. Provencher, Naval Electronics Laboratory Center, 271 Catalina Blvd., San Diego, CA 92152	12. REPORT DATE: July 1976 / 13. NUMBER OF PAGES: 131 / 133 pp.
14. MONITORING AGENCY NAME & ADDRESS (if different from Controlling Office): Mr. S. Wong, Office of Naval Research, 715 Broadway, New York, N. Y. 10003	15. SECURITY CLASS. (of this report): Unclassified / 15a. DECLASSIFICATION/DOWNGRADING SCHEDULE

16. DISTRIBUTION STATEMENT (of this Report)

Approved for public release; distribution unlimited.

17. DISTRIBUTION STATEMENT (of the abstract entered in Block 20, if different from Report)

18. SUPPLEMENTARY NOTES

None

19 KEY WORDS (Continue on reverse side if necessary and identify by block number)

antennas, conformal arrays, arrays, coupling

1/ka 1/kD

20. ABSTRACT (Continue on reverse side if necessary and identify by block number)

This report describes a stage of development of Surface Ray Methods for mutual coupling in conformal arrays of aperture elements on conducting cylindrical surfaces, with a subsequent generalization to conical surfaces. Asymptotic techniques are used to develop expressions for the dyadic Green's function for a circumferential and axial magnetic current sources. These expressions are to lowest order in $\frac{1}{ka}$ and to two orders in $\frac{1}{kD}$, where ka is the cylinder circumference in free space wavelengths and kD is the length in radians of the geodesic distance from the source to the observation point on

→ OVER

DD FORM 1 JAN 73 1473 EDITION OF 1 NOV 65 IS OBSOLETE

UNCLASSIFIED 409 203

SECURITY CLASSIFICATION OF THIS PAGE (When Data Entered)

6 pgs

20. Abstract

the cylinder surface. The region of validity of these expressions does not include the paraxial region. Rigorous transition functions for this region have not yet been derived, but instead, in this report, approximate transition functions have been developed. These transition functions are employed to obtain numerical results for the mutual admittance or the coupling coefficients between "single mode" circumferential and axial slots on cylinders with ka = 10 or 20. The numerical results are compared with those obtained via harmonic series and via GTD formulation.

SURFACE RAY METHODS FOR MUTUAL COUPLING IN CONFORMAL ARRAYS ON CYLINDRICAL AND CONICAL SURFACES

by Z. W. Chang, L. B. Felsen and A. Hessel
Department of Electrical Engineering and Electrophysics
Polytechnic Institute of New York
Farmingdale, New York 11735

Contract No. N00123-76-C-0236
Final Report
For the period
September 1975 - February 29, 1976

Prepared for

Naval Regional Procurement Office
Long Beach, California

Abstract

This report describes a stage of development of Surface Ray Methods for mutual coupling in conformal arrays of aperture elements on conducting cylindrical surfaces, with a subsequent generalization to conical surfaces. Asymptotic techniques are used to develop expressions for the dyadic Green's function for a circumferential and axial magnetic current sources. These expressions are to lowest order in $\frac{1}{ka}$ and to two asymptotic orders in $\frac{1}{kD}$, where ka is the cylinder circumference in free space wavelengths and kD is the length in radians of the geodesic distance from the source to the observation point on the cylinder surface. The region of validity of these expressions does not include the paraxial region. Rigorous transition functions for this region have not yet been derived, but instead, in this report, approximate transition functions have been developed. These transition functions are employed to obtain numerical results for the mutual admittance-or the coupling coefficients between "single mode" circumferential and axial slots on cylinders with $ka \approx 10$ or 20. The numerical results are compared with those obtained via harmonic series and via GTD formulation.

Table of Contents

List of Figures

I. Introduction

The theoretical determination of mutual admittance coefficients in arrays of aperture elements in a conducting surface requires the knowledge of the dyadic Green's function of the surface. This Green's function (G. F.) represents the magnetic field excited on the unperforated surface by a magnetic point-current element located on the surface. For the case of separable geometry G. F. is obtained by modal techniques. However, even for a separable geometry such as a conical surface, the modal series are very slowly convergent. Furthermore, modal analysis is inapplicable to non-separable geometries. A more efficient technique, also suitable to nonseparable geometry, of constructing the dyadic G. F. is that of the Geometric Theory of Diffraction (GTD) and its extensions which we may term as Surface Ray Methods. These are based, similarly to GTD, on high frequency asymptotic solutions of problems in canonical geometries, such as a circular cylinder or a sphere. These solutions are then generalized on the basis of locality of the high frequency propagation to other geometries. However in contrast to GTD which considers only lowest order asymptotic terms, Surface Ray Methods include also higher order terms.

This report describes a stage of development of Surface Ray Methods for analysis of mutual coupling in arrays of aperture elements on circular-cylindrical surfaces with application to conical surfaces.

A comprehensive survey of the state of the art of GTD as applied to both the far and the surface fields radiated by elemental magnetic currents (short slots) located on smooth curved conducting surfaces of large radii of curvature is found in Ref. [1] . Recently, this procedure has been

successfully applied, after certain modifications that preserve continuity of polarization. to the determination of far field patterns of slots on conducting conical surfaces [2] .

These calculated radiation patterns are based on the lowest order asymptotic results [1] and furthermore do not include the cone tip scattering. Nevertheless, they compare favorably with the numerical solutions based on harmonic series backed by experimental data [3] . While the lowest order asymptotic far field expressions seem to yield sufficient accuracy even for curvatures $ka \approx 9.5$, a different situation arises in calculation of surface fields, which are required for the determination of mutual admittance coefficients.

It is found that for a current element on a conducting circular cylinder, the validity of the lowest order GTD result is restricted to observation points not too close to the source and in addition these expressions do not hold in the paraxial and the circumferential regions.

In order to determine the near zone fields of the source, which are essential for calculation of the nearest neighbor mutuals, asymptotic expansions for the Green's function are required to higher order in $\frac{1}{kD}$, where D is the geodesic distance between the source and the observation point.

In this report a rigorous asymptotic expansion is obtained for both circumferential and axial magnetic current element on a conducting circular cylinder. The expressions are to lowest order in $\frac{1}{ka}$ and to second order in $\frac{1}{kD}$. These expressions correctly reproduce the H-plane behavior of the Green's functions for a circumferential current element.

However these asymptotic expressions based on Fock type integrals [4] are invalid in the paraxial region of a source. This is due to the fact that the Airy function approximation of the Hankel function $H_\nu^{(2)}(z)$ breaks down for small values of z. As a result e.g. the lowest order TM (soft) and the next order TE (hard) H_φ contributions for a circumferential magnetic current element become unbounded as the observation point tends to $\varphi = 0$, i.e. to the cylinder generator through the source.

As anticipated, the angular region of validity of the asymptotic expansions increases with larger values of ka.

The asymptotic evaluation of surface fields in paraxial region (E-plane) of a circumferential magnetic current element will necessitate a different representation than that used in this report and merits a separate study. Here we have chosen to concern ourselves with the development of an approximate "Modified Planar Formula" for the surface Green's function which provides a transition to the paraxial region. The Modified Planar Formula which is cast in an invariant vector form, includes a provision for arbitrary orientation of the tangential magnetic sources. It reduces to the planar dyadic Green's Function to $0\left(\frac{1}{(kD)^2}\right)$, when the observation point tends to the source. When the Modified Planar Formula is specialized to the case of H_φ for a circumferential magnetic current element, it will be referred to as the "Full Formula".

The "Full Formula" matches in the H-plane the exact asymptotic expansion to second order in $\frac{1}{kD}$, is finite for $\varphi = 0$ and reduces to the planar result near the source. A variant of the "Full Formula" is also considered in which one term of higher order in $\frac{1}{ka}$ has been neglected and

the soft polarization term is discarded for observation direction close to the E-plane.

In contrast to the case of circumferential sources, the asymptotic expansion to $0\left(\frac{1}{(kD)^2}\right)$ for H_z due to an axial magnetic current element and based on the Airy function approximation of $H_\nu^{(2)}(z)$, is formally well behaved in every direction. From the comparison of the numerical data for mutual admittance between axial slots on a conducting circular cylinder of $ka \approx 9.5$ with the harmonic series results [5], one may conclude that this approximation is fairly accurate for calculation of mutual admittances between axial slots and by GTD generalization, for radial slots on conical surfaces.

The structure of this report is as follows:

Chapter *II* develops *the asymptotics to second order in* $\frac{1}{kD}$ for the surface fields excited by magnetic point sources located on a conducting circular cylinder. In Section 1, the scalar TE and TM potentials are constructed for the case of an infinitely extended conducting circular cylinder. In Section 2, an integral representation suitable for development of the surface ray formalism is presented. Section 3 is devoted to the evaluation of curvature terms. Section 4 addresses the asymptotic evaluation of integrals developed in Section 2. Section 5 discusses the approximate formulae used in this report for numerical evoluation of the mutual admittance Y_{12} between rectangular slots. Section 6 presents a list of the various formulae.

Chapter III is devoted to numerical results.

Chapter IV deals with the GTD generalization from the cylinder to a cone.

Conclusions and discussion are found in Chapter V.

Appendix A reviews the theory of the alternative representations for scalar potentials.

Appendix B considers the details of analysis of the curvature terms (Fock type integrals).

Appendix C summarizes the derivation of asymptotic series for Laplace type integrals.

Appendix D deals with the vector form of the planar Green's function.

Appendices E and F contain computer program listings.

II. Surface Fields Excited by a Magnetic Current Element (Short Slot) on a Large Conducting Circular Cylinder

For evaluation of mutual coupling in conformal arrays one is particularly interested in surface magnetic fields excited by elemental magnetic currents placed tangentially on the surface of a perfectly conducting, large, circular cylinder, with the geometry shown in Figure II-1.

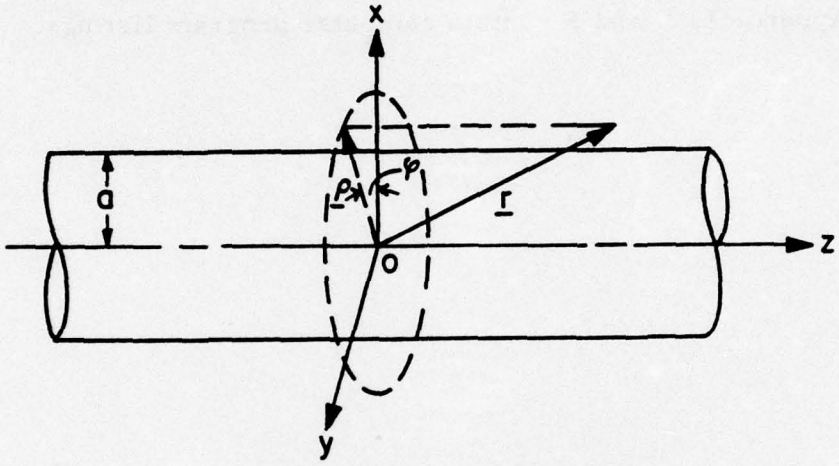

Figure II-1. Geometry of a Circular Cylinder.

Following Ref. [6, p. 197] one finds for the total, time harmonic ($e^{j\omega t}$ dependent) magnetic field excited by a magnetic point current source, the following result:

$$\underline{H}(\underline{r}, \underline{r}') = -j\omega\epsilon_o \, (\nabla x\hat{z}) \, (\nabla' x\hat{z}) S'(\underline{r}, \underline{r}') \cdot \underline{M} + \frac{1}{j\omega\mu_o} \, (\nabla x\nabla x\, \hat{z}) \, (\nabla' x \nabla' x\, \hat{z}) S''(\underline{r}, \underline{r}') \cdot \underline{M}, \tag{1}$$

where: $\underline{M}$ denotes the magnetic point source current density, ϵ_o and μ_o the free space permittivity and permeability, $\hat{z}$ the axial unit vector, and ∇' and $\underline{r}'$ refer to the source coordinates.

1. Scalar Potentials for the Circular Cylinder Problem

The aim of this study is to establish the high frequency surface ray formalism suitable for mutual coupling applications in cylindrical and conical arrays. This is facilitated by the particular integral representation of the potentials S' and S''. From Appendix A (9), (13), (19) and (21a) one finds

$$S(\underline{r},\underline{r}') = -\frac{1}{4\pi^2}\oint_{C_z} d\lambda_\mu \frac{e^{-j\sqrt{\lambda_\mu}\,|z-z'|}}{2j\sqrt{\lambda_\mu}} \oint_{C_\varphi} d\lambda_\nu \frac{-\cos\sqrt{\lambda_\nu}\left(\pi-|\varphi-\varphi'|\right)}{2\sqrt{\lambda_\nu}\,\sin\sqrt{\lambda_\nu}\,\pi} \times$$

$$\frac{-j\pi}{4}\left[H^{(2)}_{\sqrt{\lambda_\nu}}(k_t\rho_<) - \frac{QH^{(1)}_{\sqrt{\lambda_\nu}}(k_t a)}{QH^{(2)}_{\sqrt{\lambda_\nu}}(k_t a)} H^{(2)}_{\sqrt{\lambda_\nu}}(k_t\rho_<)\right] H^{(2)}_{\sqrt{\lambda_\nu}}(k_t\rho_>)\frac{1}{k_t^2}, \qquad (2)$$

where for S', $Q=1$, for S'', $Q=\frac{\partial}{\partial a}$, and $k_t = \sqrt{k^2-\lambda_\mu}$.

With $\lambda_\nu = \nu^2$, the contour C_φ in the λ_ν-plane maps into a straight line from $-\infty$ to $+\infty$ just below the real axis in the ν-plane.

$$S(\underline{r},\underline{r}') = -\frac{1}{4\pi^2}\oint_{C_z} d\lambda_\mu \frac{e^{-j\sqrt{\lambda_\mu}\,|z-z'|}}{2j\sqrt{\lambda_\mu}} \int_{-\infty-j\delta}^{\infty-j\delta} d\nu \frac{-\cos\nu(\pi-|\varphi-\varphi'|)}{\sin\nu\pi} \times$$

$$\frac{-j\pi}{4}\left[H^{(1)}_\nu(k_t\rho_<) - \frac{QH^{(1)}_\nu(k_t a)}{QH^{(2)}_\nu(k_t a)} H^{(2)}_\nu(k_t\rho_<)\right] H^{(2)}_\nu(k_t\rho_>)\frac{1}{k_t^2}, \qquad (3)$$

where δ is an arbitrarily small positive quantity. The only singularities

in the ν -plane are simple poles at $Q\overset{(2)}{H}_\nu(k_t a) = 0$ and at $\nu = 0, \pm 1, \pm 2, \cdots$.

Another transformation $\lambda_\mu = k_z^2$ maps the λ_μ -plane into k_z -plane, where one finds two branch points at $k_z = \pm k$. The complex k_z -plane is the usual two sheeted Riemann surface of the $k_t = \sqrt{k^2 - k_z^2}$. The proper branch of k_t can be determined by the large argument expansion of the Hankel function $\overset{(2)}{H}_\nu(k_t \rho_>)$ in (3). For $|k_t| \rho_> >> |\nu|$,

$$\overset{(2)}{H}_\nu(k_t \rho_>) \sim \sqrt{\frac{2}{\pi k_t \rho_>}}\, e^{-j(k_t \rho_> - \nu \frac{\pi}{2} - \frac{\pi}{4})} \quad . \tag{4}$$

The radiation condition requires that for $0 \leq k_z^2 < k^2$, $k_t = \sqrt{k^2 - k_z^2} > 0$ and for $k_z^2 > k^2$, $\mathrm{Im}(k_t) < 0$ on the integration contour running along the real axis in the k_z plane, as shown in Fig. II-2. With the branch cut as indicated, $\mathrm{Im}(k_t) < 0$ in un-shaded region and $\mathrm{Re}\, k_t > 0$ on the entire top sheet. In this fashion one finds for S' and S'' the expression

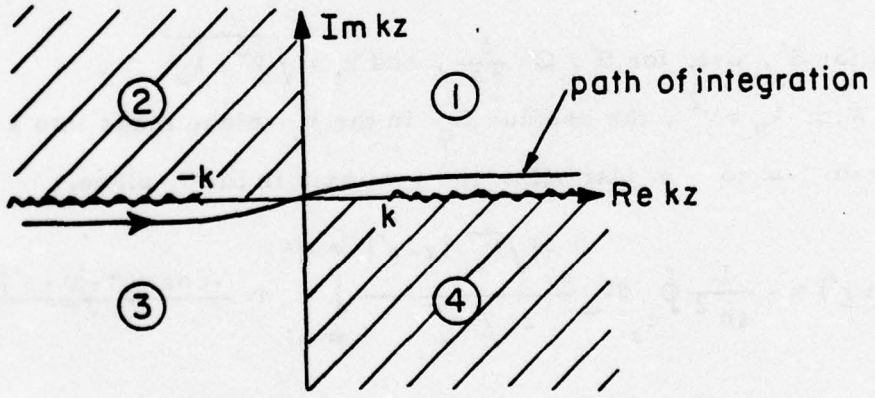

Figure II-2. Top Sheet of k_z-plane.

$$S(\underline{r}, \underline{r}') = -\frac{1}{16\pi} \int_{-\infty - j\delta'}^{\infty + j\delta'} dk_z\, e^{-jk_z|z-z'|} \int_{-\infty - j\delta}^{\infty - j\delta} \frac{\cos \nu(\pi - |\varphi - \varphi'|)}{\sin \nu\pi} \times$$

$$\left[\overset{(1)}{H}_\nu(k_t \rho_<) - \frac{Q\overset{(1)}{H}_\nu(k_t a)}{Q\overset{(2)}{H}_\nu(k_t a)}\, \overset{(2)}{H}_\nu(k_t \rho_<)\right] \overset{(2)}{H}_\nu(k_t \rho_>) \frac{1}{k_t^2} \quad , \tag{5}$$

where δ' is an arbitrarily small positive quantity.

In order to cast S into a form appropriate to the surface ray formalism, it is necessary to convert the angular Green's function into a traveling wave series.

$$\frac{\cos \nu (\pi - |\varphi - \varphi'|)}{\sin \nu\pi} = j \sum_{i=1}^{2} \sum_{\ell=0}^{\infty} e^{-j\nu (\varphi_i + 2\pi\ell)} \tag{6}$$

where $\varphi_1 = |\varphi - \varphi'|$, $\varphi_2 = 2\pi - |\varphi - \varphi'|$ and $-\pi \leq \varphi, < \pi$. Consequently

$$S(\underline{r}, \underline{r}') = -\frac{j}{16\pi} \sum_{i=1}^{2} \sum_{\ell=0}^{\infty} \int_{-\infty - j\delta'}^{\infty + j\delta'} dk_z \int_{-\infty - j\delta}^{\infty - j\delta} d\nu\, e^{-jk_z |z - z'|} e^{-j\nu (\varphi_i + 2\pi\ell)} \times$$

$$\left[H_\nu^{(1)} (k_t \rho_<) - \frac{QH_\nu^{(1)} (k_t a)}{QH_\nu^{(2)} (k_t a)} H_\nu^{(2)} (k_t \rho_<) \right] H_\nu^{(2)} (k_t \rho_>) \frac{1}{k_t^2} \tag{7}$$

One notes that for a given value of ν, the two waves $e^{-j\nu\varphi_1}$ and $e^{-j\nu\varphi_2}$ propagate in opposite directions. The terms with $\ell \neq 0$ represent waves that arrive at φ after having traveled ℓ complete circuits around the cylinder. If the cylinder radius (ka) is not too small, the terms with $\ell \neq 0$ are negligible, because of the exponential attenuation of the creeping rays, as will be shown. Also for the same reason, if $\varphi_2 >> \varphi_1$, the contributions of the $\ell = 0$, φ_2 term may be neglected compared to that of φ_1 term.

Thus, it will be sufficient, except near $|\varphi-\varphi'| = \pi$, to consider only the $\ell=0$, φ_1 term, i.e.

$$S(\underline{r},\underline{r}') = -\frac{j}{16\pi}\int_{-\infty}^{\infty} dk_z\, e^{-jk_z|z-z'|}\int_{-\infty}^{\infty} d\nu\, e^{-j\nu\Phi}\, x$$

$$\left[H_\nu^{(1)}(k_t\rho_<) - \frac{QH_\nu^{(1)}(k_t a)}{QH_\nu^{(2)}(k_t a)}\, H_\nu^{(2)}(k_t\rho_<)\right] H_\nu^{(2)}(k_t\rho_>)\,\frac{1}{k_t^2}\,. \qquad (8)$$

In the above, φ_1 was replaced by Φ and the integration contours have been shifted to the real ν and k_z axes.

2. Integral Representation for the Field Components

There are two independent tangential source configurations on the surface of a conducting cylinder giving rise to different solutions. One, an axial, the other a circumferential (transverse) magnetic current element.

a. Circumferential Magnetic Current Element (Short Slot)

In this case

$$\underline{M} = M_\varphi \hat{\varphi}$$

and therefore, from (1) one has

$$H_\varphi^c(\underline{r},\underline{r}') = \frac{M_\varphi}{j\omega\mu_o \rho\rho'} \frac{\partial^2}{\partial z \partial\varphi} \frac{\partial^2}{\partial z' \partial\varphi'} S''(\underline{r},\underline{r}') - j\omega\varepsilon_o M_\varphi \frac{\partial^2}{\partial\rho\partial\rho'} S'(\underline{r},\underline{r}') \tag{9}$$

$$H_z^c(\underline{r},\underline{r}') = \frac{M_\varphi}{j\omega\mu_o \rho'} (-\nabla_t^2) \frac{\partial^2}{\partial z' \partial\varphi'} S''(\underline{r},\underline{r}') \quad , \tag{10}$$

where the superscript "c" denotes quantities excited by a circumferential magnetic current source.

In view of the relation [Ref. 6, Eq. 33b, p. 198]

$$-\nabla_t^2 S''(\underline{r},\underline{r}') = -\nabla_t'^2 S''(\underline{r},\underline{r}') = G''(\underline{r},\underline{r}') \tag{11}$$

(10) may also be written in the form

$$H_z^c(\underline{r},\underline{r}') = \frac{M_\varphi}{j\omega\mu_o \rho'} \frac{\partial^2}{\partial z \partial\varphi'} G''(\underline{r},\underline{r}') \quad . \tag{12}$$

The formal modal representation of the scalar Green's function G'' is [Ref. 6, Eq. 33b, p. 198]

$$G''(\underline{r}, \underline{r}') = \sum_i \psi_i''(\underline{\rho}) \psi_i''^*(\underline{\rho}') g_z(z, z') \quad . \tag{13}$$

Upon combining (A2), (A18) and (13) one finds that G'' satisfies

$$(\nabla^2 + k^2) G''(\underline{r}, \underline{r}') = -\delta(\underline{r}-\underline{r}') \quad , \tag{14}$$

with

$$\frac{\partial}{\partial \rho} G''(\underline{r}, \underline{r}') \Big|_{\rho=\rho'=a} = 0 \quad . \tag{15}$$

There is no TM contribution to the z-component of the magnetic field.

Upon introducing the Wronskian

$$H_\nu^{(1)'}(z) H_\nu^{(2)}(z) - H_\nu^{(1)}(z) H_\nu^{(2)'}(z) = \frac{4j}{\pi z} \quad , \tag{16}$$

one finds that for $\rho = \rho' = a$, i.e. the case of surface magnetic field H_φ^c, excited by a circumferential magnetic current element located on the surface

$$H_\varphi^c = H_\varphi''^c + H_\varphi'^c \tag{17}$$

where H_φ'' and H_φ' denote the TE and TM contributions, respectively.

From (8), (9) and (16) one has

$$H_\varphi^{''c}(\underline{r},\underline{r}')\Big|_{\rho=\rho'=a} = \frac{jM_\varphi}{4\pi^2\omega\mu_o a^3}\int_{-\infty}^{\infty} dk_z\, e^{-jk_z|z-z'|}\frac{k_z^2}{k_t^3}\int_{-\infty}^{\infty} d\nu e^{-j\nu\Phi}\nu^2\frac{H_\nu^{(2)}(k_t a)}{H_\nu^{(2)\prime}(k_t a)} \tag{18}$$

and

$$H_\varphi^{'c}(\underline{r},\underline{r}')\Big|_{\rho=\rho'=a} = \frac{-jM_\varphi\omega\varepsilon_o}{4\pi^2 a}\int_{-\infty}^{\infty} dk_z\, e^{-jk_z|z-z'|}\frac{1}{k_t}\int_{-\infty}^{\infty} d\nu\, e^{-j\nu\Phi}\frac{H_\nu^{(2)\prime}(k_t a)}{H_\nu^{(2)}(k_t a)} \tag{19}$$

Similarly, for H_z, one obtains from (8), (12) and (16)

$$H_z^c(\underline{r},\underline{r}')\Big|_{\rho=\rho'=a} = \mathrm{sgn}(\varphi-\varphi')\mathrm{sgn}(z-z')\frac{-jM_\varphi}{4\pi^2\omega\mu_o a^2}\int_{-\infty}^{\infty} dk_z e^{-jk_z|z-z'|}\frac{k_z}{k_t}\int_{-\infty}^{\infty} d\nu e^{-j\nu\Phi}\nu\frac{H_\nu^{(2)}(k_t a)}{H_\nu^{(2)\prime}(k_t a)} \tag{20}$$

with

$$\mathrm{sgn}\, u = \begin{cases} 1, & u > 0, \\ -1, & u < 0. \end{cases} \tag{21}$$

The reason for appearance of the sgn u in (20) is the operation $\frac{\partial^2}{\partial z'\partial\varphi}$ in (12); the absence of sgn u in (18) and (19) is brought about by the operations $\frac{\partial^2}{\partial z\partial z'}$ and $\frac{\partial^2}{\partial\varphi\partial\varphi'}$ in (9) which because of the presence of $|z-z'|$ and $|\varphi-\varphi'|$ in the exponents, do not give rise to sign changes.

b. Axial Magnetic Current Element (Short Slot)

In this case

$$\underline{M} = M_z \hat{z} \tag{22}$$

and in view of (1), one has

$$\underline{H}^a(\underline{r},\underline{r}') = \frac{M_z}{j\omega\mu_o}(\nabla \times \nabla \times \hat{z})(-\nabla_t'^2) S''(\underline{r},\underline{r}')$$

$$= \frac{M_z}{j\omega\mu_o} \nabla \times \nabla \times \hat{z}\, G''(\underline{r},\underline{r}') , \tag{23}$$

where the relation (11) has been used. Therefore,

$$H_z^a(\underline{r},\underline{r}') = \frac{M_z}{j\omega\mu_o}\left(\frac{\partial^2}{\partial z^2} + k^2\right) G''(\underline{r},\underline{r}') \tag{24}$$

and

$$H_\varphi^a(\underline{r},\underline{r}') = \frac{M_z}{j\omega\mu_o\rho}\frac{\partial^2}{\partial\varphi\partial z} G''(\underline{r},\underline{r}') . \tag{25}$$

Following an analogous procedure as in (18), one obtains, via (8), (11) and (16), the following expressions

$$H_z^a(\underline{r},\underline{r}')\Big|_{\rho=\rho'=a} = \frac{-jM_z}{4\pi^2\omega\mu_o a}\int_{-\infty}^{\infty} dk_z\, e^{-jk_z|z-z'|} k_t \int_{-\infty}^{\infty} d\nu\, e^{-j\nu\Phi} \frac{H_\nu^{(2)}(k_t a)}{H_\nu^{(2)'}(k_t a)} \tag{26}$$

and

$$H_\varphi^a(\underline{r},\underline{r}')\Big|_{\rho=\rho'=a} = \mathrm{sgn}(\varphi-\varphi')\mathrm{sgn}(z-z')\frac{-jM_z}{4\pi^2\omega\mu_o a^2}\int_{-\infty}^{\infty} dk_z\, e^{-jk_z|z-z'|}\frac{k_z}{k_t}\int_{-\infty}^{\infty} d\nu\, e^{-j\nu\Phi}\nu\frac{H_\nu^{(2)}(k_t a)}{H_\nu^{(2)'}(k_t a)} \tag{27}$$

where the superscript "a" denotes the field excited by an axial magnetic current element.

It is noted, following a similar reasoning as for the case of a circumferential magnetic current element, that H_z^a does not change sign for $z \gtrless z'$ or $\varphi \gtrless \varphi'$, but H_φ^a may do so.

3. The Curvature Terms

Relations (18-20) and (26-27) involve two contour integrals with respect to the angular and the axial wavenumbers. They contain two independent large parameters, one ka the circumference of the cylinder in wavelengths, the other kD the free space phase delay along the geodesic distance from the source to the point of observation. The asymptotics will be carried out to lowest order in $\frac{1}{ka}$ in each polarization and to $O\left(\frac{1}{(kD)^{3/2}}\right)$ in the deep shadow, or equivalently to $O\left(\frac{1}{(kD)^2}\right)$ in the near zone. An evaluation to the lowest order in $\frac{1}{kD}$ is insufficient for applications to mutual coupling in conformal arrays, because the elements of the array are not necessarily far apart. Furthermore, for the case of circumferential slots, the lowest order TE contribution vanishes in the H-plane and a consistent expansion to second order in $\frac{1}{kD}$ is essential, as will be seen in Section 4.

One notes that, in principle, it is sufficient to carry out the evaluation of the fields in the first quadrant, $0 \leq \theta \leq \frac{\pi}{2}$, those in other quadrants follow, in view of (18-20 and 26-27) via the various sgn u relations. This procedure, however, will be replaced by an equivalent method that conforms naturally to the surface ray description. In this simple alternative scheme that avoids the use of the sgn symbols and will be explained with the aid of final formulae, the observation angle θ (Figure II-7) ranges over all four quadrants.

Following a standard procedure (e.g. Ref. 4) one transforms variables via

$$\nu = k_t a + f_t t \tag{28}$$

where

$$f_t = \left(\frac{k_t a}{2}\right)^{1/3} \tag{29}$$

so that

$$\nu^2 = k_t^2 a^2 + 2 k_t a f_t t + f_t^2 t^2 \tag{30}$$

Substituting (30) into (18) and making use of the Airy function approximation for the Hankel functions to the lowest order in $\frac{1}{ka}$ (see Appendix B), one finds

$$H_{\varphi}^{\prime\prime c}(\underline{r},\underline{r}')\Big|_{\rho=\rho'=} \sim \frac{-jM_{\varphi}}{4\pi^2 \omega \mu_o a}\left\{\int_{-\infty}^{\infty} dk_z\, e^{-jk_z|z-z'| - jk_t a \Phi \frac{k_z^2 f_t^2}{k_t}} V_0(x)\right.$$

$$+ \int_{-\infty}^{\infty} dk_z\, e^{-jk_z|z-z'| - jk_t a \Phi \frac{k_z^2}{k_t}} V_1(x)$$

$$\left. + \int_{-\infty}^{\infty} dk_z\, e^{-jk_z|z-z'| - jk_t a \Phi \frac{k_z^2 f_t^4}{k_t^3}} V_2(x)\right\} \tag{31}$$

where $x = f_t \Phi$ and $V_n(x)$ denote the Fock type integrals:

$$V_0(x) = \int_{\tau} dt\, e^{-jxt} \frac{w_2(t)}{w_2'(t)} \tag{32}$$

$$V_1(x) = \int_{\tau} dt\, e^{-jxt}\, t \frac{w_2(t)}{w_2'(t)} \tag{33}$$

and

$$V_2(x) = \int_{\tau} dt\, e^{-jxt}\, t^2\, \frac{w_2(t)}{w_2'(t)} \,. \tag{34}$$

The integration contour τ is depicted in Figure II-3.

The validity of the Airy function approximation of Hankel function $H_\nu^{(2)}(z)$ is predicated upon the condition of large z and $|\nu - z| < 0\,(z^{1/3})$. If z is not large as, e.g. in the paraxial region $\Phi \approx 0$,

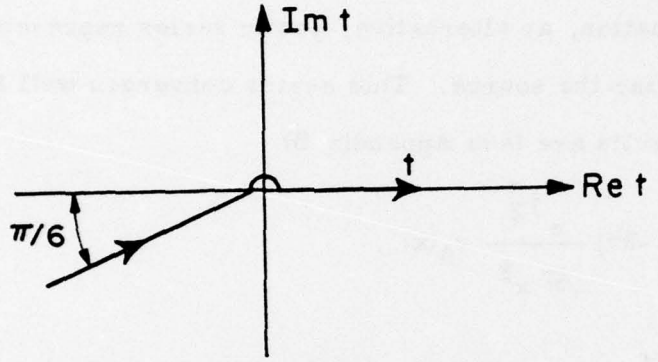

Figure II-3. Contour of Integration for Curvature Terms.

where the value of $k_t a$ at the saddle point as in (31) becomes small, this approximation of $H_\nu^{(2)}(k_t a)$ breaks down, and the above method of asymptotic evaluation becomes invalid. The extent of the paraxial region depends on the value of ka; the larger the value of ka the narrower will be the paraxial region where approximation (B1) does not hold. To date no rigorous asymptotic transition function is available for the paraxial region, but in Section 5 we shall derive an approximate transition function, which will be employed in Chapter III to obtain numerical results for mutual coupling between rectangular slots on circular cylindrical surfaces. In spite of this deficiency, it will be seen from comparison of the numerical results with those obtained via harmonic series, that the overall agreement is very reasonable for $ka \approx 10$ and 20, including the paraxial region for circumferential and axial slots.

In the deep shadow, i.e. for sufficiently large values of the parameter x, the Fock type integrals are evaluated by closing the contour at infinity in the lower half of the t-plane. The resulting residue series at the simple poles $\bar{t}_p$ of the integrand with $w_2'(\bar{t}_p) = 0$ will give rise to surface rays, one for each pole. This representation becomes poorly convergent for small value of x, necessitating too many residue terms. To amend the situation, an alternative, power series representation of $V_n(x)$ is employed near the source. This series converges well for small values of x. The results are (see Appendix B)

$$V_0(x) = -2\pi j \frac{e^{j\frac{\pi}{4}}}{\sqrt{\pi}\, x^{\frac{1}{2}}}\, v_0(x) \ , \tag{35}$$

where

$$v_0(x) = \begin{cases} 1 - \dfrac{\sqrt{j\pi}}{4} x^{3/2} + \dfrac{j7}{60} x^3 + \dfrac{7\sqrt{\pi}}{\sqrt{j}\,512} x^{9/2} + \ldots, & \text{for small } x \quad (x < 0.6) \\ \dfrac{\sqrt{\pi}\, x^{\frac{1}{2}}}{e^{j\frac{\pi}{4}}} \displaystyle\sum_{p=1}^{\infty} \frac{e^{-jx\bar{t}_p}}{\bar{t}_p}, & \text{for large } x \quad (x > 0.6), \end{cases} \tag{36}$$

$$V_1(x) = -2\pi j \frac{e^{-j\frac{\pi}{4}}}{2\sqrt{\pi}\, x^{3/2}}\, v_1(x) \ , \tag{37}$$

where

$$v_1(x) = \begin{cases} 1 + \dfrac{\sqrt{j\pi}}{2} x^{3/2} - \dfrac{j7}{12} x^3 - \dfrac{7\sqrt{\pi}}{\sqrt{j}\,64} x^{9/2} + \ldots, & \text{for small } x \quad (x < 0.6) \\ \dfrac{2\sqrt{\pi}\, x^{3/2}}{e^{-j\frac{\pi}{4}}} \displaystyle\sum_{p=1}^{\infty} e^{-jx\bar{t}_p}, & \text{for large } x \quad (x > 0.6) \end{cases} \tag{38}$$

and

$$V_2(x) = -2\pi \frac{3\, e^{-j\frac{\pi}{4}}}{4\sqrt{\pi}\, x^{5/2}}\, v_2(x) \quad , \tag{39}$$

where

$$v_2(x) = \begin{cases} 1 + \frac{j7}{12} x^3 + \frac{7\sqrt{\pi}}{\sqrt{j}\,32} x^{9/2} + \ldots, & \text{for small } x \quad (x < 0.6) \\ \frac{4\sqrt{\pi}\, x^{5/2}}{3\, e^{-j\frac{\pi}{4}}} \sum_{p=1}^{\infty} \bar{t}_p\, e^{-jx\bar{t}_p}, & \text{for large } x \quad (x > 0.6) \, . \end{cases} \tag{40}$$

Here $\bar{t}_p = |\bar{t}_p|\, e^{-j\frac{\pi}{3}}$, $Ai'(-|\bar{t}_p|) = 0$ and $Ai'(y)$ denotes the derivative of the Airy function $Ai(y)$.

Another type of Fock integral that represents the TM polarization contributions is defined by

$$U_0(x) = \int_{\tau} dt\, e^{-jxt}\, \frac{w_2'(t)}{w_2(t)} \tag{41}$$

where τ is the same contour as in Figure II-3.

Similarly to $V_n(x)$, $U_0(x)$ becomes a residue series for large values of x and may be expanded in a power series for small values of x as follows:

$$U_0(x) = -2\pi j \frac{e^{-j\frac{\pi}{4}}}{2\sqrt{\pi}\, x^{3/2}}\, u_0(x) \quad , \tag{42}$$

where

$$u_0(x) = \begin{cases} 1 - \frac{\sqrt{j\pi}}{2} x^{3/2} + \frac{j5}{12} x^3 + \frac{5\sqrt{\pi}}{\sqrt{j}\,64} x^{9/2} + \ldots, & \text{for small } x \quad (x < 0.6) \\ \frac{2\sqrt{\pi}\, x^{3/2}}{e^{-j\frac{\pi}{4}}} \sum_{p=1}^{\infty} e^{-jxt_p}, & \text{for large } x \quad (x > 0.6). \end{cases} \tag{43}$$

Here $t_p = |t_p| e^{-j\frac{\pi}{3}}$, with $Ai(-|t_p|) = 0$.

Figures (II-6, II-8) show the residue series-power series crossover regions for the curvature terms $v_0(x)$, $v_1(x)$ and $u_0(x)$. From the computed data it is found that the smoothest crossover is obtained for $x = 0.6$, where the difference Δ between the sum of ten residue terms and the sum of four power series terms is as follows:

$\Delta|v_0(x)| = 0.0025\%$ $\qquad$ $\Delta \arg v_0(x) = 0.012^\circ$

$\Delta|v_1(x)| = 0.42\%$ $\qquad$ $\Delta \arg v_1(x) = 0.126^\circ$

$\Delta|v_2(x)| = 1.7\%$ $\qquad$ $\Delta \arg v_2(x) = 0.101^\circ$

$\Delta|u_0(x)| = 0.2\%$ $\qquad$ $\Delta \arg u_0(x) = 0.10^\circ$.

In actual computations, the crossover value of $x = 0.8$ was employed, with

$\Delta|v_o(x)| = 0.13\%$ $\qquad$ $\Delta \arg v_0(x) = 0.012^\circ$

$\Delta|v_1(x)| = 0.77\%$ $\qquad$ $\Delta \arg v_1(x) = 0.13^\circ$

$\Delta|u_0(x)| = 1.26\%$ $\qquad$ $\Delta \arg u_0(x) = 0.28^\circ$.

The integrals $V_n(x)$ arise from the TE polarization in the cylindrical geometry or from the Neumann boundary conditions. In the terminology borfored from acoustics, the latter corresponds to a hard boundary. Accordingly,

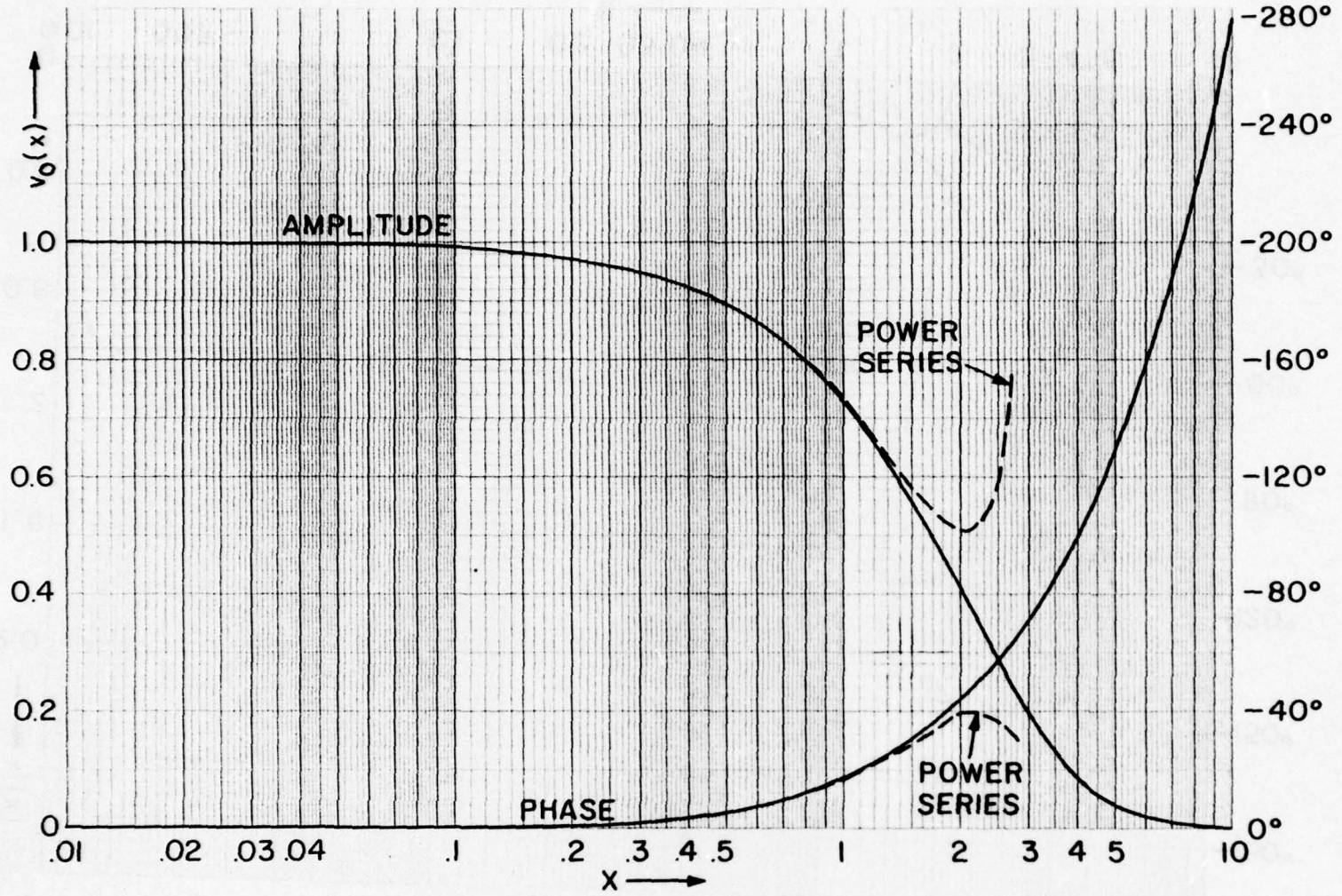

Figure II-4. Curvature Term $v_o(x)$.

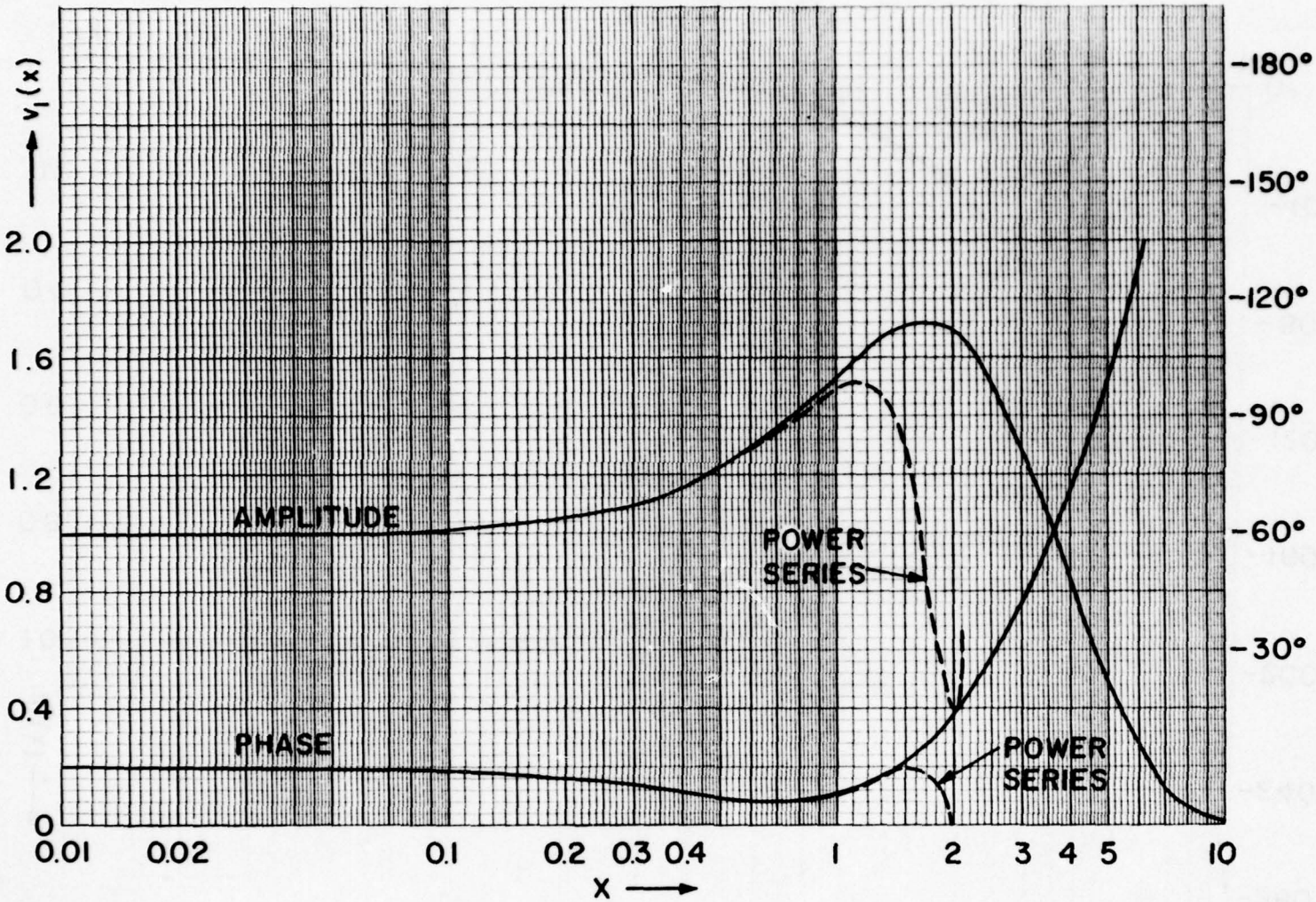

Figure II-5. Curvature Term $v_1(x)$

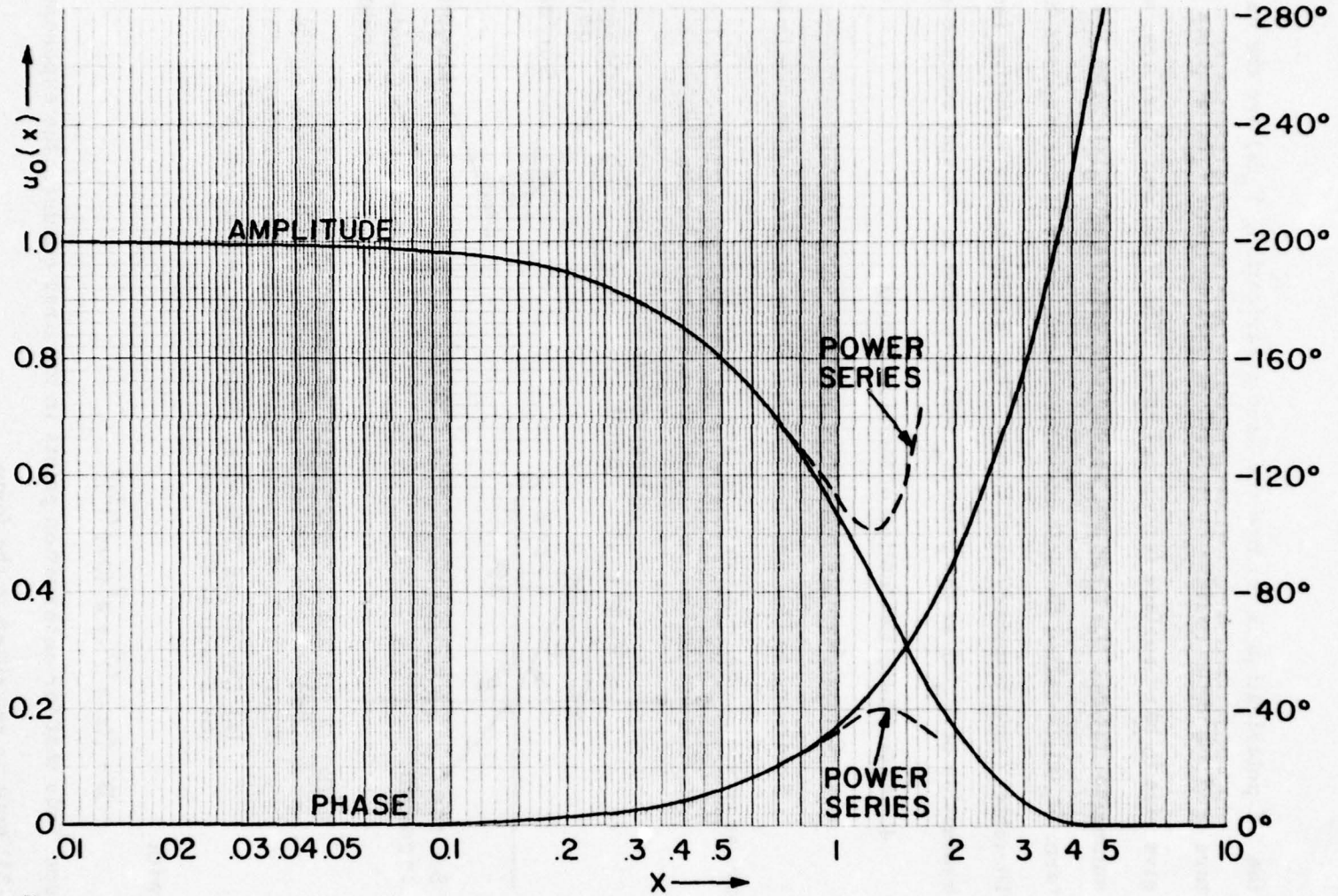

Figure II-6. Curvature Term $u_o(x)$.

the TE polarization is termed the hard polarization, $V_n(x)$ are the hard curvature terms and the residue contributions arising from $V_n(x)$ at poles $\bar{t}_p$ will give rise to hard surface (creeping) rays. The $V_1(x)$ and $V_2(x)$ are, within a numerical factor, the first and second derivatives of $V_0(x)$. The TM curvature term $U_0(x)$ is called the soft curvature term, since it corresponds to the Dirichlet (soft) boundary conditions. The residue terms resulting from evaluation of $U_0(x)$ at the poles t_p will give rise to the soft surface rays.

4. Asymptotic Evaluation of Surface Fields.

a. Circumferential Magnetic Current Element.

Returning to (31) and denoting by D the geodesic distance between the source and observation point (see Figure II-7)

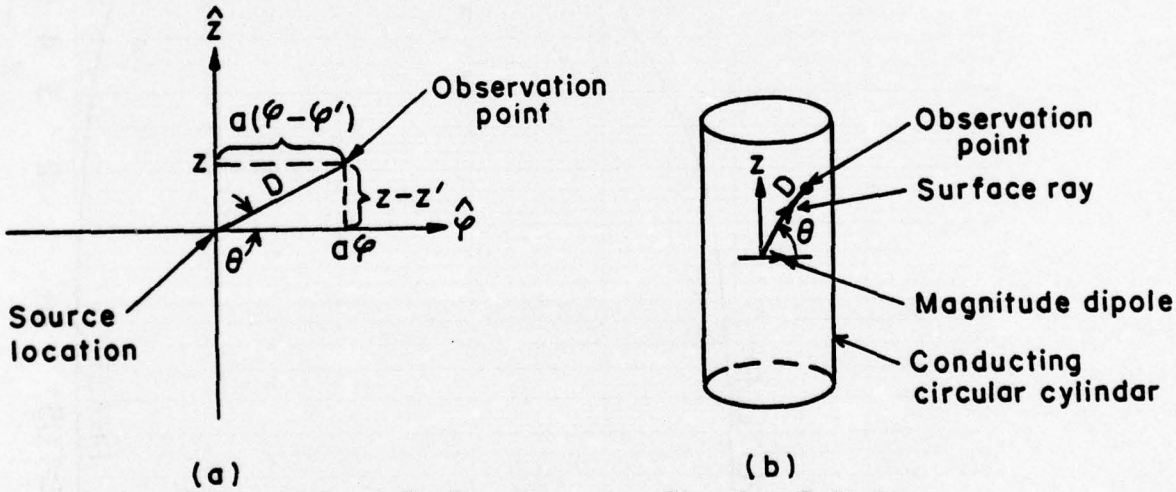

Figure II-7. A Surface Ray on a Circular Cylinder
(a) Developed Cylinder, Source located at $(a\varphi', z')$
(b) Physical Structure.

with

$$D = [(z-z')^2 + a^2(\varphi-\varphi')^2]^{\frac{1}{2}} \quad , \tag{44}$$

one finds that for observation points in the first quadrant the exponent in (31) may be rewritten in the form

$$k_z\,|z-z'| + k_t\,a\phi = D(k_z \sin\theta + k_t \cos\theta)\,, \tag{45}$$

where

$$\frac{|z-z'|}{a\phi} = \tan\theta\,. \tag{46}$$

Introducing the change of variable

$$k_z = k \sin\alpha \tag{47}$$

with

$$k_t = k \cos\alpha, \tag{48}$$

where the positive sign is chosen in order that for $k_z = 0$ ($\alpha = 0$), $k_t = k$, and substituting (47) and (48) into (45), one finds

$$k_z\,|z-z'| + k_t\,a\phi = kD \cos(\alpha - \theta). \tag{49}$$

Combining (49), and $dk_z = k_t\,d\alpha$, with (31), one obtains, for observation points in the first quadrant, the hard (TE) contributions

$$H_\phi''^{c}(\underline{r},\underline{r}')\Big|_{\rho=\rho'=a} \sim \frac{-j M_\phi}{4\pi^2 \omega\mu_o a}\left[k^2 f^2 \int_P d\alpha\, e^{-jkD\cos(\alpha-\theta)} \cos^{2/3}\alpha \sin^2\alpha\, V_0(x)\right.$$
$$+ k^2 \int_P d\alpha\, e^{-jkD\cos(\alpha-\theta)} \sin^2\alpha\, V_1(x)$$
$$\left. + \frac{f^4}{a^2} \int_P d\alpha\, e^{-jkD\cos(\alpha-\theta)} \sin^2\alpha \cos^{4/3}\alpha\, V_2(x)\right], \tag{50}$$

where

$$f = \left(\frac{ka}{2}\right)^{1/3}. \tag{51}$$

The integration contour P is the α-plane is depicted in Figure II-8.

Top Sheet of Fig. II-2

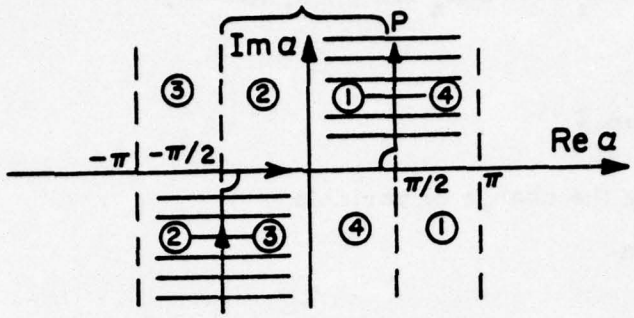

Figure II-8. One Period of the α-plane and Contour of Integration. Shaded Regions are Valleys for $e^{-jkD \cos \alpha}$. The Numbering Corresponds to Mapping of the Four Quadrants of Figure II-2.

To perform the asymptotic evaluation of the integrals in (50), one first deforms the contour of Figure II-8 into the steepest descent path (SDP) through the saddle point α_s, as depicted in Figure II-9. The SDP intersects the real α-axis at an angle $\frac{\pi}{4}$. From (C1) one has for the

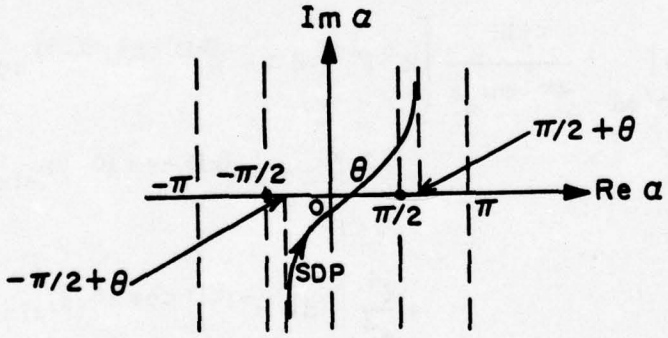

Figure II-9. SDP in the α-plane

first integral in (50)

$$q(\alpha) = -j \cos(\alpha - \theta) = -j - s^2 \tag{52}$$

$$F(\alpha) = \sin^2\alpha \cos^{2/3}\alpha \, V_0(x) \tag{53}$$

and

$$G(s) = F(\alpha) \frac{d\alpha}{ds} . \tag{54}$$

From (52), the saddle point is

$$\alpha_s = \theta \, . \tag{55}$$

The even power terms in the Taylor series expansion of (54) about s=0 are found below

$$G(0) = F(\theta)\,\alpha_s' \tag{56}$$

$$G''(0) = F''(\theta)\,(\alpha_s')^3 + 3F'(\theta)\,\alpha_s'\,\alpha_s'' + F(\theta)\,\alpha_s''' \, , \tag{57}$$

where

$$\alpha_s^{(n)} = \frac{d^n \alpha}{ds^n}\Bigg|_{s=0} \tag{58}$$

and

$$F^{(n)}(\theta) = \frac{d^n F(\alpha)}{d\alpha^n}\Bigg|_{\alpha=\theta} \, . \tag{59}$$

From (53) one finds

$$F'(\theta) = -\frac{2}{3}\cos^{-1/3}\theta \sin^3\theta\, V_0(x_s) + 2\cos^{5/3}\theta \sin\theta\, V_0(x_s) + \cos^{2/3}\sin^2\theta\, V_0'(x_s)\,x_s' \, , \tag{60}$$

$$\begin{aligned} F''(\theta) = {} & -\frac{2}{9}\cos^{-4/3}\theta \sin^4\theta\, V_0(x_s) - \frac{4}{3}\cos^{-1/3}\theta \sin^3\theta\, V_0'(x_s)\,x_s' - \frac{16}{3}\cos^{2/3}\theta \sin^2\theta\, V_0(x_s) \\ & + 2\cos^{8/3}\theta\, V_0(x_s) + 4\cos^{5/3}\theta \sin\theta\, V_0'(x_s)x_s' + \cos^{2/3}\theta \sin^2\theta\, V_0''(x_s)(x_s')^2 \\ & + \cos^{2/3}\theta \sin^2\theta\, V_0(x_s)\,x_s'' \, , \end{aligned} \tag{61}$$

where

$$x_s = x\Big|_{\alpha=\theta} = \frac{kD}{2f_g^2} = f\cos^{1/3}\theta\,\Phi \, , \tag{62}$$

with f defined in (51) and

$$f_g = \left(\frac{k\rho_g}{2}\right)^{1/3} = \left(\frac{ka}{2\cos^2\theta}\right)^{1/3}, \tag{63}$$

$$x_s' = \frac{dx}{d\alpha}\bigg|_{\alpha=\theta} = -\frac{1}{3}x_s \tan\theta, \tag{64}$$

and

$$x_s'' = \frac{d^2x}{d\alpha^2}\bigg|_{\alpha=\theta} = -\frac{2}{9}x_s \tan^2\theta - \frac{1}{3}x_s . \tag{65}$$

The mapping derivative can be found via (52) and the proper branch is determined by the condition that at $\alpha=\theta$, $\arg\left(\frac{d\alpha}{ds}\right) = \frac{\pi}{4}$. Therefore,

$$\frac{d\alpha}{ds} = \sqrt{2j}\left(1 - j\frac{s^2}{2}\right)^{-\frac{1}{2}}, \tag{66}$$

and

$$\alpha_s' = \sqrt{2j} . \tag{67}$$

Consequently, the higher order derivatives become

$$\alpha_s'' = 0, \tag{68}$$

$$\alpha_s''' = \frac{j\sqrt{j2}}{2} . \tag{69}$$

As a result, one has

$$G(0) = \sqrt{2j}\,\sin^2\theta\cos^{2/3}\theta\, V_0(x_s) \tag{70}$$

and

$$\begin{aligned} G''(0) = 2j\sqrt{2j}\Big[& -\frac{2}{9}\cos^{-4/3}\theta\sin^4\theta\, V_0(x_s) - \frac{4}{3}\cos^{-1/3}\theta\sin^3\theta\, V_0'(x_s)x_s' \\ & - \frac{16}{3}\cos^{2/3}\theta\sin^2\theta\, V_0(x_s) + 2\cos^{8/3}\theta\, V_0(x_s) + 4\cos^{5/3}\theta\sin\theta\, V_0'(x_s)x_s' \\ & + \cos^{2/3}\theta\sin^2\theta\, V_0''(x_s)(x_s')^2 + \cos^{2/3}\sin^2\theta\, V_0'(x_s)x_s''\Big] \\ & + \frac{j\sqrt{j2}}{2}\sin^2\theta\cos^{2/3}\theta\, V_0(x_s) . \end{aligned} \tag{71}$$

Thus, one has, with $\Omega = kD$

$$H''^{c}_{\varphi,1}(\underline{r},\underline{r}')\Big|_{\rho=\rho=a} \sim \frac{-jM_\varphi k^2 f^2}{4\pi^2 \omega \mu_o a}\Bigg\{\sqrt{2\pi j}\sin^2\theta\cos^{2/3}\theta\, V_0(x_s)\frac{e^{-jkD}}{(kD)^{\frac{1}{2}}}$$

$$+\frac{j\sqrt{2\pi j}}{2}\Big[(2\cos^{8/3}\theta - \frac{61}{12}\cos^{2/3}\theta\sin^2\theta - \frac{2}{9}\cos^{-4/3}\theta\sin^2\theta)V_0(x_s)$$

$$+(4\cos^{5/3}\theta\sin\theta - \frac{4}{3}\cos^{-1/3}\theta\sin^3\theta)V_0'(x_s)x_s'$$

$$+\cos^{2/3}\theta\sin^2\theta\, V_0'(x_s)\,x_s''$$

$$+\cos^{2/3}\theta\sin^2\theta\, V_0''(x_s)(x_s')^2\Big]\frac{e^{-jkD}}{(kD)^{3/2}}\Bigg\}, \qquad (72)$$

where the second subscript "1" denotes the first integral in (50).

Carrying out the various derivatives in the bracket, one finds

$$H''^{c}_{\varphi,1}(\underline{r},\underline{r}')\Big|_{\rho=\rho'=a} \sim \frac{-jM_\varphi k^2 f^2}{4\pi^2\omega\mu_o a}\sqrt{2\pi j}\, V_0(x_s)\cos^{2/3}\theta\sin^2\theta\frac{e^{-jkD}}{\sqrt{kD}}$$

$$+\frac{M_\varphi k^2 f^2}{4\pi^2\omega\mu_o a}\frac{\sqrt{2\pi j}}{2}V_0(x_s)\Big(-\frac{2}{9}\cos^{-4/3}\theta\sin^4\theta + 2\cos^{8/3}\theta$$

$$-\frac{61}{12}\cos^{2/3}\theta\sin^2\theta\Big)\frac{e^{-jkD}}{(kD)^{3/2}}$$

$$+\frac{M_\varphi k^2}{4\pi^2\omega\mu_o a}\frac{\sqrt{2\pi j}}{12}V_1(x_s)\Big(-\frac{2}{3}\sin^4\theta + 5\cos^2\theta\sin^2\theta\Big)\frac{e^{-jkD}}{\sqrt{kD}}, \qquad (73)$$

where the term with $V_2(x_s)$ has been neglected due to its lower order in $\frac{1}{ka}$. One observes that the three terms in (73) have the same exponential order in ka, because the residue series for $V_0(x)$, $V_1(x)$ contains the same "hard" exponents (see 36 and 38). However, the algebraic orders in $\frac{1}{ka}$ of the terms differ. Therefore, for consistency, the third term is also discarded.

If one transforms $V_0(x)$ into the near zone form $v_0(x)$ via (35), one finds the form

$$H''^{c}_{\varphi,1}(\underline{r},\underline{r}')\Big|_{\rho=\rho'=a} \sim -jM_{\varphi}\frac{k^2 Y}{2\pi}\sin^2\theta\, v_0(x_s)\frac{e^{-jkD}}{kD}$$

$$+ M_{\varphi}\frac{k^2 Y}{2\pi}\left(\cos^2\theta - \frac{61}{24}\sin^2\theta - \frac{1}{9}\frac{\sin^4\theta}{\cos^2\theta}\right)v_0(x_s)\frac{e^{-jkD}}{(kD)^2} \qquad (74)$$

where for small values of x_s one uses for $v_o(x_s)$ the power series expressions and for large values of x_s the residue series (see (36)).

The second integral yields

$$H''^{c}_{\varphi,2}(\underline{r},\underline{r}')\Big|_{\rho=\rho'=a} \sim \frac{-M_{\varphi}k^2}{4\pi^2\omega\mu_o a}\sqrt{2\pi j}\sin^2\theta\, V_1(x_s)\frac{e^{-jkD}}{(kD)^{\frac{1}{2}}} + O(\tfrac{1}{ka})\,O\left(\frac{1}{(kD)^{3/2}}\right) \qquad (75)$$

Because $H''^{c}_{\varphi,2}$ is $O(\frac{1}{ka})$, it is also discarded, as compared to $O\left(\frac{1}{ka}\right)^{1/3}$ of the first two terms in (73).

The TM contribution follows via an analogous procedure. From (19) one finds

$$H'^{c}_{\varphi}(\underline{r},\underline{r}')\Big|_{\rho=\rho=a} \sim \frac{j\omega\epsilon_o M_{\varphi}}{4\pi^2 a}\int_P d\alpha\, e^{-jkD\cos(\alpha-\theta)}\, U_o(x)\,, \qquad (76)$$

where the integration contour P is same as for the TE case.

The asymptotic evaluation yields

$$H'^{c}_{\varphi}(\underline{r},\underline{r}')\Big|_{\rho=\rho'=a} \sim \frac{j\omega\epsilon_o M_{\varphi}}{4\pi^2 a}\left[\sqrt{2\pi j}\, U_o(x_s)\frac{e^{-jkD}}{(kD)^{\frac{1}{2}}} + \frac{j\sqrt{2\pi j}}{8}\, U_o(x_s)\frac{e^{-jkD}}{(kD)^{3/2}}\right]$$

$$+ O\left(\frac{1}{(ka)^{5/3}}\right)O\left(\frac{1}{(kD)^{3/2}}\right) \qquad (77)$$

The $O\left(\frac{1}{(kD)^{3/2}}\right)$ term results in the near zone in $\frac{1}{(kD)^3}$. To $O\left(\frac{1}{(kD)^2}\right)$ in the near zone one needs to consider only the leading soft contribution.

$$H_\varphi'^{c}(\underline{r},\underline{r}')\Big|_{\rho=\rho'=a} \sim M_\varphi \frac{k^2 Y}{2\pi}\frac{1}{\cos^2\theta}\, u_o(x_s)\,\frac{e^{-jkD}}{(kD)^2} \tag{78}$$

Combining (74) and (78), one has the total φ-component of the surface magnetic field excited by a circumferential magnetic current element:

$$\begin{aligned} H_\varphi^{c}(\underline{r},\underline{r}')\Big|_{\rho=\rho'=a} \sim & -jM_\varphi \frac{k^2 Y}{2\pi}\sin^2\theta\, v_o(x_s)\,\frac{e^{-jkD}}{kD} \\ & + M_\varphi \frac{k^2 Y}{2\pi}\left(\cos^2\theta - \frac{61}{24}\sin^2\theta - \frac{1}{9}\frac{\sin^4\theta}{\cos^2\theta}\right) v_o(x_s)\,\frac{e^{-jkD}}{(kD)^2} \\ & + M_\varphi \frac{k^2 Y}{2\pi}\frac{1}{\cos^2\theta}\, u_o(x_s)\,\frac{e^{-jkD}}{(kD)^2} \quad . \end{aligned} \tag{79}$$

Besides those already neglected additional terms of order $\frac{1}{(kD)^2}$ but of lower order in $\frac{1}{ka}$ appear when the uniform expansion of $H_\nu^{(2)\prime}(z)$ is used. These terms are similarly discarded.

The above asymptotic evaluation is valid as long as $ka\cos\theta$ is not too small, because otherwise the Airy function approximation breaks down. The failure of the Airy function approximation of $H_\nu^{(2)}(z)$ for small values of z manifests itself in appearance of a spurious algebraic branch point at $\alpha = \frac{\pi}{2}$ in the various integrands and of $\Phi^{-1/2}$ and $\Phi^{-3/2}$ factors (see 30, 35 and 62) with $V_0(x) \to \frac{1}{\sqrt{x}} \to \frac{1}{\Phi^{\frac{1}{2}}}$, $U_0(x) \to \frac{1}{x^{3/2}} \to \frac{1}{\Phi^{3/2}}$ as $\Phi \to 0$ or $\theta \to \frac{\pi}{2}$. Although the proximity of the saddle point to the branch point for paraxial propagation could be taken into account by appropriate parabolic cylinder transition function [7], the presence of $\Phi^{-1/2}$ and $\Phi^{-3/2}$ factors yields infinity in the axial direction ($\Phi=0$) which cannot be removed by constructing a transition function based on the assumed validity of (B1). An approximate transition function and

its variant which render the field finite for $\Phi=0$ will be given in Section 5.

From (20) one finds, in a similar manner, for the z-component of the surface magnetic field to lowest order in $\frac{1}{ka}$:

$$H_z^c(\underline{r},\underline{r}')\Big|_{\rho=\rho'=a} \sim \operatorname{sgn}(\varphi-\varphi')\operatorname{sgn}(z-z')\frac{jM_\varphi k^2 f^2}{4\pi^2\omega\mu_o a}\int_P d\alpha\, e^{-jkD\cos(\alpha-\theta)}\sin\alpha\cos^{5/3}\alpha\, V_0(x). \tag{80}$$

Following the same procedure as in (79), one finds

$$H_z^c(\underline{r},\underline{r}')\Big|_{\rho=\rho'=a} \sim \operatorname{sgn}(\varphi-\varphi')\operatorname{sgn}(z-z')\, jM_\varphi\frac{k^2 Y}{2\pi}\sin\theta\cos\theta\, v_0(x_s)\frac{e^{-jkD}}{kD}$$

$$-M_\varphi\frac{k^2 Y}{2\pi}\left(-\frac{23}{8}\sin\theta\cos\theta+\frac{5}{9}\frac{\sin^3\theta}{\cos\theta}\right)v_0(x_s)\frac{e^{-jkD}}{(kD)^2}\quad . \tag{81}$$

Again the second order terms are inadequate as $\theta\to\frac{\pi}{2}$. As mentioned previously, the sgn symbols in (81) may be removed when the range of θ is extended to all four quadrants i.e. $0\le\theta<2\pi$.

b. Axial Magnetic Current Element

In contrast to the case of circumferential magnetic current element, in spite of the fact that the Airy function approximation of $H_\nu^{(2)}(z)$ breaks down in the paraxial region, the asymptotic series terms $O\left(\frac{1}{(kD)^2}\right)$ are bounded.

The z- and φ- components of the surface magnetic field may be obtained from (26) and (27). For mutual coupling between axial slots, one is particularly interested in H_z. Proceeding in a similar manner as in Section (4a) with (28) and (32) one has

$$H_z^a(\underline{r},\underline{r}')\Big|_{\rho=\rho'=a} \sim \frac{-jM_z k^2 f^2}{4\pi^2\omega\mu_o a}\int_{SDP} d\alpha\, e^{-jkD\cos(\alpha-\theta)}\cos^{8/3}\alpha\, V_0(x_s) \tag{82}$$

where SDP is shown in Figure II-9 and $V_0(x_s)$ is the hard curvature term, with x_s given by (62).

One finds in (82)

$$\alpha_s = \theta \tag{83}$$

$$F(\alpha) = \cos^{8/3}\alpha\, V_0(x) \tag{84}$$

$$F''(\alpha) = \frac{40}{9}\cos^{2/3}\alpha \sin^2\alpha\, V_0(x) - \frac{8}{3}\cos^{8/3}\alpha\, V_0(x) - \frac{16}{3}\cos^{5/3}\alpha \sin\alpha\, V_0'(x)\, x'$$

$$+ \cos^{8/3} V_0''(x)\,(x')^2 + \cos^{8/3}\alpha\, V_0'(x)\, x'' \tag{85}$$

Therefore

$$G(0) = \sqrt{2j}\cos^{8/3}\theta\, V_0(x_s) \tag{86}$$

and

$$G''(0) = 2j\sqrt{2j}\left[\frac{40}{9}\cos^{2/3}\theta \sin^2\theta\, V_0(x_s) - \frac{8}{3}\cos^{8/3}\theta\, V_0(x_s)\right.$$

$$\left. - \frac{16}{3}\cos^{5/3}\theta \sin\theta\, V_0'(x_s)x_s' + \cos^{8/3}\theta\, V_0''(x_s)(x_s')^2 + \cos^{8/3}\theta\, V_0'(x_s)x_s''\right]$$

$$+ \frac{j\sqrt{2j}}{2}\cos^{8/3}\theta\, V_0(x_s) \quad . \tag{87}$$

In accordance with (C6), one has

$$H_z^a(\underline{r}, \underline{r}')\Big|_{\rho=\rho'=a} \sim \frac{-j M_z k^2 f^2}{4\pi^2 \omega \mu_o a}\left\{\sqrt{2\pi j}\cos^{8/3}\theta\, V_0(x_s)\,\frac{e^{-jkD}}{\sqrt{kD}}\right.$$

$$+ \frac{j\sqrt{2\pi j}}{2}\left[\left(\frac{40}{9}\cos^{2/3}\theta \sin^2\theta - \frac{29}{12}\cos^{8/3}\theta\right)V_0(x_s)\right.$$

$$- \frac{16}{3}\cos^{5/3}\theta \sin\theta\, V_0'(x_s)x_s' + \cos^{8/3}\theta\, V_0'(x_s)x_s''$$

$$\left.\left. + \cos^{8/3}\theta\, V_0''(x_s)(x_s')^2\right]\right\}\frac{e^{-jkD}}{(kD)^{3/2}} \tag{88}$$

Carrying out the derivatives in the bracket yields

$$H_z^a(\underline{r},\underline{r}')\Big|_{\rho=\rho'=a} \sim -\frac{-jM_z k^2 f^2}{4\pi^2 \omega\mu_o a}\sqrt{2\pi j}\, V_0(x_s)\cos^{8/3}\theta\,\frac{e^{-jkD}}{\sqrt{kD}}$$

$$-\frac{jM_z k^2 f^2}{4\pi^2\omega\mu_o a}\frac{j\sqrt{2\pi j}}{2}V_0(x_s)\left(\frac{40}{9}\cos^{2/3}\theta\sin^2\theta-\frac{29}{12}\cos^{8/3}\theta\right)\frac{e^{-jkD}}{(kD)^{3/2}}$$

$$+\frac{jM_z k^2}{4\pi^2\omega\mu_o a}\frac{\sqrt{2\pi j}}{2}V_1(x_s)\left(-\frac{7}{9}\cos^2\theta\sin^2\theta+\frac{1}{6}\cos^4\theta\right)\frac{e^{-jkD}}{(kD)^{1/2}}\,. \quad (89)$$

Note, the last term is of $O\frac{1}{(ka)^{2/3}}$ below the leading term and is therefore neglected.

Finally one arrives at the following simpler form

$$H_z^a(\underline{r},\underline{r}')\Big|_{\rho=\rho'=a} \sim -jM_z\frac{k^2 Y}{2\pi}\cos^2\theta\, v_0(x_s)\frac{e^{-jkD}}{kD}$$

$$+M_z\frac{k^2 Y}{2\pi}\left(\frac{20}{9}\sin^2\theta-\frac{29}{24}\cos^2\theta\right)v_0(x_s)\frac{e^{-jkD}}{(kD)^2} \quad (90)$$

Because of a similarity between (25) and (12), H_φ^a component excited by an axial magnetic current element becomes

$$H_\varphi^a(\underline{r},\underline{r}')\Big|_{\rho=\rho'=a} \sim jM_z\frac{k^2 Y}{2\pi}\sin\theta\cos\theta\, v_0(x_s)\frac{e^{-jkD}}{kD}$$

$$-M_z\frac{k^2 Y}{2\pi}\left(-\frac{23}{4}\sin\theta\cos\theta+\frac{5}{9}\frac{\sin^3\theta}{\cos\theta}\right)v_0(x_s)\frac{e^{-jkD}}{(kD)^2},\quad 0\le\theta<2\pi \quad (91)$$

5. Approximate Formulae

a. The "Full Formula" for Circumferential Current Element.

Since the limits of validity of the rigorous asymptotic expansion (79),

(81) and (91) do not extend to the paraxial region, we shall derive an approximate, simple transition function which is finite for $\theta \to \frac{\pi}{2}$, matches to $O\left(\frac{1}{(kD)^2}\right)$ the rigorous formula at $\theta=0$ and reduces to a planar result to $O\left(\frac{1}{(kD)^2}\right)$ when the observation point approaches the source.

The derivation of the "Full Formula" is given below.

Starting with (31), we immediately discard the integral containing $V_2(x)$, since it gives rise to a lower order of $\frac{1}{kD}$ than considered here. The first integral in (31) is replaced by

$$\frac{jM_\varphi}{4\pi^2\omega\mu_o a}\frac{\partial^2}{\partial z^2}\int_{-\infty}^{\infty} dk_z\, e^{-ik_z|z-z'|-jk_t a\Phi}\frac{f_t^2}{k_t}V_0(x)\,, \tag{92}$$

while the second integral is left in its original form which contains k_z^2. Hence,

$$H_\varphi''^{c}(\underline{r},\underline{r}')\Big|_{\rho=\rho'=a} \sim \frac{jM_\varphi}{4\pi^2\omega\mu_o a}\left[\frac{\partial^2}{\partial z^2}\int_P d\alpha\, e^{-jkD\cos(\alpha-\theta)} f_t^2 V_0(x) - k^2\int_P d\alpha\, e^{-jkD\cos(\alpha-\theta)}\sin^2\alpha\, V_1(x)\right]. \tag{93}$$

The contour P is deformed into SDP of Figure II-9 and the asymptotic evaluation yields the leading terms

$$\int_{SDP} d\alpha\, e^{-jkD\cos(\alpha-\theta)} f_t^2 V_0(x) \sim f^2 V_0(x_s)\cos^{2/3}\theta\sqrt{\frac{2\pi j}{kD}}e^{-jkD} \tag{94}$$

and

$$\int_{SDP} d\alpha\, e^{-jkD\cos(\alpha-\theta)}\sin^2\alpha\, V_1(x) \sim V_1(x_s)\sin^2\theta\sqrt{\frac{2\pi j}{kD}}\,e^{-jkD} \tag{95}$$

where x_s denotes the value of x evaluated at the saddle point $\alpha_s=\theta$.

In view of the relation (35) and (37) one finds

$$f^2 V_0(x_s)\cos^{2/3}\theta \sqrt{\frac{2\pi j}{kD}}\, e^{-jkD} = 2\pi ka\, v_0(x_s)\frac{e^{-jkD}}{kD} \tag{96}$$

and

$$V_1(x_s)\sin^2\theta \sqrt{\frac{2\pi j}{kD}}\, e^{-jkD} = -j\,2\pi k^3 a\, v_1(x_s)\frac{\sin^2\theta}{\cos^2\theta}\,\frac{e^{-jkD}}{(kD)^2} \quad . \tag{97}$$

Substituting (96) and (97) into (93), one has approximately

$$H_\varphi''^{c}(\underline{r},\underline{r}')\Big|_{\rho=\rho'=a} \approx \frac{jM_\varphi}{4\pi^2\omega\mu_o a}\left\{2\pi ka\,\frac{\partial^2}{\partial z^2}\left[v_0(x_s)\,\frac{e^{-jkD}}{kD}\right]\right.$$

$$\left. + j\,2\pi k^3 a\, v_1(x_s)\frac{\sin^2\theta}{\cos^2\theta}\,\frac{e^{-jkD}}{(kD)^2}\right\} \tag{98}$$

Rigorously, the asymptotic evaluation of the integral in (94) should be carried out to next order.

Since for $x < 1$, $v_0(x_s)$ is slowly varying (see Figure II-4), one may employ the approximation

$$\frac{\partial^2}{\partial z^2}\left[v_0(x_s)\,\frac{e^{-jkD}}{kD}\right] \approx v_0(x_s)\frac{\partial^2}{\partial z^2}\frac{e^{-jkD}}{kD}$$

$$\approx -k^2 v_0(x_s)\left(\sin^2\theta - \sin^2\theta\,\frac{j}{kD} + \cos^2\theta\,\frac{2j}{kD} - \frac{j}{kD}\right)\frac{e^{-jkD}}{kD}, \tag{99}$$

where after differentiation terms $O\left(\frac{1}{(kD)^3}\right)$ have geen neglected. Meanwhile, the next term in (95)is $O\left(\frac{1}{(kD)^{3/2}}\right)$ in the deep shadow, so that in view of (37) the corresponding near zone expression will be $O\left(\frac{1}{(kD)^3}\right)$ and is neglected.

Substituting (99) into (98), one finds the approximate field expression

$$H_\varphi''^{c}(\underline{r},\underline{r}')\Big|_{\rho=\rho'=a} \approx M_\varphi\,\frac{k^2 Y}{2\pi}\left[-j\left(\sin^2\theta - \sin^2\theta\,\frac{2j}{kD}\right)\right.$$

$$\left. - \frac{\sin^2\theta}{\cos^2\theta}\,\frac{1}{kD}\,v_1(x_s)\right]\frac{e^{-jkD}}{kD} \tag{100}$$

The soft contribution is obtained directly from (78). Combining (78) with (100) one finds the "Full Formula"

$$H_\varphi^c(\underline{r},\underline{r}')\Big|_{\rho=\rho'=a} \approx -j M_\varphi \frac{k^2 Y}{2\pi}\left(\sin^2\theta - \sin^2\theta \frac{j}{kD} + \cos^2\theta \frac{2j}{kD}\right) v_0(x_s)\, e^{\frac{-jkD}{kD}}$$

$$- M_\varphi \frac{k^2 Y}{2\pi}\left[v_0(x_s) + \frac{\sin^2\theta\, v_1(x_s) - u_0(x_s)}{\cos^2\theta}\right] \frac{e^{-jkD}}{(kD)^2} \qquad (101)$$

The properties of this Full Formula are as follows:

a) it matches to $O\left(\frac{1}{(kD)^2}\right)$ the asymptotic formula (79) for $\theta=0$, i.e. in the circumferential (H-plane),

b) it is finite on $\theta = \frac{\pi}{2}$, and

c) as $D \to 0$ H_φ^c tends to the planar result to $O\left(\frac{1}{(kD)^2}\right)$..

This is seen as follows:

$$w(x_s) = v_0(x_s) + \frac{\sin^2\theta\, v_1(x_s) - u_0(x_s)}{\cos^2\theta}$$

$$= \frac{\sqrt{j\pi}}{4}\left(\frac{fD}{a}\right)^{3/2}(1+3\sin^2\theta) - \frac{j}{60}\left(\frac{fD}{a}\right)^3 (18+42\sin^2\theta)\cos^2\theta + O\left(\frac{fD}{a}\right)^{9/2} \qquad (102)$$

Consequently $w(x_s) \to 0$ as $D \to 0$ and (101) reduces to the planar result for H_ζ, where ζ denotes the Cartesian coordinate in the direction of the magnetic dipole on a ground plane and θ is the angle of the radius vector with the ζ direction.

Following the same line of reasoning one has from (12) and in the first quadrant

$$H_z^c(\underline{r},\underline{r}')\Big|_{\rho=\rho'=a} = \frac{j M_\varphi}{4\pi^2 \omega\mu_0 a^2} \frac{\partial^2}{\partial z' \partial\varphi'} \int_{-\infty}^{\infty} dk_z\, e^{-jk_z|z-z'|} \frac{1}{k_t} \int_{-\infty}^{\infty} d\nu\, e^{-j\nu\Phi} \frac{H_\nu^{(2)}(k_t a)}{H_\nu^{(2)\prime}(k_t a)} \qquad (103)$$

After certain amount of algebra one finds

$$H_z^c(\underline{r},\underline{r}')\Big|_{\rho=\rho'=a} \approx -j\frac{M_\varphi Y}{2\pi a} v_0(x_s)\frac{\partial^2}{\partial z'\,\partial\varphi'}\frac{e^{-jkD}}{kD} \tag{104}$$

where the integrals were evaluated to lowest order in $\frac{1}{kD}$ and $v_0(x_s)$ was assumed slowly varying. Hence approximately

$$H_z^c(\underline{r},\underline{r}')\Big|_{\rho=\rho'=a} \approx jM_\varphi\frac{k^2Y}{2\pi}\sin\theta\cos\theta\left(1-\frac{3j}{kD}\right)v_0(x_s)\frac{e^{-jkD}}{kD} \tag{105}$$

b. Variant of the "Full Formula"

This formula is obtained from (101) by retaining, in addition to the soft polarization contribution $u_0(x)$, only hard terms to lowest order in $\frac{1}{ka}$, in line with the rigorously asymptotic procedure used in (74). Examining in the deep shadow the hard polarization terms $v_0(x)$ and $v_1(x)$ one observes, in view of (35) and (37), that for a given distance D

$$\frac{v_1(x)}{v_0(x)} = O\left(\frac{1}{(ka)^{2/3}}\right), \tag{106}$$

since from (62) and (63) one has $x = \frac{kD}{2f_g^2} = \frac{kD}{2}\left(\frac{2\cos^2\theta}{ka}\right)^{2/3}$. Thus, for consistency, the term involving $v_1(x_s)$ should be discarded. As a result, in the paraxial region, for $x_s < 0.8$ or 0.6, it is necessary to neglect the soft polarization term $u_0(x)$, which becomes unbounded for $\theta \to \frac{\pi}{2}$.

Thus, the variant formula becomes

$$H_\varphi^c(\underline{r},\underline{r}')\Big|_{\rho=\rho'=a} \approx -jM_\varphi \frac{k^2 Y}{2\pi}\left(\sin^2\theta - \sin^2\theta\,\frac{2j}{kD} + \cos^2\theta\,\frac{j}{kD}\right) v_0(x_s)\,\frac{e^{-jkD}}{kD}$$

$$+ M_\varphi \frac{k^2 Y}{2\pi}\,\frac{u_0(x)}{\cos^2\theta}\,\frac{e^{-jkD}}{(kD)^2}\,, \qquad \text{for } x > 0.6 \tag{107}$$

$$\approx -jM_\varphi \frac{k^2 Y}{2\pi}\left(\sin^2\theta - \sin^2\theta\,\frac{2j}{kD} + \cos^2\theta\,\frac{j}{kD}\right) v_0(x_s)\,\frac{e^{-jkD}}{kD}\,,$$

$$\text{for } x \leq 0.6 \tag{108}$$

It should be noted that in the $\theta=0^\circ$ (H-plane) both the "Full Formula" and its variant coincide with the rigorously asymptotic result of (79).

c. Axial Magnetic Current Element

From (8), (11), (16) and (24) one has

$$H_z^a(\underline{r},\underline{r}')\Big|_{\rho=\rho'=a} \sim \frac{jM_z}{4\pi^2\omega\mu_o a}\left(\frac{\partial^2}{\partial z^2}+k^2\right)\int_{-\infty}^{\infty} dk_z\, e^{-jk_z|z-z'|}\,\frac{1}{k_t}\int_{-\infty}^{\infty} d\nu\, e^{-j\nu\Phi}\,\frac{H_\nu^{(2)}(k_t a)}{H_\nu^{(2)\prime}(k_t a)}$$

$$\sim \frac{-jM_z}{4\pi^2\omega\mu_o a}\left(\frac{\partial^2}{\partial z^2}+k^2\right)\int_P d\alpha\, e^{-jkD\cos(\alpha-\theta)}\cos^{2/3}\alpha\, V_0(x). \tag{109}$$

In a similar manner, retaining in the integral of (109) only the leading term, one has

$$H_z^a(\underline{r},\underline{r}')\Big|_{\rho=\rho'=a} \approx -jM_z\,\frac{Y}{2\pi}\left(\frac{\partial^2}{\partial z^2}+k^2\right)\left[v_0(x_s)\,\frac{e^{-jkD}}{kD}\right]. \tag{110}$$

Again, assuming that $v_0(x_s)$ is slowly varying for $x_s < 1$, one finds

$$H_z^a(\underline{r},\underline{r}')\Big|_{\rho=\rho'=a} \approx -jM_z\,\frac{k^2 Y}{2\pi}\left(\cos^2\theta - \cos^2\theta\,\frac{j}{kD} + \sin^2\theta\,\frac{2j}{kD}\right) v_0(x_s)\,\frac{e^{-jkD}}{kD}\,. \tag{111}$$

In view of the identical form of (25) and (12) and because

$\frac{\partial^2}{\partial z\,\partial\varphi} G'' = \frac{\partial^2}{\partial z'\,\partial m'} G''$, one has, via (105)

$$H_z^a(\underline{r},\underline{r}')\Big|_{\rho=\rho'=a} \approx j M_z \frac{k^2 Y}{2\pi} \cos\theta \sin\theta \left(1 - \frac{3j}{kD}\right) v_0(x_s) \frac{e^{-jkD}}{kD} \tag{112}$$

The range of θ in (101) and (105) and (11-112) is $0 \leq \theta < 2\pi$, i.e. over all four quadrants. This feature automatically accounts for the sign changes from quadrant to quadrant, as required by (80) and (91).

d. Modified Planar Vector Formula for Arbitrary Orientation of Current Source

The set of approximate relations (101), (105), (111) and (112) can be cast in a vector form similar to that for the planar case (see Appendix D). In Figures II-10(a) and (b), the unit vectors $\hat{t}$ and $\hat{t}'$ are tangent vectors, $\hat{b}$ and $\hat{b}'$ binormals to a typical surface ray and $\hat{s}$ denotes the source

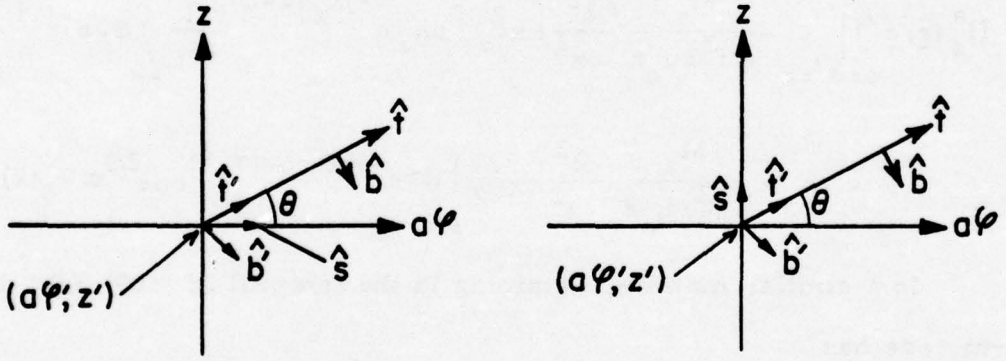

(a) Circumferential $\underline{M}$ (b) Axial $\underline{M}$

Figure II-10. Surface Rays on a Developed Cylinder

direction. The prime indicates source coordinates while the unprimed quantities refer to the observation point. The angle θ is given to $\tan^{-1}\frac{z-z'}{a(\varpi-\varpi')}$ One now obtains for a circumferential magnetic current element (Figure II-10a); i.e. $\hat{s} = \hat{m}$

$$\sin^2\theta = \hat{s} \cdot \hat{b}' \hat{b} \cdot \hat{\varphi} \,, \tag{113}$$

$$\cos^2\theta = \hat{s} \cdot \hat{t}' \hat{t} \cdot \hat{\varphi} \tag{114}$$

and

$$\sin\theta\cos\theta = \hat{s} \cdot \hat{b}(-\hat{b} \cdot \hat{z}) = (\hat{s} \cdot \hat{t}')(\hat{t} \cdot \hat{z}) \,. \tag{115}$$

Therefore,

$$H^c_\varphi(\underline{r}, \underline{r}')\Big|_{\rho=\rho'=a} \approx -j M_\varphi \frac{k^2 Y}{2\pi} \hat{s} \cdot \left[\hat{b}' \hat{b} \cdot \hat{\varphi}\left(1 - \frac{j}{kD}\right) + \hat{t}' \hat{t} \cdot \hat{\varphi} \frac{2j}{kD}\right] v_0(x_s) \frac{e^{-jkD}}{kD}$$

$$- M_\varphi \frac{k^2 Y}{2\pi} w(x_s) \frac{e^{-jkD}}{(kD)^2} \,. \tag{116}$$

The second term in the bracket in (105) may also be written $\sin\theta\cos\theta + 2\cos\theta\sin\theta$. Therefore, one has, via (115),

$$H^c_z(\underline{r}, \underline{r}')\Big|_{\rho=\rho'=a} \sim -j M_\varphi \frac{k^2 Y}{2\pi} \hat{s} \cdot \left[\hat{b}' \hat{b} \cdot \hat{z}\left(1 - \frac{j}{kD}\right) + \hat{t}' \hat{t} \cdot \hat{z} \frac{2j}{kD}\right] v_0(x_s) \frac{e^{-jkD}}{kD} \,, \tag{117}$$

Making use of the unit dyadic $\hat{\varphi}\hat{\varphi} + \hat{z}\hat{z} = 1$, one finds

$$\underline{H}^c(\underline{r}, \underline{r}')\Big|_{\rho=\rho'=a} = \hat{\varphi} H^c_\varphi(\underline{r}, \underline{r}') + \hat{z} H^c_z(\underline{r}, \underline{r}')$$

$$\approx -j M_\varphi \frac{k^2 Y}{2\pi} \hat{s} \left[\hat{b}' \hat{b}\left(1 - \frac{j}{kD}\right) + \hat{t}' \hat{t} \frac{2j}{kD}\right] v_0(x_s) \frac{e^{-jkD}}{kD}$$

$$- M_\varphi \frac{k^2 Y}{2\pi} w(x_s) \frac{e^{-jkD}}{(kD)^2} \hat{\varphi} \,. \tag{118}$$

For an axial $\underline{M}$, (see Figure II-10b)

$$\cos^2\theta = \hat{s} \cdot \hat{b}' \hat{b} \cdot \hat{z} \tag{119}$$

$$\sin^2\theta = \hat{s} \cdot \hat{t}' \hat{t} \cdot \hat{z} \tag{120}$$

and

$$\cos\theta \sin\theta = -\hat{s}\cdot\hat{\theta}'\hat{\theta}\cdot\hat{\varphi} = \hat{t}\cdot\hat{\varphi}\hat{s}\cdot\hat{t}' \,. \tag{121}$$

Hence, in a similar manner as in (118), one has

$$\underline{H}^a(\underline{r},\underline{r}')\Big|_{\rho=\rho'=a} \approx -j M_z \frac{k^2 Y}{2\pi}\hat{s}\cdot\left[\hat{\theta}'\hat{\theta}\left(1-\frac{j}{kD}\right)+\hat{t}'\hat{t}\,\frac{2j}{kD}\right] v_0(x_s)\,\frac{e^{-jkD}}{kD} \tag{122}$$

Combining both slot orientations, one finally has

$$\underline{H}(\underline{r},\underline{r}')\Big|_{\rho=\rho'=a} \sim -j\frac{k^2 Y}{2\pi}\underline{M}\cdot\left[\hat{\theta}'\hat{\theta}\left(1-\frac{j}{kD}\right)+\hat{t}'\hat{t}\,\frac{2j}{kD}\right] v_0(x_s)\,\frac{e^{-jkD}}{kD}$$

$$-\underline{M}\cdot\hat{\varphi}'\hat{\varphi}\,\frac{k^2 Y}{2\pi}\,w(x_s)\,\frac{e^{-jkD}}{(kD)^2} \,, \tag{123}$$

where $\underline{M}$ denotes an arbitrarily oriented magnetic point source. Note, this formula is identical with the planar formula (D8), save for the curvature terms $v_0(x_s)$ and $w(x_s)$.

The analysis of the circular cylinder problem was carried out in terms of the φ and z coordinates which simultaneously constitute the directions of principal curvature of the surface. In its generalization to a conical surface $\varphi \to \varphi$ and $z \to r$, φ and r again being the principal curvature directions on a cone (see Chapter IV).

For a more general surface of revolution, the tangential $\underline{M}$ will have to be decomposed prior to further treatment into components along the two principal directions.

6. Summary of Formulae

a. Strictly Asymptotic Expressions to Lowest Order in $\frac{1}{ka}$ and to Second Order in $\frac{1}{kD}$:

A. Circumferential Magnetic Current Element

$$H_\varphi^c(\underline{r},\underline{r}')\Big|_{\rho=\rho'=a} \sim -j\,M_\varphi \frac{k^2 Y}{2\pi}\sin^2\theta\, v_0(x_s)\frac{e^{-jkD}}{kD}$$

$$+ M_\varphi \frac{k^2 Y}{2\pi}\left(\cos^2\theta - \frac{61}{24}\sin^2\theta - \frac{1}{9}\frac{\sin^2\theta}{\cos^2\theta}\right) v_0(x_s)\frac{e^{-jkD}}{(kD)^2}$$

$$+ M_\varphi \frac{k^2 Y}{2\pi}\frac{1}{\cos^2\theta}\, u_0(x_s)\frac{e^{-jkD}}{(kD)^2} \qquad (124)$$

$$H_z^c(\underline{r},\underline{r}')\Big|_{\rho=\rho'=a} \sim j\,M_\varphi \frac{k^2 Y}{2\pi}\sin\theta\cos\theta\, v_0(x_s)\frac{e^{-jkD}}{kD}$$

$$- M_\varphi \frac{k^2 Y}{2\pi}\left(-\frac{23}{8}\sin\theta\cos\theta + \frac{5}{9}\frac{\sin^3\theta}{\cos\theta}\right) v_0(x_s)\frac{e^{-jkD}}{(kD)^2} \qquad (125)$$

B. Axial Magnetic Current Element

$$H_z^a(\underline{r},\underline{r}')\Big|_{\rho=\rho'=a} \sim -j\,M_z \frac{k^2 Y}{2\pi}\cos^2\theta\, v_0(x_s)\frac{e^{-jkD}}{kD}$$

$$+ M_z \frac{k^2 Y}{2\pi}\left(\frac{20}{9}\sin^2\theta - \frac{29}{24}\cos^2\theta\right) v_0(x_s)\frac{e^{-jkD}}{(kD)^2} \qquad (126)$$

$$H_\varphi^a(\underline{r},\underline{r}')\Big|_{\rho=\rho'=a} \sim j\,M_z \frac{k^2 Y}{2\pi}\sin\theta\cos\theta\, v_0(x_s)\frac{e^{-jkD}}{kD}$$

$$- M_z \frac{k^2 Y}{2\pi}\left(-\frac{23}{4}\sin\theta\cos\theta + \frac{5}{9}\frac{\sin^3\theta}{\cos\theta}\right) v_0(x_s)\frac{e^{-jkD}}{(kD)^2} \qquad (127)$$

Validity of these formulae is restricted to θ not too close to $\pi/2$.

b. The Modified Planar Formula

This formula is not strictly asymptotic. It applies to an arbitrary $\underline{M}$, and is written in a vector form.

$$\underline{H}(\underline{r},\underline{r}')\Big|_{\rho=\rho'=a} \sim -j\frac{k^2Y}{2\pi}\underline{M}\cdot\left[\hat{\theta}'\hat{\theta}\left(1-\frac{j}{kD}\right)+\hat{t}'\hat{t}\,\frac{2j}{kD}\right]v_0(x_s)\,\frac{e^{-jkD}}{kD}$$

$$-\underline{M}\cdot\hat{\varphi}'\hat{\varphi}\,\frac{k^2Y}{2\pi}\,w(x_s)\,\frac{e^{-jkD}}{(kD)^2} \qquad (128)$$

where

$$w(x_s) = v_0(x_s) + \frac{\sin^2\theta\, v_1(x_s) - u_o(x_s)}{\cos^2\theta} \qquad (129)$$

c. The "Full Formula"

The expression for H_φ excited by a circumferential magnetic current element derived in (101) or obtainable from (128) - (129) is termed here the "Full Formula."

$$H_\varphi^c(\underline{r},\underline{r}')\Big|_{\rho=\rho} \sim -j\,M_\varphi\frac{k^2Y}{2\pi}\left(\sin^2\theta-\sin^2\theta\,\frac{j}{kD}+\cos^2\theta\,\frac{2j}{kD}\right)v_0(x_s)\,\frac{e^{-jkD}}{kD}$$

$$-M_\varphi\frac{k^2Y}{2\pi}\,w(x_s)\,\frac{e^{-jkD}}{(kD)^2}\quad, \qquad (130)$$

where $w(x_s)$ is shown in (129).

d. The Variant of the "Full Formula"

$$H_\varphi^c(\underline{r},\underline{r}')\Big|_{\rho=\rho} \sim -j\,M_\varphi\frac{k^2Y}{2\pi}\left(\sin^2\theta-\sin^2\theta\,\frac{2j}{kD}+\cos^2\theta\,\frac{j}{kD}\right)v_0(x_s)\,\frac{e^{-jkD}}{kD}$$

$$+M_\varphi\frac{k^2Y}{2\pi}\frac{1}{\cos^2\theta}\,u_o(x_s)\,\frac{e^{-jkD}}{(kD)^2}, \qquad \text{for } x_s > 0.6$$

$$\sim -j\,M_\varphi\frac{k^2Y}{2\pi}\left(\sin^2\theta-\sin^2\theta\,\frac{2j}{kD}+\cos^2\theta\,\frac{j}{kD}\right)v_0(x_s)\,\frac{e^{-jkD}}{kD}, \qquad \text{for } x_s < 0.6 \qquad (132)$$

where $x_s = \frac{kD}{2f_g^2}$, $f_g = \left(\frac{k\rho_g}{2}\right)^{1/3}$ and $\rho_g = \frac{a}{\cos^2\theta}$ (see 62 and 63).

The curvature terms $v_o(x_s)$, $v_1(x_s)$ and $u_0(x_s)$ are listed in (35-43).

III. Numerical Results

This chapter is devoted to numerical tests of validity of surface ray methods for mutual coupling in conformal arrays. Specifically, these methods are applied to mutual coupling between slots on conducting circular cylindrical surfaces. Once the limits of validity of the surface ray techniques have been established, the asymptotic results of the cylindrical problem can easily be extended in a GTD manner to conical surfaces. This is described in Chapter IV.

A literature search has disclosed the availability of numerical and experimental results for mutual admittance between "single mode" rectangular slots in a conducting circular cylinder [5], [9]. These were obtained via harmonic series in Φ and a numerically evaluated Fourier integral with respect to the axial wave-number spectrum. To enforce convergence, a small loss was assumed in the surrounding medium. The authors were helpful in supplying us with some of their numerical data in a computer print-out form. They also made available their computer program to Drs. Kummer and Villeneuve of Hughes Aircraft Co., Culver City, California, who in turn furnished us with additional numerical harmonic series results.

The surface ray computations of mutual admittances between "single mode" rectangular slots in an infinite conducting circular cylinder were carried out by numerical integration of the mutual admittance integral

$$Y_{12} = \frac{\iint_{\text{Aperture 2}} \underline{E}_2 \times \underline{H}_{21} \cdot \hat{n}_2 \, dS}{V_1 V_2} \tag{1}$$

where $\underline{E}_2 = V_2 \underline{e}_2$, $\underline{E}_1 = V_1 \underline{e}_1$, denote the tangential fields in aperture (2) and (1) respectively, $\underline{e}_1$ and $\underline{e}_2$ representing the respective TE_{10} mode functions,

normalized so that

$$\iint_{\text{Aperture 2}} |\underline{e}_2|^2 \, dS = \iint_{\text{Aperture 1}} |e_1|^2 \, dS = 1 \ , \tag{2}$$

and $\underline{H}_{21}$ is the surface magnetic field intensity due to aperture 1 on the unperforated surface in the location of aperture 2. The surface magnetic current density is

$$\underline{M} = \underline{E} \times \hat{n} \, dS \tag{3}$$

where $\hat{n}$ is the local outward unit normal of the cylindrical surface and dS denotes an infinitesimal area in the slot. In the case of circumferential slots, it follows from (1) and (3) that only H_φ needs to be considered, while for axial slots only H_z is required.

To compare to Stewart-Golden's data, the slot dimensions were chosen those of a standard X-band 0.9" x 0.4" waveguide.

a. Circumferential Slots

Two formulae for H_φ were used in obtaining the numerical values for Y_{12}, the "Full Formula" (II-101) and its variant, (II-107, 108) as described in Section 5 of Chapter II.

In the following, Z_o and Φ_o denote the axial and the angular center-to-center separation of two circumferential slots (see Fig. III-1.

For further comparison, curves based on Hwang and Kouyoumjians GTD formulation [10]are also included. These formulae consist solely of the dominant hard and soft terms of (II-123). For a circumferential

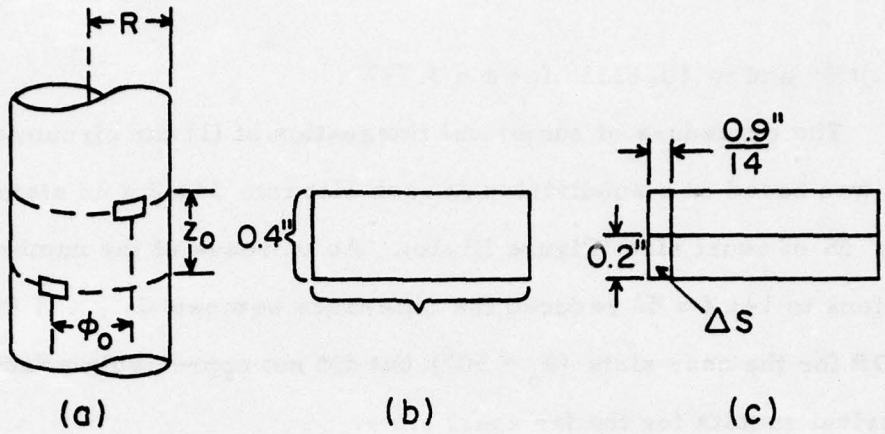

Figure III-1. (a) Two Circumferential Slots on a Cylinder of Radius a ≡ R,
(b) Slot Geometry,
(c) Partitioning of Slots for Numerical Integration.

magnetic current element, in our notation, these formulae are

$$H^c_{\varphi}(\underline{r},\underline{r}')\Big|_{\rho=\rho'=a} \sim -\,j M_{\varphi} \frac{k^2 Y}{2\pi} \sin^2\theta\, v_0(x_s) \frac{e^{-jkD}}{kD}$$

$$+ M_{\varphi} \frac{k^2 Y}{2\pi} \frac{1}{\cos^2\theta}\, u_0(x_s) \frac{e^{-jkD}}{(kD)^2} \qquad (4)$$

and for an axial magnetic current element,

$$H^a_z(\underline{r},\underline{r}')\Big|_{\rho=\rho'=a} \sim -\,j M_z \frac{k^2 Y}{2\pi} \cos^2\theta\, v_0(x_s) \frac{e^{-jkD}}{kD} \quad . \qquad (5)$$

We shall consider the mutual admittance between circumferential 0.9" x 0.4" single mode slots in conducting cylinder with a ≡ R = 1.991" at f = 9 GHz (ka ≈ 9.5) and subsequently with a = 3.777" at f = 0.975 GHz (ka ≈ 19.6). In each case the data are normalized to the magnetic of the self admittance $|Y_{11}|$, where $Y_{11}/Y_g = 0.8588 + j\,0.3834$ for a = 1.991" at 9 GHz and $Y_{11}/Y_g = 0.8440 + j\,0.4040$ at 9.75 GHz, for a = 3.777", Y_g being the TE_{10} modal admittance of the rectangular feed waveguide with 0.9" x 0.4" I.D. The computed points are in 10° steps of angular separation Φ_o for

a = 1.991" and in 10.1333° for a = 3.777".

The procedure of numerical integration of (1) for circumferential slots was based on a subdivision of each slot into 14x2 = 28 elemental areas ΔS of equal size (Figure III-1c). An increase of the number of subdivisions to 14x4 = 56 reduced the difference between S-G and PINY by 0.3 DB for the near slots ($\Phi_o < 50^o$) but did not appreciably affect the numerical results for the far apart slots.

We shall begin with the H-plane coupling ($Z_o = 0$) and increase Z_o in steps. Figure (III-2) shows $|Y_{12}/Y_{11}|$ calculated by the Full Formula (PINY) for $Z_o = 0$, in comparison with the harmonic series data (S-G), and GTD . The PINY curves show good agreement with S-G, but the GTD curve markedly deviates from S-G and shows a different slope. As discussed in Chapter I, the reason for this discrepancy is that the lowest order in $\frac{1}{kD}$ hard contribution vanishes for $\theta=0$ and the behavior of H_φ is dominated not by the soft contribution, but rather by the second order in $\frac{1}{kD}$ hard contribution, the exponential attenuation rate of which is identical with that of the lowest order hard contribution, the attenuation constant of the dominant hard surface ray being $\sim\frac{1}{2}$ that of the dominant soft surface ray for the same geodesic. Figure III-3 shows the effect of neglecting the $v_1(x)$ term in (II-101) and in addition discarding the soft contribution $u_0(x)$ for $x < 0.3$ (actually $x = 0.6$ would be more appropriate). In the H-plane the $v_1(x)$ term has a negligible effect, because its pattern $\frac{\sin^2\theta}{\cos^2\theta}$ has a null for $\theta=0$.

Table I gives the phase comparison. It is seen that the "Full Formula" (F.F.) yields, except for $\Phi_o = 110^o$, a maximum phase difference of $\approx 13^o$ from S-G.

Figure III-4 shows $\left|\frac{Y_{12}}{Y_{11}}\right|$ for the case of $Z_o = 0.5''$. The departure of the F.F. from the S-G result increases and the departure of GTD decreases. Table II summarizes the phase comparison and it is seen that the correlation of the F.F. to S-G is very good, next comes the variant formula and finally GTD.

Figure III-5 shows the $Z_o = 1''$ case. The F.F. curve is now above S-G and so is the variant formula which shows now a better amplitude correlation than F.F. with the harmonic series result. The phase comparison is shown in Table III. Again best phase correlation is obtained via F.F.

Figure III-6 and III-7 and Table IV present the case of $Z_o = 2''$. The F.F. is about 2 DB higher than S-G, while GTD correlates better for $\Phi_o \geq 30^o$, but tends to diverge for small Φ_o values. On the other hand the variant formula result, to the accuracy of the graph, is indistinguishable from S-G except towards the E-plane where it falls below S-G by about 1 DB. Similar comments apply to the case $Z_o = 3''$, represented Figure III-8 and III-9 and Table V. It is seen that in Figure III-8 the difference between the F.F. and the harmonic series result is ~2 DB. On the other hand the variant formula and GTD track S-G quite well.

Figures III-10 and III-11 and Table VI summarize the comparison for the case of $Z = 4''$. There is about 1.7 DB difference in the E-plane for either F.F. or the variant formula. The F.F. phases track very well, next best is the variant formula.

Figure III-12 and Table VII present the results for $Z = 8''$. The maximum deviation of the F.F. result from that of harmonic series is about 3 DB. However, it is to be noted that in view of the assumed loss, i.e. $\varepsilon = \varepsilon_o(1 - j\,0.0025)$ the actual discrepancy should be reduced to no more than 2 DB.

As a general comment, the GTD formulae show good agreement in amplitude with the harmonic series for $Z_o > 2''$ and $\Phi_o > 30^o$. The variant formula matches very well to S-G in amplitude over the entire range of Z_o including the H-plane, but falls below the harmonic series result in the E-plane. Also the phase of the variant formula tracks better that of S-G than the GTD result. The phase of the F.F. tracks best of all. The discrepancy in $\left|\frac{Y_{12}}{Y_{11}}\right|$ is increasing with Z_o, but seems to level off for large values of Z_o, in view of the loss assumed in S-G program.

Figures III-13 to III-17 and Tables VIII to XII show the amplitude and phase of $\frac{Y_{12}}{Y_{11}}$ for a = 3.777", f = 9.75 GHz and 0.9" x 0.4" apertures for different axial slot separations Z_o. In this case, the harmonic series computer program employed a loss tangent of 0.003. As expected, for this increased value of $ka \approx 19.6$, the correlation between the harmonic series and the asymptotic surface ray results is improved in amplitude.

b. Axial Slots

Since the expressions (II-90) are finite as $\theta \to \frac{\pi}{2}$, they may be adequate for the description of the field in the neighborhood of a slot uniformly in all directions and thus, suitable for the determination of the mutual admittance. One observes that for axial slots only the hard polarization is excited, so that the soft transition function $u_o(x)$ does not appear in (II-90).

Samples of numerical results, obtained via harmonic series, for mutual coupling between single mode axial slots on a circular cylinder can be found in [9]. These data are in the form of isolation $20 \log_{10} |S_{12}|$ between two open-ended rectangular waveguides feeding the slot apertures, where S_{12} is the scattering (coupling coefficient between the waveguides).

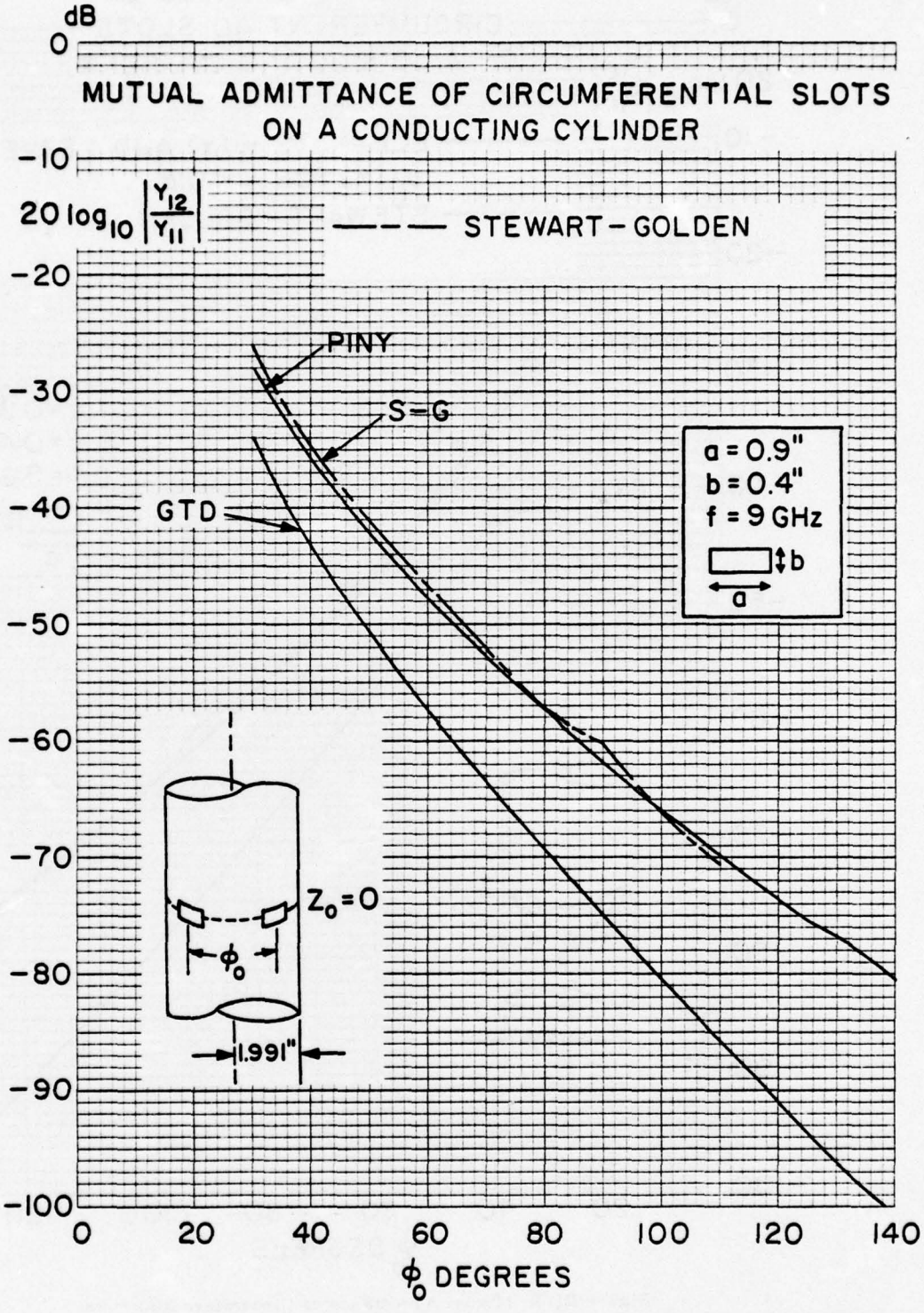

Figure III-2. Mutual Admittance of Circumferential Slots on a Conducting Cylinder, a = 1.991", $Z_0 = 0$

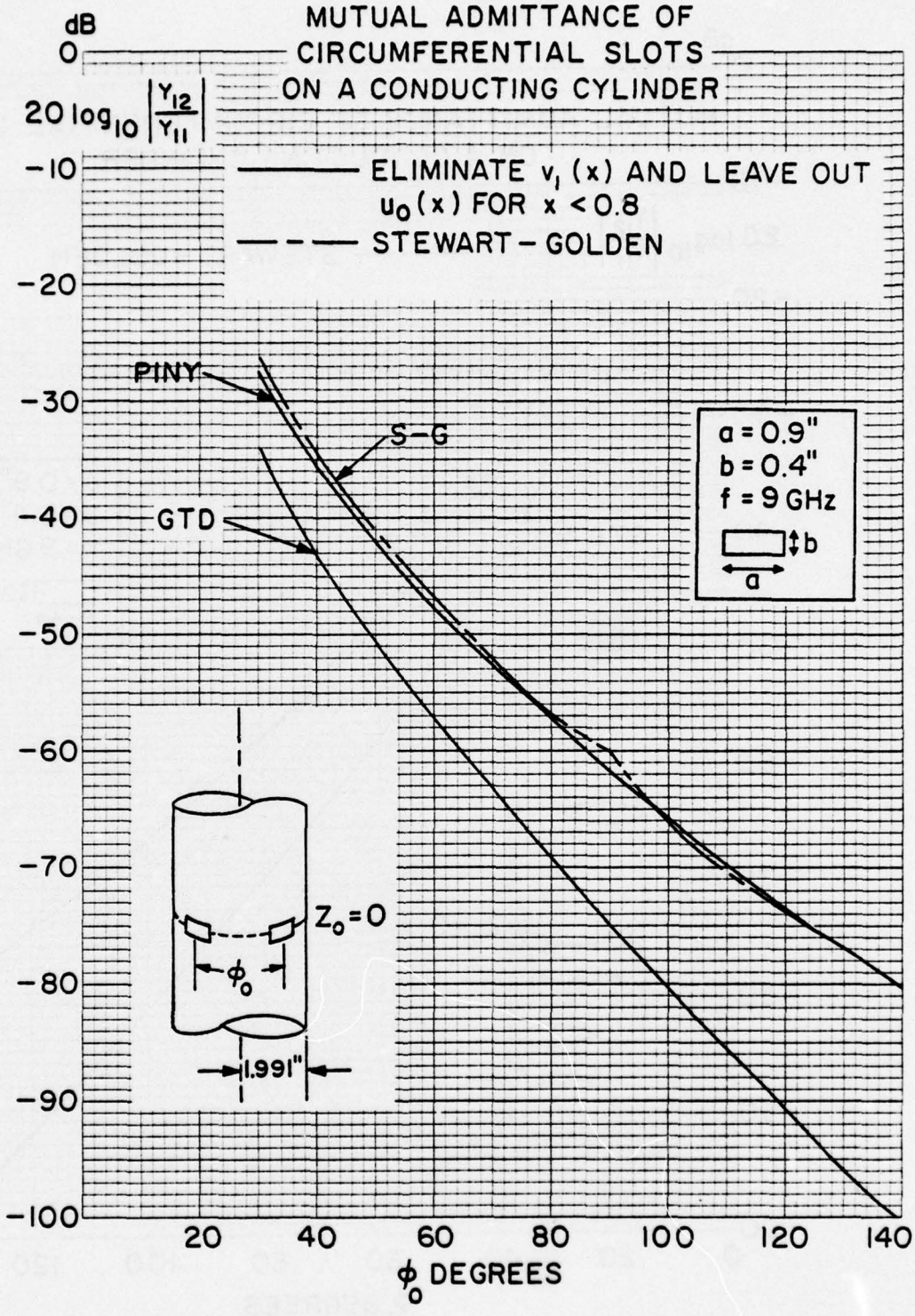

Figure III-3. Mutual Admittance of Circumferential Slots on a Conducting Cylinder, a = 1.991", $Z_0 = 0$

TABLE I Phase Comparison, Arg. Y_{12}

Z_o=0, R=1.991", f=9 GHz

ϕ_o	No. V_1 DEGREES	Full Formula DEGREES	GTD DEGREES	S-G DEGREES
	-	-	-	-
0	-	-	-	-
10	-	-	-	-
20	-	-	-	-
30	-60.23	-62.77	-56.01	-76.85
40	176.68	179.36	178.02	167.74
50	71.18	69.28	60.54	58.18
60	-38.10	-39.66	-54.93	-48.51
70	-145.75	-147.10	-169.76	-154.31
80	107.89	106.63	75.63	93.19
90	2.34	1.29	-38.86	-8.28
100	-102.09	-103.25	-153.17	-99.86
110	153.70	152.82	92.71	121.91

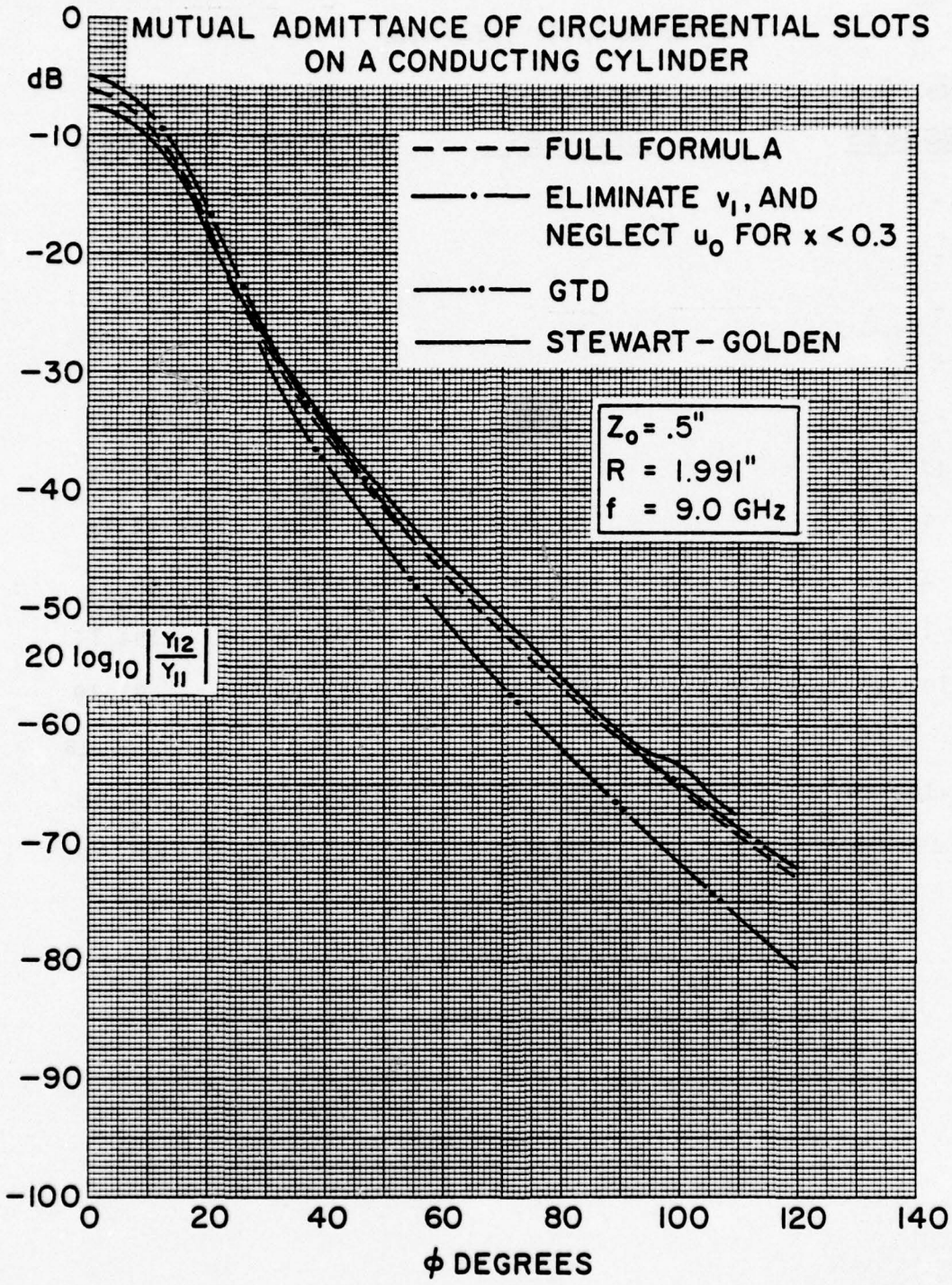

Figure III-4. Mutual Admittance of Circumferential Slots on a Conducting Cylinder $a = 1.991"$, $Z_0 = 0.5$

TABLE II

Phase Comparison Arg. Y_{12}

$Z_o = .5''$, $R = 1.991''$, $f = 9$ GHz

θ^o	No V_1 DEGREES	Full Formula DEGREES	GTD DEGREES	S-G DEGREES
0	-81.84	-70.85		-72.38
10	-85.57	-77.63		-77.88
20	-99.46	-107.29		-105.71
30	-151.36	-172.00	-144.44	-172.93
40	-117.03	103.28	108.76	103.17
50	19.18	8.77	2.51	7.45
60	-81.43	-90.17	-104.95	-92.63
70	176.65	168.89	146.80	168.20
80	74.26	67.15	38.17	67.67
90	-28.18	-34.79	-70.49	-41.51
100	-130.46	-136.65	-178.93	-142.26
110	127.49	121/69	73.03	131/22

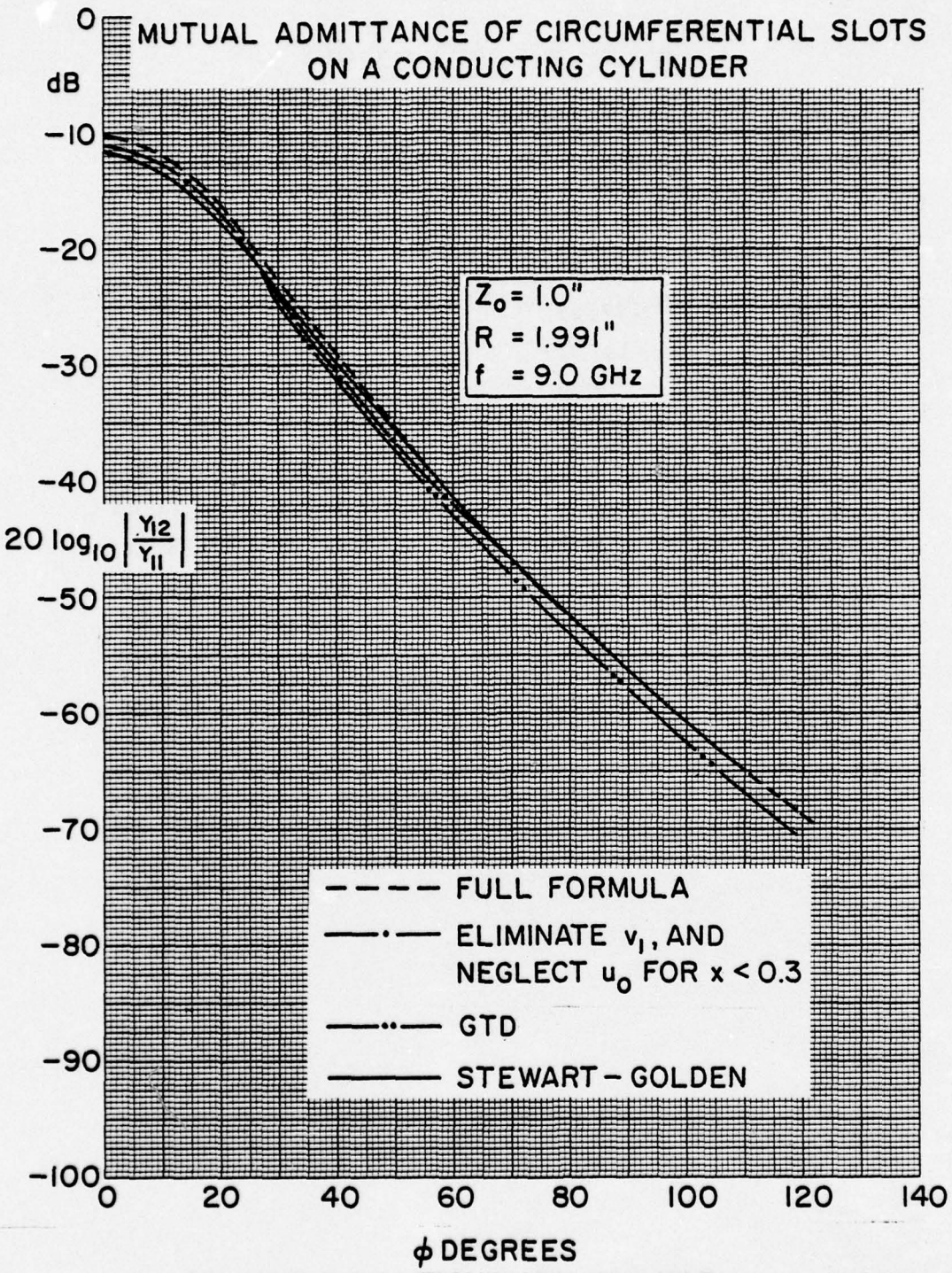

Figure III-5. Mutual Admittance of Circumferential Slots on a Conducting Cylinder a = 1.991", Z_o = 1"

TABLE III Phase Comparison, Arg. Y_{12}

$Z_o = 1''$, $R = 1.991''$, $f = 9$ GHz

ϕ^o	No V_1 DEGREES	Full Formula DEGREES	GTD DEGREES	S-G DEGREES
0	152.62	152.99	-	154.67
10	151.24	142.84	-	144.69
20	134.53	111.19	-	113.51
30	86.51	57.95	101.53	61.20
40	9.01	-12.30	13.62	-7.90
50	-75.81	-93.86	-77.03	-88.37
60	-165.88	177.49	-172.19	-176.18
70	100.36	84.48	89.47	91.39
80	4.22	-11.27	-10.91	-3.58
90	-93.40	-108.69	-112.58	-100.29
100	168.07	152.88	144.99	161.02
110	69.00	53.87	42.12	61.96

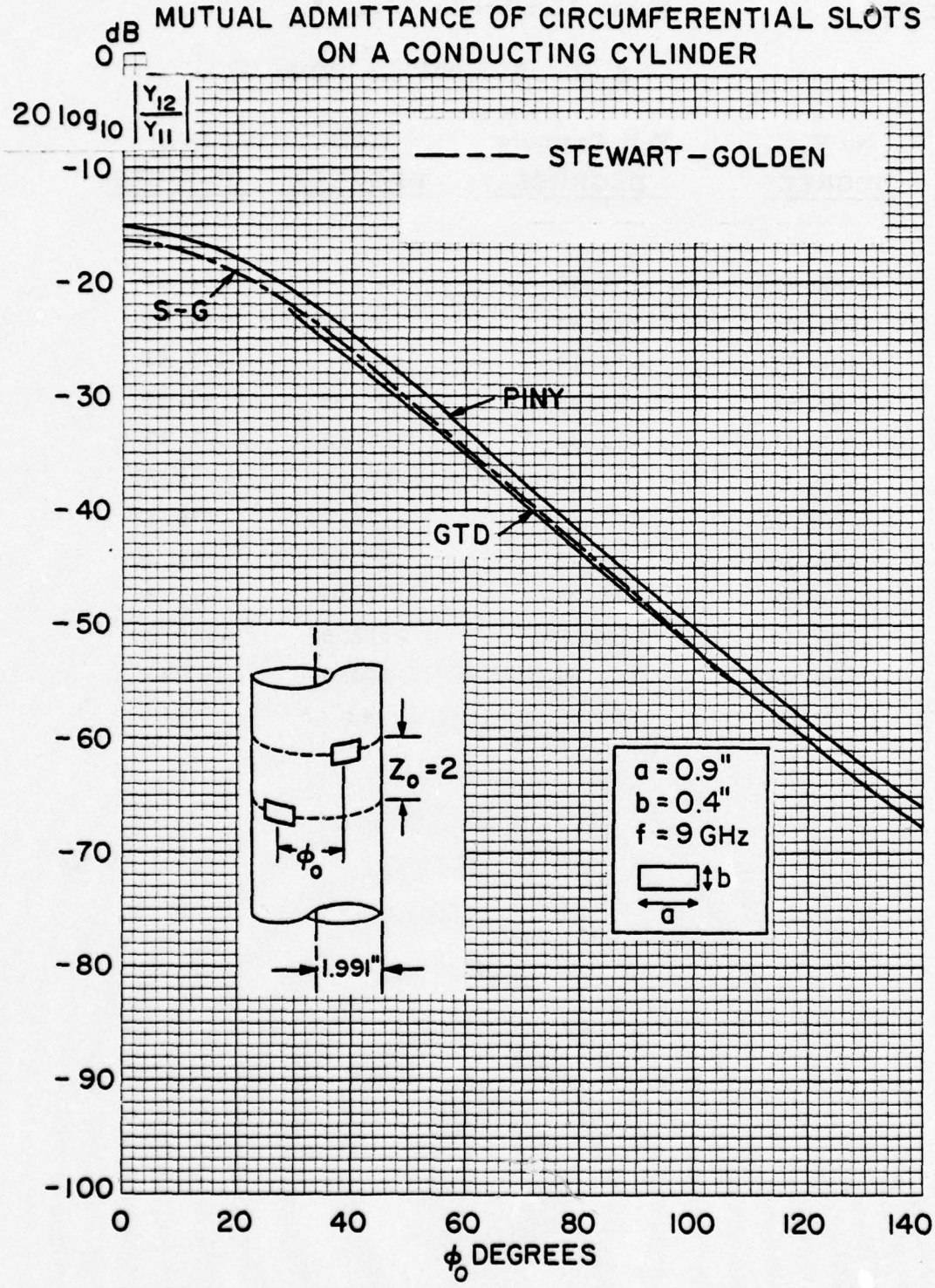

Figure III-6. Mutual Admittance of Circumferential Slots on a Conducting Cylinder, a = 1.991", Z_o = 2"

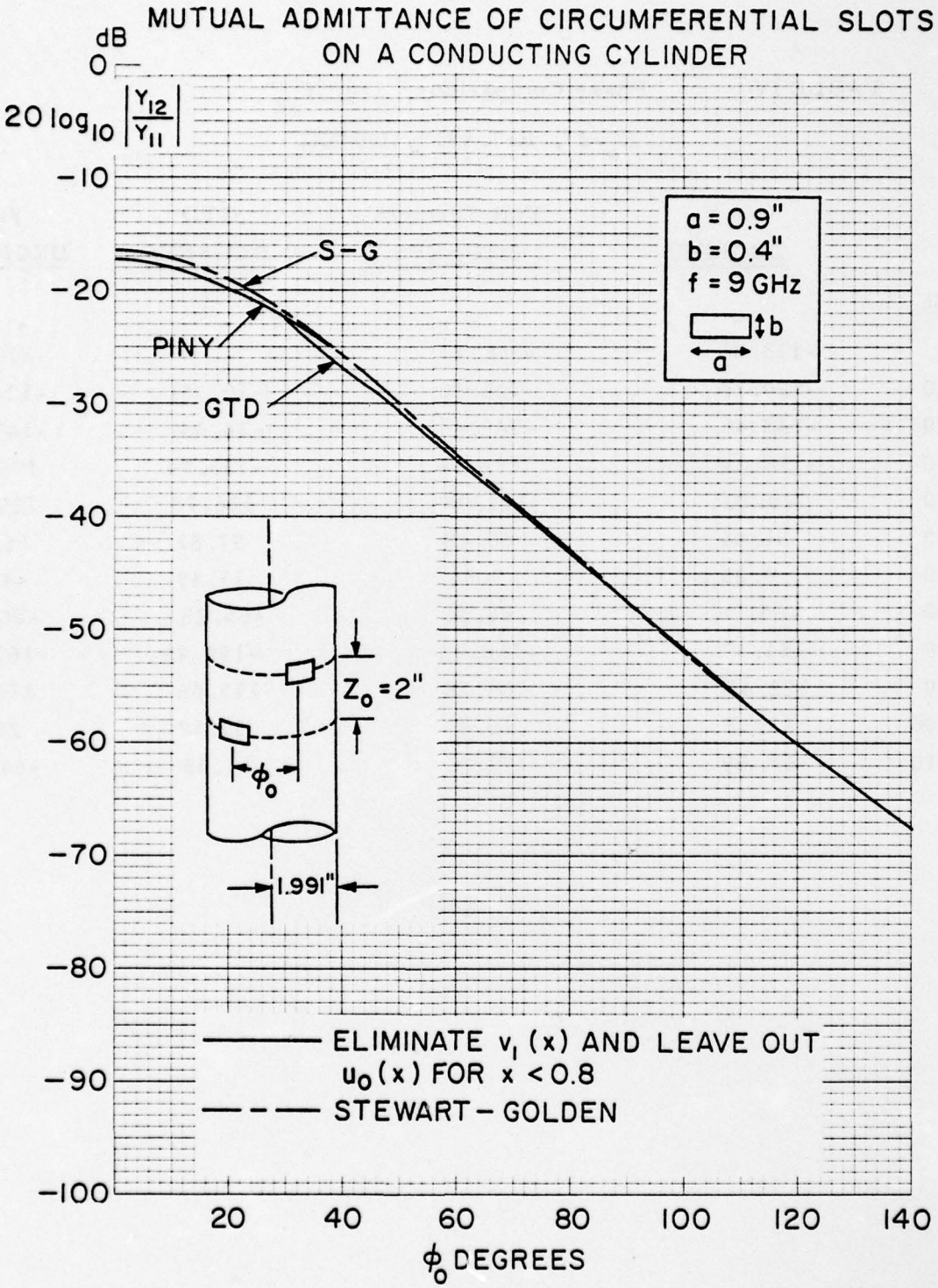

Figure III-7. Mutual Admittance of Circumferential Slots on a Conducting Cylinder, a = 1.991", Z_o = 2"

TABLE IV Phase Comparison, Arg. Y_{12}

Z_o=2", R=1.991", f=9 GHz

θ_o	No V_1 DEGREES	Full Formula DEGREES	GTD DEGREES	S-G DEGREES
	-	-	-	-
0	-113.06	-118.21	-	-117.01
10	-120.75	-126.10	(-10.33)	-124.73
20	-143.46	-149.45	(-14.44)	-147.59
30	-178.14	172.64	-133.74	175.34
40	140.10	121.90	156.78	125.66
50	81.44	60.48	87.81	65.19
60	9.25	-9.56	13.48	-4.26
70	-68.76	-86.36	-66.25	-80.58
80	-151.37	-168.32	-150.49	-161.05
90	122.46	105.78	115.55	115.55
100	33.33	16.87	31.12	26.12
110	-57.59	-73.26	-61.35	-69.08

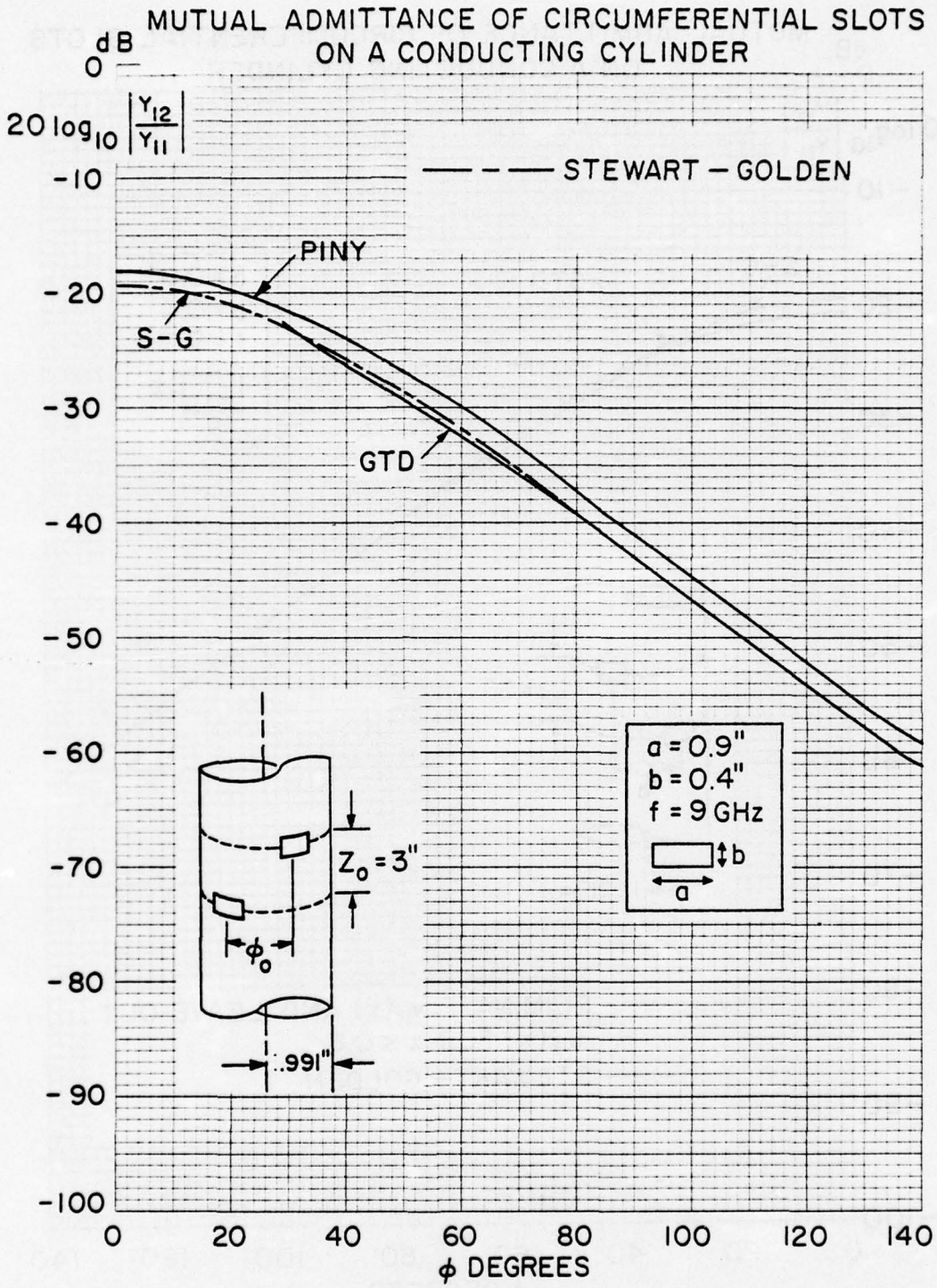

Figure III-8. Mutual Admittance of Circumferential Slots on a Conducting Cylinder, a = 1.991", Z_o = 3"

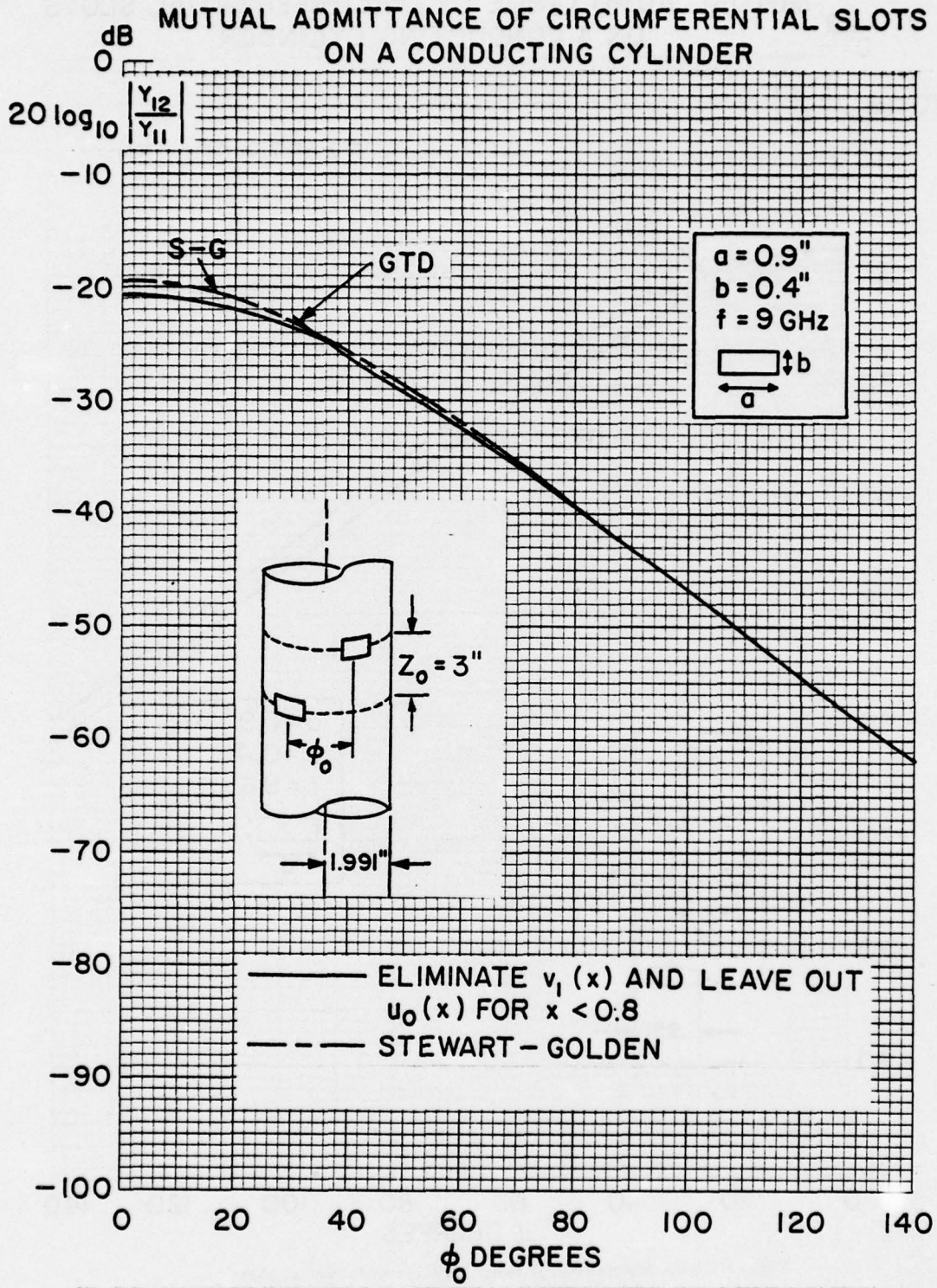

Figure III-9. Mutual Admittance of Circumferential Slots on a Conducting Cylinder, a = 1.991", Z_o = 3"

TABLE V Phase Comparison, Arg. Y_{12}

$Z_o = 3''$, $R = 1.991''$, $f = 9$ GHz

ϕ^o	No V_1 DEGREES	Full Formula DEGREES	GTD DEGREES	S-G DEGREES
0	-22.89	-32.33	-	-30.90
10	-28.67	-38.19	(75.84)	-36.72
20	-45.76	-55.67	(72.46)	-54.11
30	-71.91	-84.27	-22.20	-82.33
40	-103.96	-123.14	-83.23	-120.52
50	-147.55	-171.15	-140.36	-167.78
60	153.96	132.82	+158.90	137.00
70	88.94	69.90	93.13	74.88
80	19.01	1.15	22.42	6.78
90	-55.24	-72.46	-52.59	-66.24
100	-133.40	-150.12	-131.53	-143.17
110	145.59	129.69	146.75	137.29

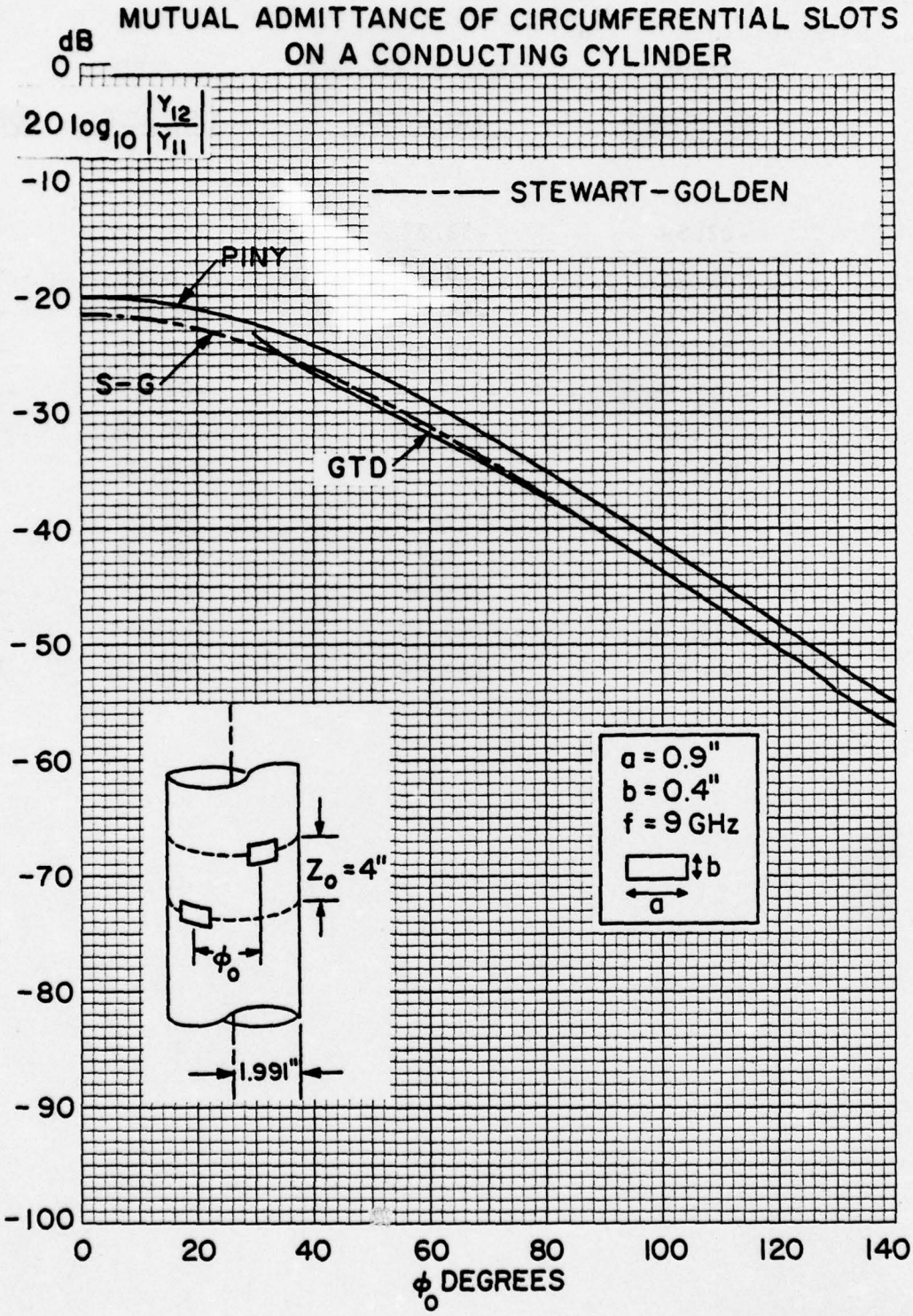

Figure III-10. Mutual Admittance of Circumferential Slots on a Conducting Cylinder, a = 1.991", Z_o = 4"

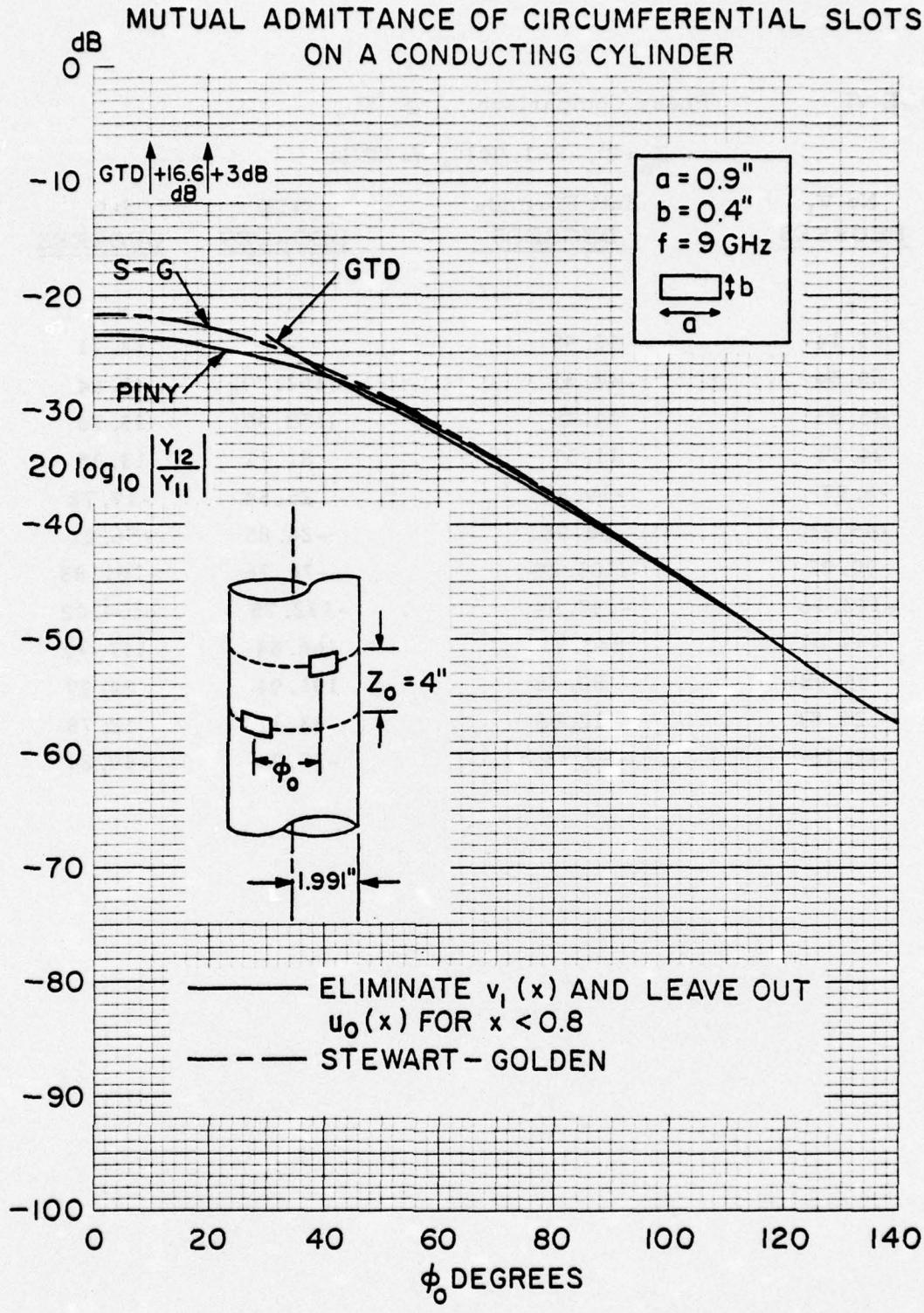

Figure III-11. Mutual Admittance of Circumferential Slots on a Conducting Cylinder, a = 1.991", Z_0 = 4"

TABLE VI Phase Comparison, Arg. Y_{12}

Z_o=4", R=1.991", f=9GHz

θ^o	No V_1 DEGREES	Full Formula DEGREES	GTD DEGREES	S-G DEGREES
	-	-	-	-
0	65.14	52.98	-	54.11
10	60.54	48.33	(161.79)	49.54
20	46.83	34.45	(158.99)	35.73
30	24.31	11.57	81.11	13.08
40	-6.57	-19.81	25.54	-17.72
50	-45.21	-58.98	-24.85	-56.21
60	-90.97	-105.25	-76.76	-101.83
70	-143.16	-157.94	-132.75	-154.02
80	159.01	143.71	166.84	147.94
90	95.98	80.36	101.94	84.99
100	28.81	12.66	33.31	18.78
110	-42.76	-58.53	-39.34	-50.84

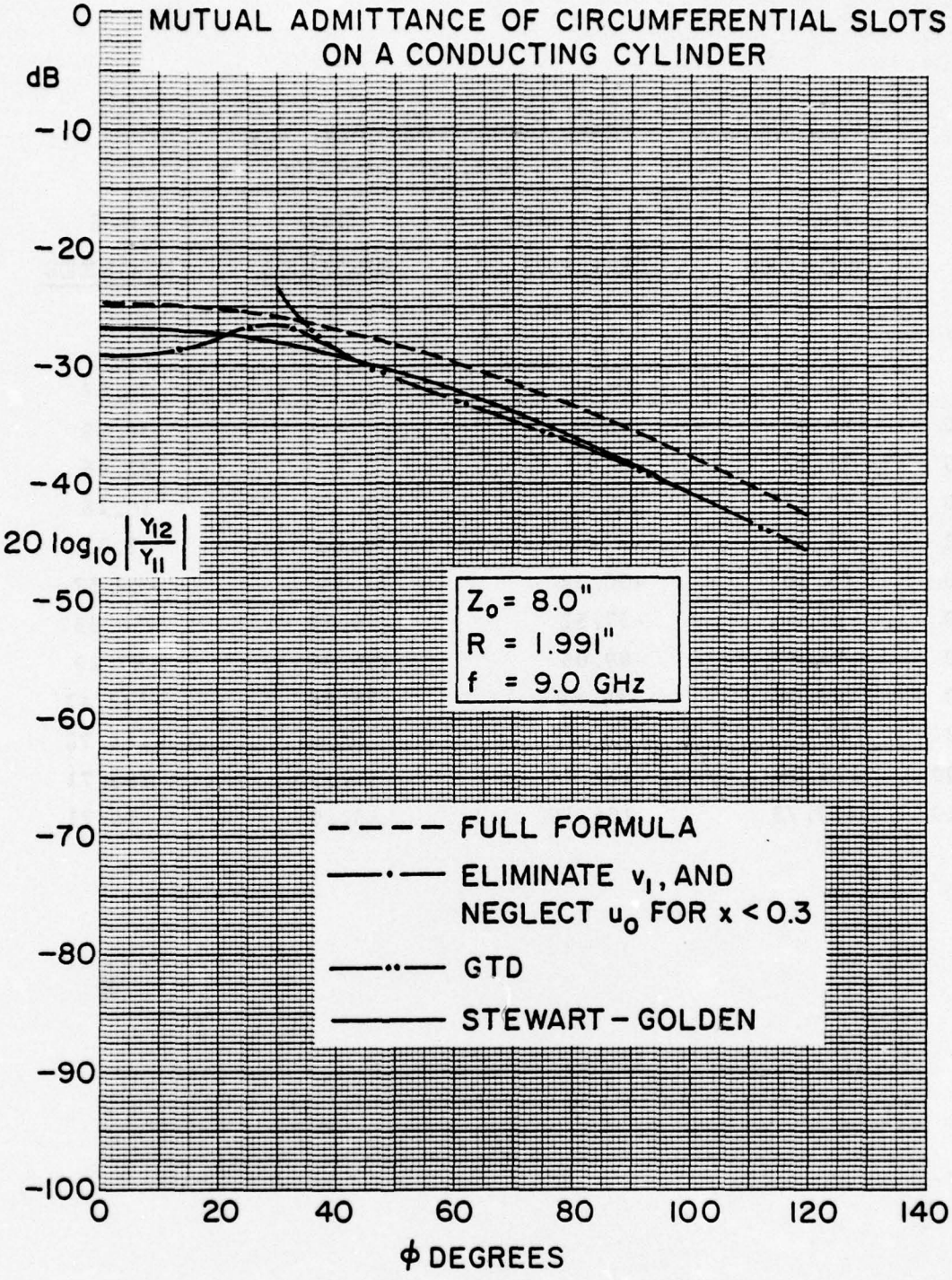

Figure III-12. Mutual Admittance of Circumferential Slots on a Conducting Cylinder a = 1.991", Z_o = 8"

TABLE VII Phase Comparison, Arg. Y_{12}

Z_o=8", R=1.991", f=9GHz

Φ^o	No V_1 DEGREES	Full Formula DEGREES	GTD DEGREES	S-G DEGREES
0	51.61	33.42	-	36.67
10	56.82	30.84	-	30.09
20	71.02	23.10	-	22.65
30	78.17	10.29	98.60	10.18
40	53.09	-7.66	56.43	-7.33
50	15.30	-30.32	17.55	-29.57
60	-21.60	-57.52	-19.13	-56.33
70	-58.87	-89.05	-56.35	-87.29
80	-98.08	-124.69	-95.58	-122.47
90	-139.91	-164.18	-137.45	-161.78
100	175.38	152.71	177.77	155.71
110	127.73	106.19	130.05	70.71

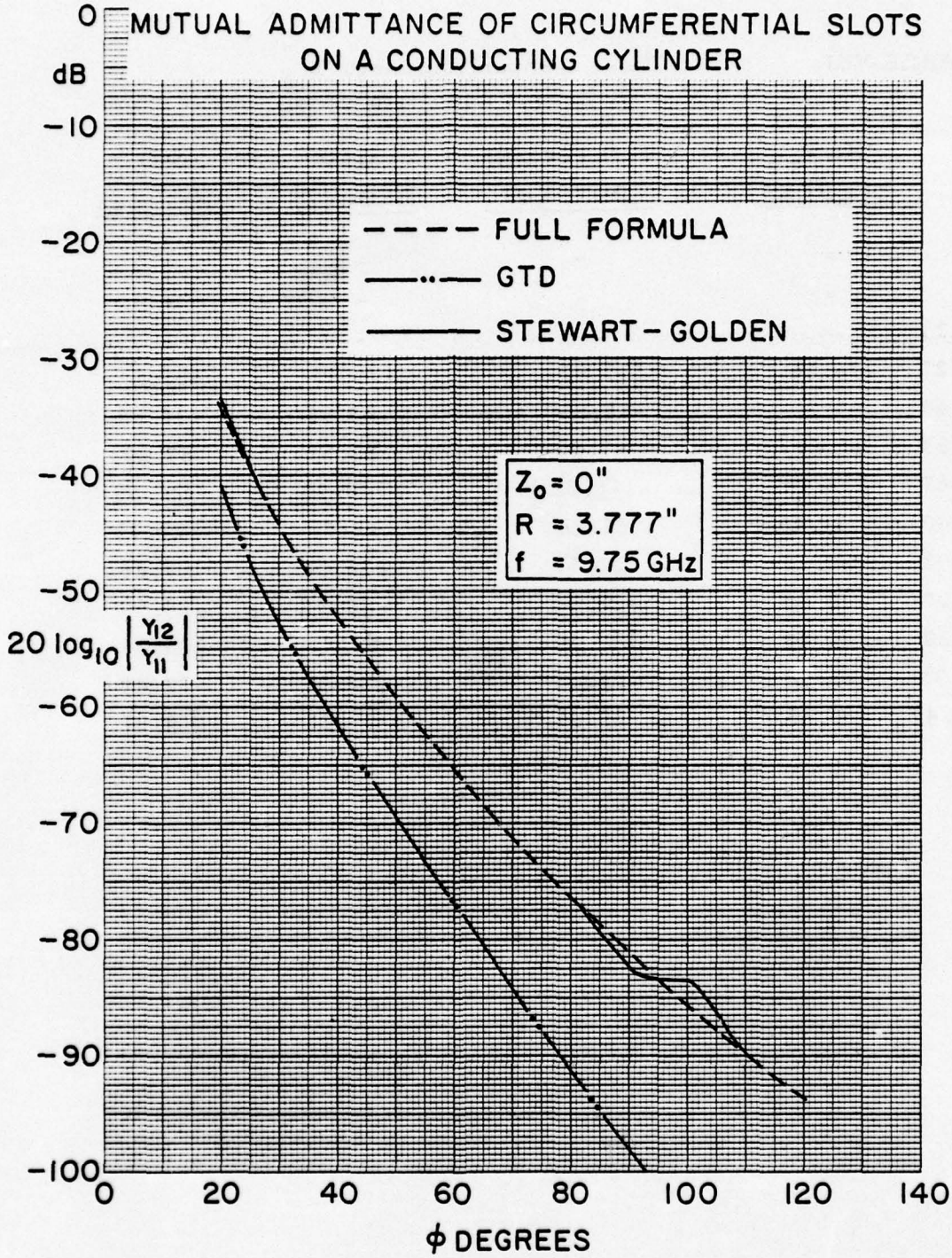

Figure III-13. Mutual Admittance of Circumferential Slots on a Conducting Cylinder a=3.777", Z_o = 0.

TABLE VIII Phase Comparison, Arg. Y_{12}

Z_o=0, R=3.777", f=9,75GHz

φ^o	No V_1 DEGREES	Full Formula DEGREES	GTD DEGREES	S-G DEGREES
0	-	-	-	-
10.13	-	-	-	-
20.27	178.24	177.92	176.11	166.5
30.40	-45.28	-45.63	53.53	-54.65
40.53	97.81	97.55	82.59	89.20
50.67	-116.29	-116.52	-140.40	-124.89
60.80	31.46	31.26	-3.36	27.71
70.93	180.73	180.55	133.64	167.26
81.07	-28.80	-28.96	-89.23	-29.50
91.20	-122.44	122.29	48.11	105.03
101.33	-85.98	-86.11	-173.96	-77.49
111.47	65.68	65.46	-35.23	9.97

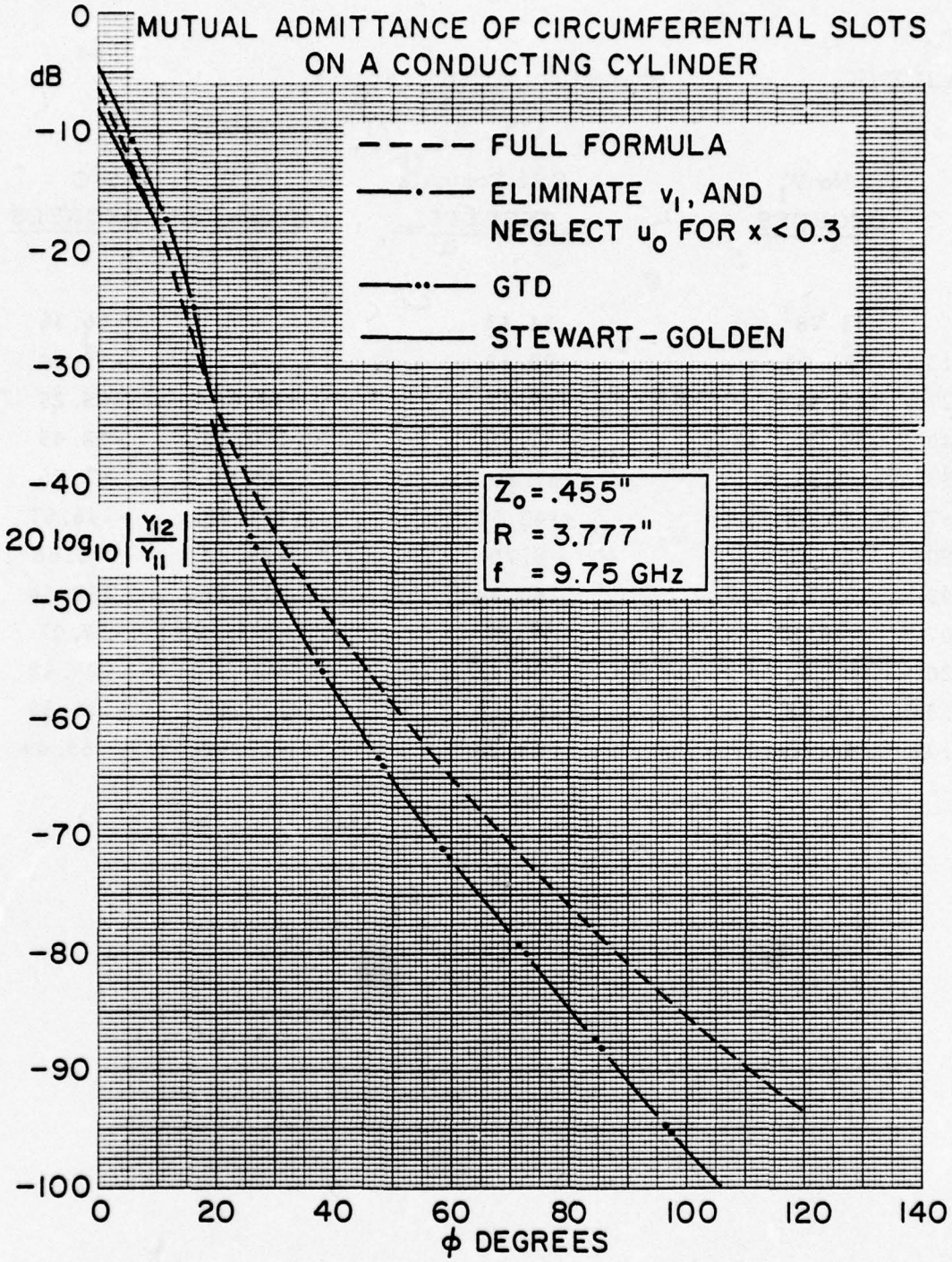

Figure III-14. Mutual Admittance of Circumferential Slots on a Conducting Cylinder a = 3.777", Z_o = 0.455"

TABLE IX Phase Comparison, Arg. Y_{12}

Z_o = .455", R = 3.777", f = 9.75GHz

φ^o	No V_1 DEGREES	Full Formula DEGREES	GTD DEGREES	S-G DEGREES
0	-81.78	-64.43	-	-66.36
10.13	-111.94	-98.63	-	-98.84
20.27	118.33	109.17	112.06	105.25
30.40	-83.20	-87.79	-100.20	-92.43
40.53	69.35	65.99	44.90	61.76
50.67	-139.68	-142.50	-171.76	-146.67
60.80	11.22	8.70	-29.22	3.66
70.93	162.64	160.34	113.27	158.34
81.07	-45.27	-47.37	-103.72	-57.03
91.20	107.33	105.42	40.24	109.48
101.33	-99.88	-101.58	-174.55	-116.88
111.47	52.80	51.28	-27.91	65.49

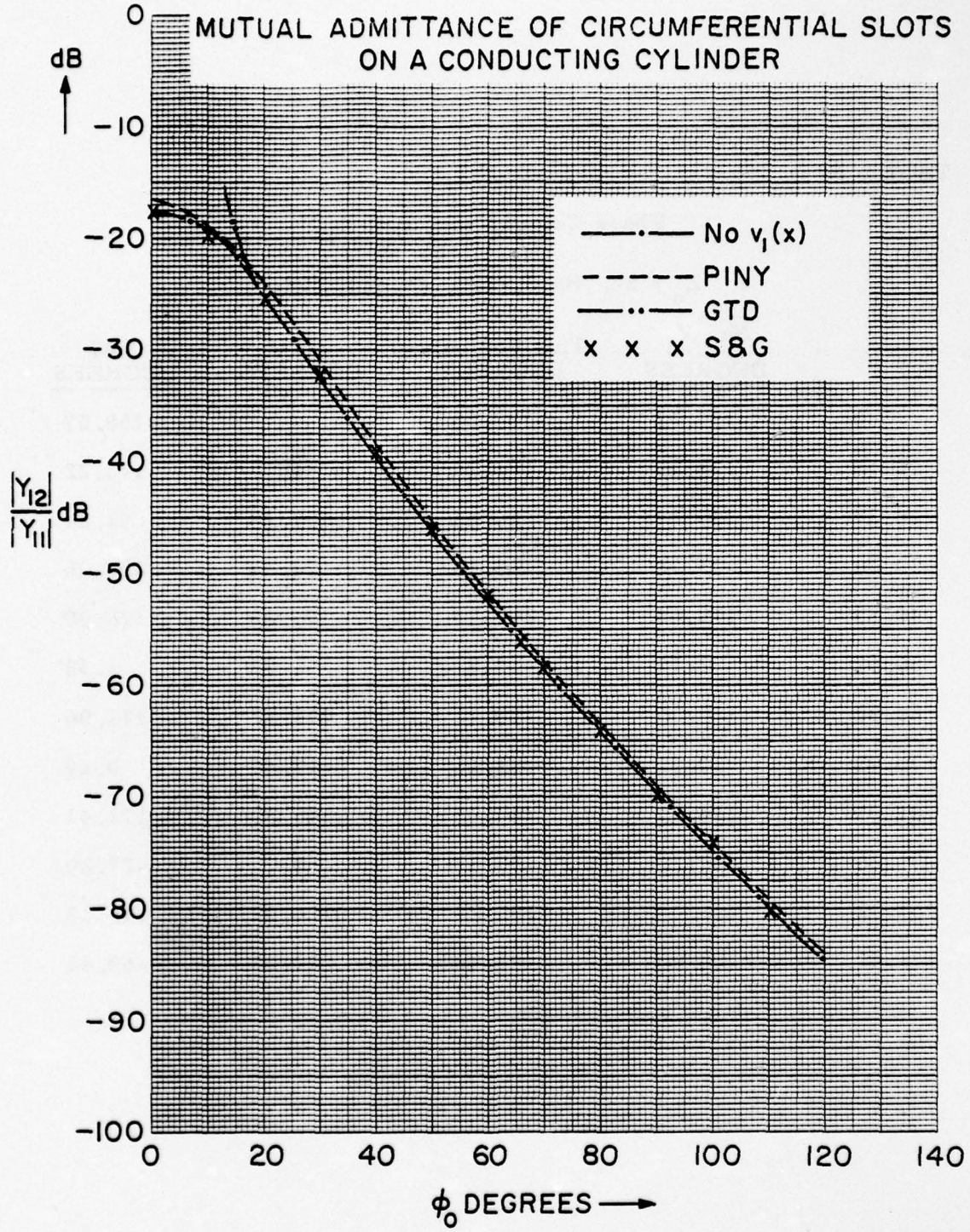

Figure III-15. Mutual Admittance of Circumferential Slots on a Conducting Cylinder a = 3.777", Z_o = 2"

TABLE X

Phase Comparison, Arg Y_{12}

$Z_o = 2''$, $R = 3.777''$, $f = 9.75$ GHz

ϕ^o	No V_1 DEGREES	Full Formula DEGREES	GTD DEGREES	S-G DEGREES
0	-157.72	-159.06	-	-158.07
10.13	178.45	171.24	-	173.22
20.27	109.69	86.80	117.89	91.24
30.40	-25.78	-40.14	-21.49	-32.46
40.53	176.63	164.75	177.88	176.39
50.67	3.11	-7.87	1.87	1.58
60.80	179.35	168.71	175.27	-171.96
70.93	-10.92	-21.46	-17.40	0.29
81.07	154.59	144.02	145.82	171.41
91.20	-42.70	-53.37	-53.70	-27.29
101.33	118.09	107.29	104.92	145.33
111.47	-82.52	-93.46	-97.81	-69.45

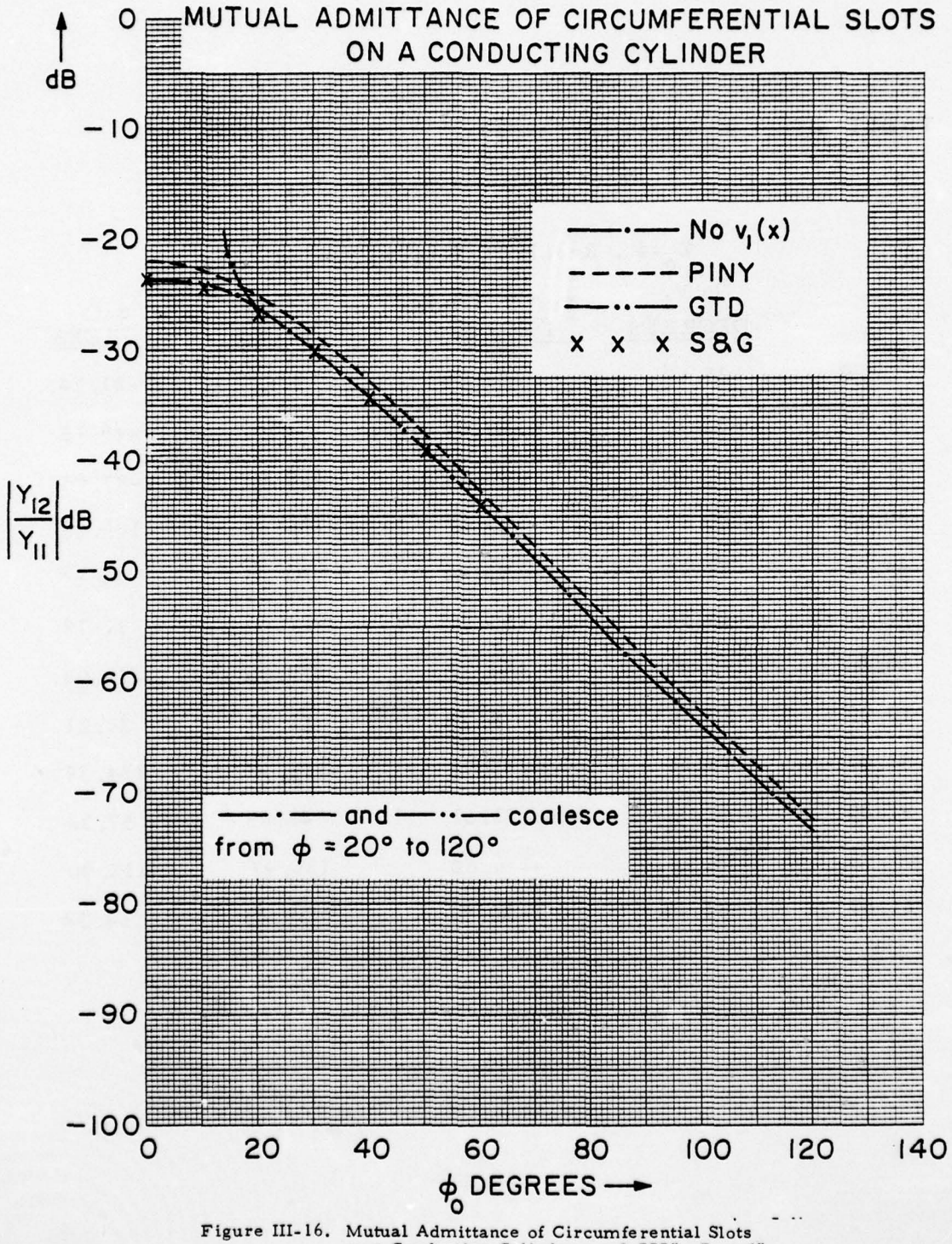

Figure III-16. Mutual Admittance of Circumferential Slots on a Conducting Cylinder a = 3.777", Z_o = 4"

TABLE XI

Phase Comparison, Arg. Y_{12}

Z_o=4", R=3.777", f=9.75 GHz

θ^o	No V_1 DEGREES	Full Formula DEGREES	GTD DEGREES	S-G DEGREES
0	-25.69	-32.26	-	-31.74
10.13	-35.18	-49.52	-	-48.15
20.27	-67.04	-100.03	-58.55	-97.04
30.40	-160.52	-179.47	-156.31	-175.26
40.53	88.30	73.46	91.82	81.67
50.67	-40.36	-53.06	-37.61	-41.78
60.80	175.89	164.21	177.86	179.08
70.93	20.10	8.94	21.29	27.21
81.07	-145.11	-155.98	-144.67	-134.39
91.20	42.35	31.61	42.05	57.36
101.33	-135.96	-146.62	-136.97	-118.90
111.47	41.15	30.51	39.45	64.32

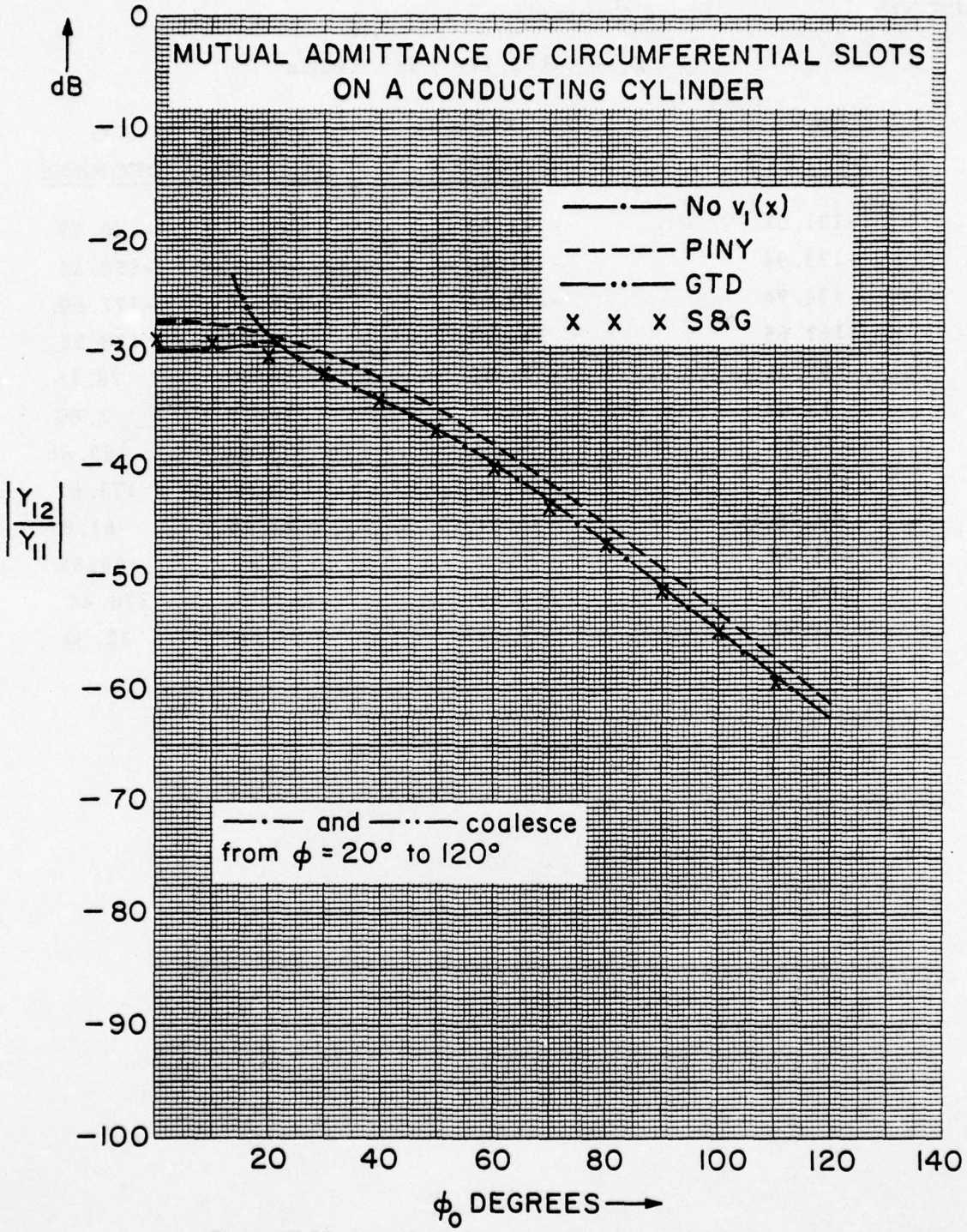

Figure III-17. Mutual Admittance of Circumferential Slots on a Conducting Cylinder a = 3.77", Z_o = 8"

TABLE XII Phase Comparison, Arg. Y_{12}

Z_o=8", R=3.777", f=9.75GHz

ϕ^o	No V_1 DEGREES	Full Formula DEGREES	GTD DEGREES	S-G DEGREES
0	-131.01	-142.09	-	-140.77
10.13	-133.94	-151.40	-	-150.35
20.27	-134.94	-179.04	-119.36	-177.69
30.40	167.65	135.71	169.93	138.36
40.53	95.66	73.59	98.00	78.16
50.67	13.91	-3.74	16.15	2.89
60.80	-79.61	-94.97	-77.51	-85.86
70.93	175.36	161.32	177.30	173.67
81.07	59.72	46.51	61.48	61.87
91.20	-65.48	-78.13	-63.91	-60.59
101.33	160.79	148.54	162.17	170.44
111.47	19.47	7.53	20.66	32.90

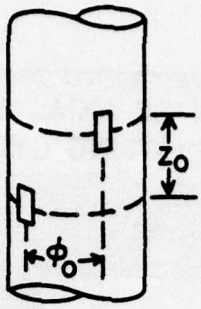

Figure III-18. Axial Slots on a Cylinder

To arrive at a comparison, it was necessary to convert the Y_{12} values obtained via (1) and (3) to S_{12} via

$$S_{12} = \frac{-2\, Y_g\, Y_{12}}{(Y_g + Y_{11} + Y_{12})(Y_g + Y_{11} - Y_{12})} \tag{6}$$

where, again Y_g is the characteristic admittance of the dominant feed-waveguide mode and Y_{11} the slot self-admittance. To save computer time the number of subdivisions for the axial slot was chosen 10 x 2 = 20, and the tests with 14 x 4 = 56 subdivisions changed the result by 0.1 DB even for the nearby slots.

Figure III-19 and III-20 show the comparison between the harmonic series and the surface ray results of E-plane coupling ($Z_o = 0$) and $Z_o = 1.5$" at 9 GHz, for ka $\approx$ 9.5. A very good agreement is found everywhere within the angular separation of 20° to 150° for the case of $Z_o = 0$, and 0° to 150° for Z = 1.5". The GTD formula is completely inadequate in the H-plane (axial direction).

From [9], $\frac{Y_{11}}{Y_g} = 0.748 + j\, 0.434.$

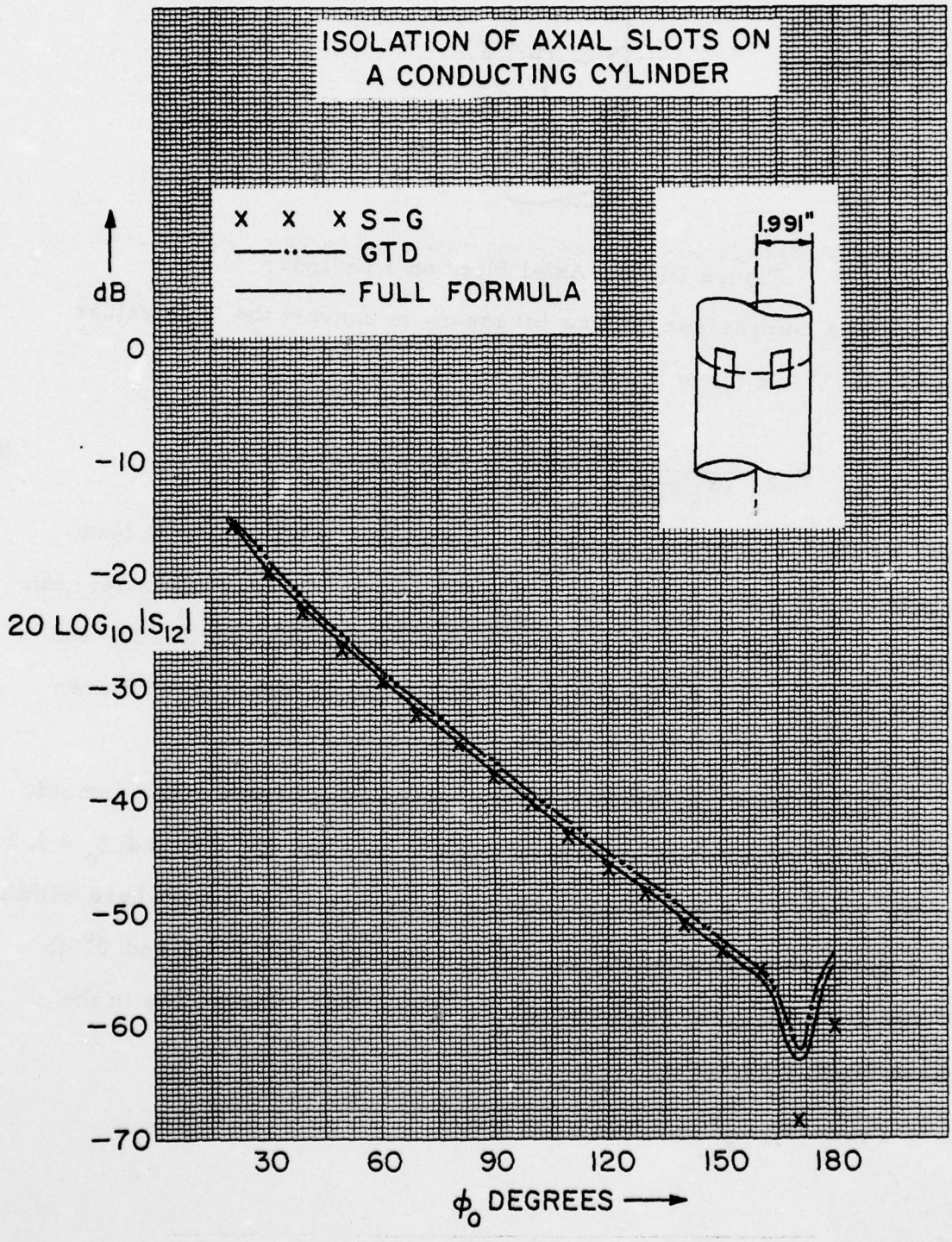

Figure III-19. Isolation of Axial Slots on a Conducting Cylinder, $a = 1.991$, $Z_o = 0$.

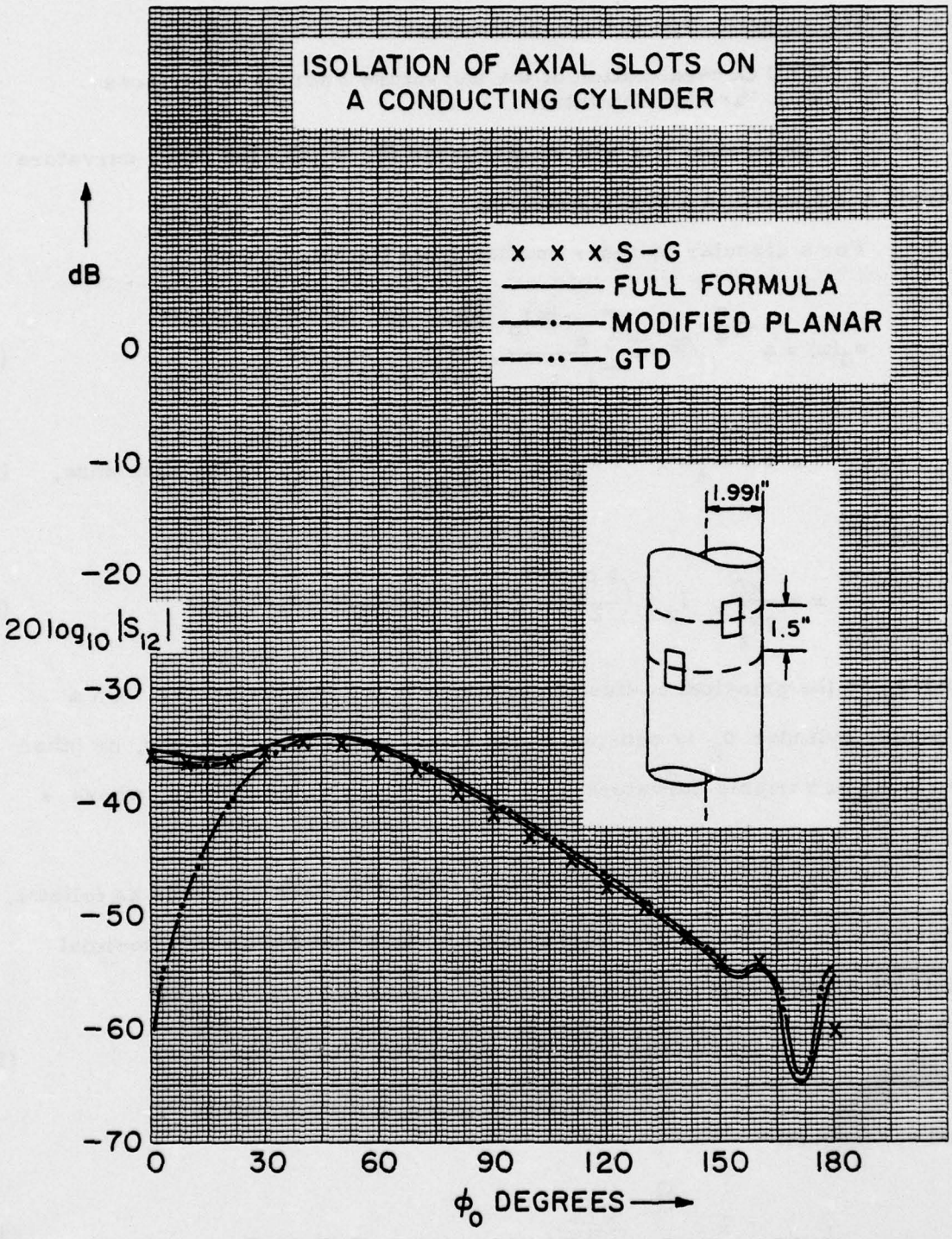

Figure III-20. Isolation of Axial Slots on a Conducting Cylinder, $a = 1.991"$, $Z_o = 1.50"$.

IV. GTD Generalization to Conical Surfaces

a. GTD Generalization of the Curvature Factors to Surfaces with Variable Curvature

The generalization will be discussed for $v_0(x)$, the other curvature terms are treated in a similar fashion.

For a circular cylinder one has from (II-36)

$$v_0(x) = e^{-j\frac{\pi}{4}} \sqrt{\pi}\sqrt{x} \sum_{p=1}^{\infty} \frac{e^{-jx\bar{t}_p}}{\bar{t}_p}, \text{ in deep shadow,} \tag{1a}$$

$$= 1 - \frac{\sqrt{j\pi}}{4} x^{3/2} + \frac{j7}{60}x^3 + \frac{7\sqrt{\pi}}{\sqrt{j}\,512}x^{9/2} + \ldots, \text{ in the near zone,} \tag{1b}$$

where

$$x = \frac{kD}{2f_g^2}, \quad f_g = \left(\frac{k\rho_g}{2}\right)^{1/3}, \quad \rho_g = \frac{a}{\cos^2\theta} \tag{2}$$

and ρ_g is the principal radius of curvature of the ray trajectory. On a circular cylinder ρ_g is constant along a ray. On a cone however, or other surfaces of variable curvature $\rho_g = \rho_g(s)$, varies along the ray, where s is distance parameter along a ray.

The generalization of $v_0(x)$ to a conical surface proceeds as follows. Firstly x in the exponent is replaced by $\bar{x}$ such that for an infinitesimal distsnce along a ray

$$d\bar{x}(s) = \frac{k\,ds}{2f_g^2(s)} \tag{3}$$

and consequently

$$\bar{x} = \int_{Q'}^{Q} \frac{k\,ds}{2f_g^2(s)} \tag{4}$$

In (4) Q' denotes the source point, Q the observation point and the ray trajectory passes along a geodesic path from Q' to Q.

Secondly, in (1a), $\sqrt{x}$ which represents the product of the launching and attachment coefficients [1], is symmetrized in order to preserve reciprocity with respect to an interchange of the source point (Q') and observation point (Q). Thus,

$$\sqrt{x} = \sqrt{\frac{kD}{2f_g^2}} \rightarrow \sqrt{\frac{kD}{2f_g(Q')f_g(Q)}} \quad , \tag{5}$$

where

$$f_g(Q') = \left[\frac{k\rho_g(Q')}{2}\right]^{1/3} \tag{6}$$

and

$$f_g(Q) = \left[\frac{k\rho_g(Q)}{2}\right]^{1/3} \quad . \tag{7}$$

Therefore,

$$v_0(x) \rightarrow e^{-j\frac{\pi}{4}}\sqrt{\pi}\sqrt{\frac{kD}{2f_g(Q')f_g(Q)}}\sum_{p=1}^{\infty}\frac{e^{-j\bar{x}\bar{t}_p}}{\bar{t}_p} \quad . \tag{8}$$

But from (1a)

$$e^{-j\frac{\pi}{4}}\sqrt{\pi}\sqrt{\bar{x}}\sum_{p=1}^{\infty}\frac{e^{-jx\bar{t}_p}}{\bar{t}_p} = v_0(\bar{x}) \tag{9}$$

Consequently,

$$v_0(x) \rightarrow \sqrt{\frac{kD}{2\bar{x}f_g(Q')f_g(Q)}}\, v_0(\bar{x}) = \tilde{v}_0(\bar{x}) \tag{10}$$

Similarly,

$$v_1(x) \to \left[\frac{kD}{2\bar{x} f_g(Q') f_g(Q)}\right]^{3/2} v_1(\bar{x}) = \tilde{v}_1(\bar{x}) \tag{11}$$

and

$$u_0(x) \to \left[\frac{kD}{2\bar{x} f_g(Q') f_g(Q)}\right]^{3/2} u_0(\bar{x}) = \tilde{u}_0(\bar{x}) \tag{12}$$

b. Example:

Generalization of the Full Formula to a Conical Surface

The formula (II-101) generalizes for a conical surface to:

$$H_\varphi^c = -j M_\varphi \frac{k^2 Y}{2\pi}\left[\sin\theta' \sin\theta - \frac{2j}{kD}\sin\theta' \sin\theta + \frac{j}{kD}\cos\theta' \cos\theta\right]\frac{e^{-jkD}}{kD}$$

$$+ M_\varphi \frac{k^2 Y}{2\pi}\frac{1}{\cos\theta' \cos\theta}\left[\tilde{u}_0(\bar{x}) - \sin\theta' \sin\theta\, \tilde{v}_1(\bar{x})\right]\frac{e^{-jkD}}{k(D)^2} \tag{13}$$

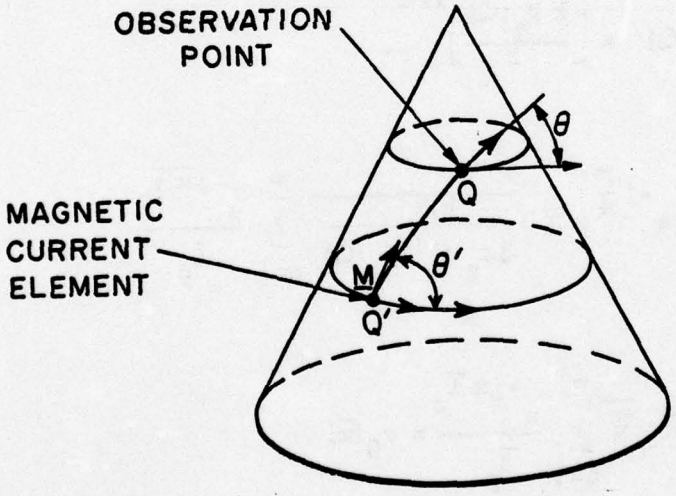

Figure IV-1. Surface Ray on a Cone

In (13) on a conical surface the pattern factors $\sin^2\theta$ and $\cos^2\theta$ have been replaced by $\sin\theta' \sin\theta$ and $\cos\theta' \cos\theta$ (see Figure IV-1), in order to preserve reciprocity.

Samples of numerical results for circumferential slots on a conical surface may be found in [2].

V. Conclusions

This report is a study of the validity of Surface Ray Methods for application to mutual coupling in conformal arrays. The study consists of an analytical part and a numerical part.

The classical GTD [1] includes leading terms in either polarization of the high frequency asymptotic expansion. These correspond to rays which propagate along geodesic trajectories of the unperforated conducting array surface with a near free space velocity, and attenuate exponentially during their travel. Furthermore, because of the ray spreading there is an algebraic ray divergence coefficient $\frac{1}{\sqrt{kD}}$.

In this report it is shown that, in addition to the surface ray terms, diffraction of surface rays must also be included in certain angular regions. These diffraction effects amount to the inclusion of terms $O\left(\frac{1}{(kD)^{3/2}}\right)$ in the deep shadow or $O\left(\frac{1}{(kD)^{2}}\right)$ in the near zone. The significance of the $O\left(\frac{1}{(kD)^{3/2}}\right)$ terms shows up clearly in the circumferential (H-plane) coupling which would be grossly underestimated on the basis of $\frac{1}{\sqrt{kD}}$ terms. The $\frac{1}{(kD)^{2}}$ terms in the near zone are also necessary for the near neighbor coupling.

A basic difficulty is observed in the paraxial (E-plane) region for circumferential slots. It has to do with the break-down of the Airy function approximation of $H_{\nu}^{(2)}(z)$ for small values of the argument z. A correct treatment of the dyadic Green's function in this region requires a different approach than used in this report. For example a harmonic series could be used. Here, the Fourier integral with respect to the axial wavenumber would be evaluated asymptotically to second order of the inverse distance from the source. This representation which is not a surface ray representation

should yield a smooth, valid transition to the surface ray representation. A further question that arises is the generalization of this transition function to the conical geometry.

Instead of proceeding along these lines this report establishes first the correct asymptotic expansion of the surface H_φ for circumferential magnetic current element on a circular cylinder. This expression is valid in the circumferential plane and its angular neighborhood. An approximate transition function is then constructed that blends with the above representation in the circumferential plane, is finite along the axis (E-plane) and reduces to the planar Green's function to $O\left(\frac{1}{(kD)^2}\right)$ in the proximity of the source. A variant of this formula is also provided.

The correlation of the numerical results in Section III with those obtained on the basis of harmonic series for cylinders with $ka \approx 9.5$ and 19.6 justifies the use of these approximate formulae. These above approximate formulae are easily generalized to conical surfaces.

As mentioned, the numerical data for Y_{12} between circumferential slots indicate a good agreement with the harmonic series results for cylinders with $ka \approx 9.5$ and an improved correlation for $ka \approx 19.6$.

The agreement for Y_{12} between axial slots on a cylinder with $ka \approx 9.5$ and based on formula (II-90) is very good, although no phase comparison is available.

References

1. P.H. Pathak and R.G. Kouyoumjian: "An Analysis of the Radiation from Apertures in Curved Surfaces by the Geometrical Theory of Diffraction," Proceedings IEEE, Vol. 62, pp. 1438-1461, November 1974.
2. A. Hessel, J. Shmoys and Z.W. Chang: "Surface Ray Analysis of Conformal Arrays," Report Poly-EE/EP-75-149, Contract N00123-73-C-1481.
3. W. Kummer, A.T. Villeneuve: "Pattern Synthesis of Conformal Arrays," Hughes Aircraft Co., Culver City, Calif., Report 2265.30/297 HAC Ref. D-0741, Contract N00019-74-C-0127. 1 Jan. - 1 April 1974, 1 April - 1 July 1974.
4. J.R. Wait "Electromagnetic Radiation from Cylindrical Structures," New York, Pergamon, 1959.
5. K.E. Golden, G.E. Stewart and D.C. Pridmore-Brown: "Approximation Techniques for the Mutual Admittance of Slot Antennas on Metallic Cones," IEEE Trans. on Antennas and Propagation, Vol. 22, pp. 43-48, Jan. 1974.
6. L.B. Felsen and N. Marcuvitz: "Radiation and Scattering of Waves," New Jersey, Prentice-Hall, 1973.
7. M. Abramowitz and I.A. Stegun: "Handbook of Mathematical Functions," National Bureau of Standards, Applied Mathematics Series 55, June 1964.
8. G. Hasserjian and A. Ishimaru: "Excitation of a Conducting Cylindrical Surface of Large Radius of Curvature," IRE Trans. on Antennas and Propagation, Vol. 10, pp. 264-273, May, 1962.

AD-A033 544 POLYTECHNIC INST OF NEW YORK FARMINGDALE DEPT OF ELE--ETC F/G 9/3
SURFACE RAY METHODS FOR MUTUAL COUPLING IN CONFORMAL ARRAYS ON --ETC(U)
JUL 76 Z W CHANG, L B FELSEN, A HESSEL N00123-76-C-0236

UNCLASSIFIED POLY-EE/EP-76-016 NL

2 OF 2
ADA033544

END

DATE
FILMED
2 -77

9. G. E. Stewart and K. E. Golden: "Mutual Admittance for Axial Rectangular Slots in a Large Conducting Cylinder," IEEE Trans. on Antennas and Propagation, Vol. 19, pp. 120-122, Jan. 1971.

10. Y. Hwang and R. G. Kouyoumjian: "The Mutual Coupling Between Slots on an Arbitrary Convex Cylinder", The Ohio State University Electroscience Laboratory, Department of Electrical Engineering, Semi-Annual Report 2902-21, 1975, prepared under Grant NGL36-003-138.

Appendix A. Review of the Theory of Alternative Representations

The procedure for obtaining electromagnetic field solutions in cylindrical regions of uniform cross-section, utilize various representations of fields and their sources in terms of a complete set of vector eigen functions, with the resultant scalarization of the relevant vector problem.

The scalar potentials are defined via [Ref. 6, Eqs. 24a and 25a, pp. 196-197]

$$S^{(\prime)(\prime\prime)}(\underline{r}, \underline{r}') = \sum_i \frac{\psi_i^{(\prime)(\prime\prime)}(\underline{\rho})\, \psi_i^{(\prime)(\prime\prime)*}(\underline{\rho}')}{k_{t_i}^{(\prime)(\prime\prime)\,2}} g_z(z, z') . \tag{1}$$

In (1) the prime and double prime denote TM- and TE- polarizations, respectively, $\underline{\rho}$ and $\underline{\rho}'$ are the transverse position vectors of the observation and of the source point, and $g_z(z, z')$ is given in (A18). The subscript i stands for a double index, one corresponding to the radial, the other to the angular domain. The mode potentials $\psi_i'(\underline{\rho})$ and $\psi_i''(\underline{\rho})$ individually satisfy in the cross-section the Helmholtz equation

$$\nabla_t^2 \psi_i^{(\prime)(\prime\prime)}(\rho, \varphi) + k_{t_i}^{(\prime)(\prime\prime)\,2} \psi_i^{(\prime)(\prime\prime)}(\rho, \varphi) = 0 \tag{2}$$

with periodicity of 2π in φ of the function and its φ derivative, and with

$$\psi_i'(a, \varphi) = 0, \quad \frac{\partial}{\partial \rho} \psi_i''(\rho, \varphi) \Big|_{\rho=a} = 0 \tag{3}$$

In (1) and (2), k_{t_i} denote the radial eigenvalues (wavenumbers).

The normalization is such that

$$\iint_{\text{cross-section}} |\underline{e}_i^{(\prime)(\prime\prime)}(\underline{\rho})|^2 \, dS = 1, \tag{4}$$

where $$\underline{e}_i'(\underline{\rho}) = -\frac{\nabla_t \psi_i'(\underline{\rho})}{k_{t_i}'} \quad \text{and} \quad \underline{e}_i''(\underline{\rho}) = -\frac{\nabla_t \psi_i''(\underline{\rho})}{k_{t_i}''} \times \hat{z} \tag{5}$$

To facilitate conversion of the various alternative representations, it is useful to define three one-dimensional characteristic Green's functions as follows:

a. Angular Green's Function

This Green's function satisfies

$$\left(\frac{d^2}{d\varphi^2} + \lambda_\nu\right) g_\varphi(\varphi, \varphi'; \lambda_\nu) = -\delta(\varphi - \varphi'), \tag{6}$$

subject to the periodicity conditions

$$g_\varphi(\varphi + \pi, \varphi'; \lambda_\nu) = g_\varphi(\varphi - \pi, \varphi'; \lambda_\nu) \tag{7}$$

and

$$\frac{d}{d\varphi} g_\varphi(\varphi + \pi, \varphi'; \lambda_\nu) = \frac{d}{d\varphi} g_\varphi(\varphi - \pi, \varphi'; \lambda_\nu) . \tag{8}$$

This Green's function is found in Ref. [6, Eq. 51c, p. 310] and is given below

$$g_\varphi(\varphi, \varphi'; \lambda_\nu) = -\frac{\cos\sqrt{\lambda_\nu}\,(\pi - |\varphi - \varphi'|)}{2\sqrt{\lambda_\nu}\,\sin\sqrt{\lambda_\nu}\,\pi}, \quad -\pi \leq \varphi, \varphi' < \pi . \tag{9}$$

The corresponding completeness relation Ref. [6, p. 277] reads

$$-\frac{1}{2\pi j}\oint_{C_\varphi} d\lambda_\nu \, g_\varphi(\varphi, \varphi'; \lambda_\nu) = \frac{1}{\pi}\sum_{\nu=0} \varepsilon_\nu \cos\nu(\varphi - \varphi') = -\delta(\varphi - \varphi'), \tag{10}$$

where $\varepsilon_\nu = \frac{1}{2}$ for $\nu = 0$ and $\varepsilon_\nu = 1$, $\nu \neq 0$.

The simple pole singularities of g_φ and the contour C_φ enclosing them

are shown in Figure A-1.

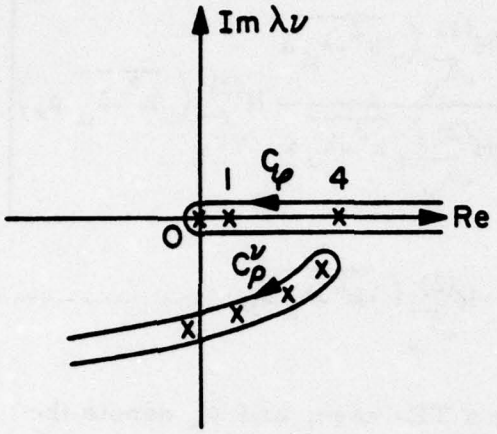

Figure A-1. Complex λ_ν-plane

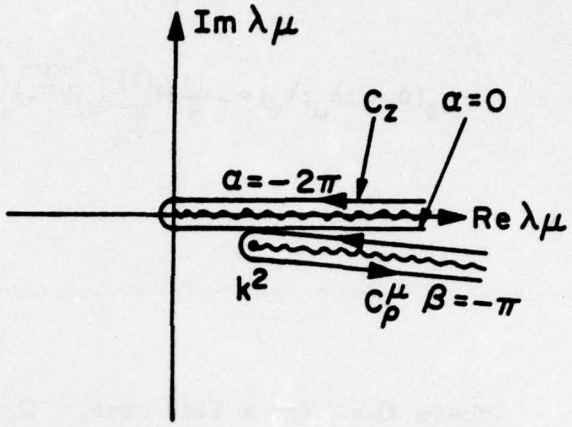

Figure A-2. Complex λ_μ-plane

$\alpha = \arg(\lambda_\mu)$, $\beta = \arg(k^2 - \lambda_\mu)$

b. The Radial Green's Function

This Green's function is defined by

$$\left[\frac{1}{\rho}\frac{d}{d\rho}\rho\frac{d}{d\rho} + (k^2 - \lambda_\mu) - \frac{\lambda_\nu}{\rho^2}\right] g_\rho(\rho, \rho'; \lambda_\mu; \lambda_\nu) = -\frac{\delta(\rho-\rho')}{\rho} \quad , \tag{11}$$

subject to the boundary conditions:

$$g'_\rho \Big|_{\rho=a} = 0, \text{ for the TM case} \tag{12a}$$

$$\frac{d}{d\rho} g''_\rho \Big|_{\rho=a} = 0, \text{ for the TE case} \tag{12b}$$

and the radiation condition at $\rho \to \infty$ for either polarization. While g_φ is a function of one parameter λ_ν, g_ρ depends on two parameters λ_ν and λ_μ. This feature follows from the separation of variables for Helmholtz equation in cylindrical coordinates. One finds [Ref. 6, p. 277]

$$g_\rho(\rho, \rho';\lambda_\mu;\lambda_\nu) = -\frac{j\pi}{4}\left[H^{(1)}_{\sqrt{\lambda_\nu}}\left(\sqrt{k^2-\lambda_\mu}\,\rho_<\right) - \frac{Q H^{(1)}_{\sqrt{\lambda_\nu}}\left(\sqrt{k^2-\lambda_\mu}\,a\right)}{Q H^{(2)}_{\sqrt{\lambda_\nu}}\left(\sqrt{k^2-\lambda_\mu}\,a\right)} H^{(2)}_{\sqrt{\lambda_\nu}}\left(\sqrt{k^2-\lambda_\mu}\,\rho_<\right)\right] \times$$

$$H^{(2)}_{\sqrt{\lambda_\nu}}\left(\sqrt{k^2-\lambda_\mu}\,\rho_>\right) \tag{13}$$

where $Q = 1$ for a TM- case, $Q = \frac{\partial}{\partial a}$ for a TE- case, and $\rho_{\gtrless}$ denote the greater and the lesser of ρ and ρ', respectively.

There is no branch point at $\lambda_\nu = 0$, since, in view of the relation

$$H^{(1,2)}_{-\alpha}(Z) = e^{\pm j\alpha\pi} H^{(1,2)}_{\alpha}(Z)\,, \tag{14}$$

g_ρ *is an even function of* $\sqrt{\lambda_\nu}$.

It is convenient to introduce the transformations $\sqrt{\lambda_\nu} = \nu$ and $\sqrt{k^2 - \lambda_\mu} = k_t$, whereupon g_ρ becomes

$$g_\rho(\rho, \rho';\lambda_\mu;\lambda_\nu) = -\frac{j\pi}{4}\left[H^{(1)}_\nu(k_t\rho_<) - \frac{Q H^{(1)}_\nu(k_t a)}{Q H^{(2)}_\nu(k_t a)} H^{(2)}_\nu(k_t\rho_<)\right] H^{(2)}_\nu(k_t\rho_>)\,. \tag{15}$$

The singularities of g_ρ in the λ_ν-plane are simple poles at the zeros of $Q H^{(2)}_{\sqrt{\lambda_\nu}}(k_t a)$. They are indicated in Figure A-1, which also shows the contour of integration C^ν_ρ enclosing these singularities in the completeness relation [Ref. 6, Eq. 3-4-98, p. 326]

$$-\frac{1}{2\pi j}\oint_{C^\nu_\rho} d\lambda_\nu\, g_\rho(\rho, \rho';k_t^2;\lambda_\nu) = -j\frac{\pi}{2}\sum_{\ell=1}^{\infty} \nu_\ell H^{(2)}_{\nu_\ell}(k_t\rho_>) H^{(2)}_{\nu_\ell}(k_t\rho_<) \frac{Q H^{(1)}_{\nu_\ell}(k_t a)}{\frac{\partial}{\partial\nu_\ell} Q H^{(2)}_{\nu_\ell}(k_t a)}$$

$$= -\rho'\,\delta(\rho-\rho') \tag{16}$$

In the λ_μ-plane g_ρ exhibits a branch point at $\lambda_\mu = k^2$. The choice of the proper branch of $\sqrt{k^2 - \lambda_\mu}$ is such as to satisfy radiation condition for $\rho \to \infty$. A convenient branch cut and the path of integration C_ρ^μ for the completeness relation [Ref. 6, Eq. 99, p. 327]

$$-\frac{1}{2\pi j}\oint_{C_\rho^\mu} d\lambda_\mu \, g_\rho(\rho, \rho';\lambda_\mu;\nu^2) = \frac{\delta(\rho-\rho')}{\rho'} \tag{17}$$

is shown in Figure A-2.

c. The Axial Green's Function

This Green's function satisfies

$$\left(\frac{d^2}{dz^2} + \lambda_\mu\right) g_z(z, z';\lambda_\mu) = -\delta(z-z') \tag{18}$$

subject to radiation condition for $|z| \to \infty$. Therefore

$$g_z(z, z';\lambda_\mu) = \frac{e^{-j\sqrt{\lambda_\mu}\,|z-z'|}}{2j\sqrt{\lambda_\mu}} \quad ; \qquad \mathrm{Im}\,\sqrt{\lambda_\mu} \leq 0. \tag{19}$$

One observes that g_ρ has a branch point singularity at $\lambda_\mu = 0$. The proper sheet of $\sqrt{\lambda_\mu}$ is defined as $0 \geq \arg(\lambda_\mu) > -2\pi$. For convenience, if the positive real λ_μ-axis is chosen as the branch cut (see Figure A-2), one obtains the completeness relation for the z-domain

$$-\frac{1}{2\pi j}\oint_{C_z} d\lambda_\mu \, g_z(z, z';\lambda_\mu) = -\delta(z-z') \tag{20}$$

To facilitate the conversion between alternative representations one transforms the modal potentials S' and S'' of (A1) into the integral representation of (21a) involving the above three one dimensional Green's functions. This representation, in turn, enables one to deduce the various alternative

representations merely by deforming the paths of integration C_ϖ or C_z into C_ρ^ν or C_ρ^μ, respectively. Examples of alternative representations for S are:

$$S(\underline{r},\underline{r}') = \begin{cases} \dfrac{1}{(-2\pi j)^2}\oint_{C_z} d\lambda_\mu \dfrac{1}{k^2-\lambda_\mu} g_\rho(\rho,\rho';\lambda_\mu;\lambda_\nu) g_\varpi(\varpi,\varpi';\lambda_\nu) g_z(z,z';\lambda_\mu) & (21a) \\ -\dfrac{1}{2\pi^2 j}\sum_{\nu=0}^{\infty} \epsilon_\nu \cos\nu(\varpi-\varpi') \displaystyle\int_{C_z} d\lambda_\mu \dfrac{1}{k^2-\lambda_\mu} g_\rho(\rho,\rho';\lambda_\mu;\nu^2) g_z(z,z';\lambda_\mu) & (21b) \\ \dfrac{1}{4}\displaystyle\sum_{\ell=1}^{\infty} \dfrac{\cos\nu_\ell(\pi-|\varpi-\varpi'|)}{\sin\nu_\ell\pi} \int_{C_z} d\lambda_\mu \dfrac{1}{k^2-\lambda_\mu} H_{\nu_\ell}^{(2)}\left(\sqrt{k^2-\lambda_\mu}\,\rho\right) H_{\nu_\ell}^{(2)}\left(\sqrt{k^2-\lambda_\mu}\,\rho'\right) \times & \\ \qquad \dfrac{QH_{\nu_\ell}^{(1)}\left(\sqrt{k^2-\lambda_\mu}\,a\right)}{QH_{\nu_\ell}^{(2)}\left(\sqrt{k^2-\lambda_\mu}\,a\right)} g_z(z,z';\lambda_\mu) & (21c) \end{cases}$$

where $Q=1$ for $S=S'$ and $Q = \frac{\partial}{\partial a}$ for $S=S''$.

Representation of the potentials S' and S'' in (A1) follows from the relation [Ref. 6, p. 198 Eqs. (32b), (33b)]

$$-\nabla_t^2 S^{(\prime)(\prime\prime)}(\underline{r},\underline{r}') = G^{(\prime)(\prime\prime)}(\underline{r},\underline{r}') \ , \tag{22}$$

where

$$G^{(\prime)(\prime\prime)}(\underline{r},\underline{r}') = \sum_i \psi_i^{(\prime)(\prime\prime)}(\underline{\rho})\, \psi_i^{(\prime)(\prime\prime)*}(\underline{\rho}')\, g_z(z,z') \ . \tag{23}$$

In a similar fashion (21a) follows from [Ref. 6, p. 285 Eq. 37] and (A-22).

To obtain (21b), the integral in (21a), with contour C_ϖ, is evaluated as a sum of residues at the simple poles of g_ϖ. To derive (21c), the contour C_ϖ is deformed into C_ρ^ν and the resulting integral is expressed as a residue series at the simple poles ν_ℓ of g_ρ.

Appendix B: Curvature Terms and their Derivatives

Basically, there are two curvature terms, hard and soft.

They are derived from the integrals $\int_{-\infty}^{\infty} e^{-j\nu\Phi} \frac{H_\nu^{(2)}(Z)}{H_\nu^{(2)\prime}(Z)} d\nu$ and

$$\int_{-\infty}^{\infty} e^{-j\nu\Phi} \frac{H_\nu^{(2)\prime}(Z)}{H_\nu^{(2)}(Z)} d\nu .$$

a. The hard curvature term and its derivatives

For large and almost equal argument and order the asymptotic expansion of the Hankel function $H_\nu^{(2)}(Z)$ and its derivative with respect to argument is found in the form of a combination of the Airy functions[4]. The leading term of this expansion is

$$\begin{aligned} H_\nu^{(2)}(Z) &\sim \frac{j}{\sqrt{\pi}} f^{-1} w_2(t) \\ H_\nu^{(2)\prime}(Z) &\sim -\frac{j}{\sqrt{\pi}} f^{-2} w_2'(t) \end{aligned} \qquad \text{for } \nu \approx Z \text{ and } |Z| >> |\,| , \tag{1}$$

where $$t = \frac{\nu - Z}{f}, \quad f = \left(\frac{Z}{2}\right)^{1/3} . \tag{2}$$

Here

$$w_2(t) = \sqrt{\pi}\,[B_i(t) - j\,A_i(t)] , \tag{3}$$

where $A_i(t)$ and $B_i(t)$ are the two independent real solutions of the Airy differential equation. Therefore $w_2(t)$ satisfies

$$\left(\frac{d^2}{dt^2} - t\right) w_2(t) = 0. \tag{4}$$

The lowest order (in Z) asymptotic term of the ratio of Hankel functions is, from(B1)

$$\frac{H_\nu^{(2)}(Z)}{H_\nu^{(2)\prime}(Z)} \sim -f\frac{w_2(t)}{w_2'(t)} \quad . \tag{5}$$

If $Z \gg 1$, this ratio exhibits a peak value near the poles of the integrand. Therefore the major contribution of the Fourier transform of this ratio is derived from the region of the ν-plane where $\nu \approx Z$. For $Z \gg 1$, one may use the asymptotic form of this ratio. Thus,

$$\int_{-\infty}^{\infty} e^{-j\nu\Phi} \frac{H_\nu^{(2)}(Z)}{H_\nu^{(2)\prime}(Z)}\, d\nu \sim -e^{-jZ\Phi} f^2 \int_\tau e^{-jf\Phi t} \frac{w_2(t)}{w_2'(t)}\, dt \ , \tag{6}$$

where $\Phi > 0$, is a parameter, and the integration contour τ depends on Z. one notes that for $|t| \to \infty$, $\frac{w_2(t)}{w_2'(t)}$ is algebraic [Ref. 6, pp. 394-395]. When arg Z=0, arg t = 0 and τ runs from $-\infty$ to $+\infty$ along the real axis in the t-plane, the valley regions being the entire lower half t-plane. But when arg $Z = -\frac{\pi}{2}$, arg $t = -\frac{5\pi}{6}$ as $\nu \to -\infty$, and arg $t = \frac{\pi}{6}$ as $\nu \to +\infty$, with the valley regions below the

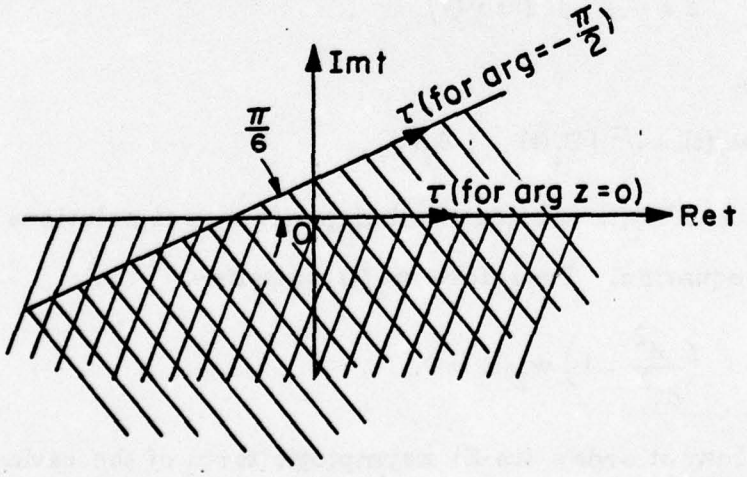

Figure B-1. Complex t-plane and the Integration Contours for arg Z = 0 and $-\frac{\pi}{2}$.

contour τ. Figure B-1 shows the contours τ for both arg Z=0 and $-\frac{\pi}{2}$.

To find a contour valid for either case, one deforms that part of the straight line with Im t > 0 (for arg $Z = -\frac{\pi}{2}$) to the real t axis and, in this fashion, recovers the usual, broken contour τ of Figure II-3 running from $\infty e^{-j\frac{5\pi}{6}}$ to $+\infty$.

The hard curvature term $V_0(x)$ is defined by

$$V_0(x) = \int_\tau e^{-jxt} \frac{w_2(t)}{w_2'(t)}\, dt \tag{7}$$

where $x = f\Phi$.

There are two expressions for $V_0(x)$; one is for large, the other for small values of x. For large values of x, one may close the contour τ in the respective valley regions (i.e. those of arg Z=0 and $-\frac{\pi}{2}$) at infinity in the lower half plane. This procedure results in a residue series evaluated at the simple poles of $w_2'(t) = 0$:

$$V_0(x) = -2\pi j \sum_{p=1}^{\infty} e^{-jx\bar{t}_p} \frac{w_2(\bar{t}_p)}{w_2''(\bar{t}_p)}, \tag{8}$$

where $\bar{t}_p = |\bar{t}_p|\, e^{-j\frac{\pi}{3}}$, with $Ai'(-|\bar{t}_p|) = 0$. Numerical values of $|\bar{t}_p|$ may be found in [7].

From (B4), one finds

$$V_0(x) = -2\pi j \sum_{p=1}^{\infty} \frac{e^{-jx\bar{t}_p}}{\bar{t}_p} \tag{9}$$

For large values of x, this residue series converges rapidly. In contrast, for small values of x the residue series becomes poorly convergent.

An alternative, more efficient representation in this range is a "power series" in x which can be established by an asymptotic expansion for large values of t of $\frac{w_2(t)}{w_2'(t)}$ and a term by term integration. To this end, one may rotate the contour τ clockwise by 90°. For arg Z=0, τ maps into a Bromwich contour τ' by letting

$$t = j s, \tag{10}$$

whereupon

$$V_0(x) = j \int_{\infty e^{-j\frac{\pi}{2}}}^{\infty e^{j\frac{\pi}{2}}} e^{x s} \frac{w_2(js)}{w_s'(js)}\, ds \tag{11}$$

For arg $Z = -\frac{\pi}{2}$ one rotates the contour clockwise by 120° by the transformation

$$t = j e^{j\frac{\pi}{6}} s\ , \tag{12}$$

which again yields the same Bromwich contour τ', i.e.

$$V_0(x) = j e^{j\frac{\pi}{6}} \int_{\tau'} e^{|x| s} \frac{w_2\left(j e^{j\frac{\pi}{6}} s\right)}{w_2'\left(j e^{j\frac{\pi}{6}} s\right)}\, ds\ . \tag{13}$$

Following [8], one has

$$\frac{w_2(js)}{w_2'(js)} \sim e^{-j\frac{\pi}{4}}\left[\frac{1}{s^{\frac{1}{2}}} - \frac{\sqrt{j}}{4s^2} + \frac{7j}{32 s^{7/2}} + \frac{21}{\sqrt{j}\, 64\, s^5} + O\left(s^{-13/2}\right)\right] \tag{14}$$

Similarly, one finds

$$\frac{w_2\left(j e^{j\frac{\pi}{6}} s\right)}{w_2'\left(j e^{j\frac{\pi}{6}} s\right)} \sim e^{-j\frac{\pi}{4}}\left[\frac{e^{-j\frac{\pi}{12}}}{s^{\frac{1}{2}}} - \frac{e^{-j\frac{\pi}{3}}\sqrt{j}}{4s^2} + \frac{7j\, e^{-j\frac{7\pi}{12}}}{32\, s^{7/2}}\right.$$

$$\left. + \frac{21\, e^{-j\frac{5\pi}{6}}}{\sqrt{j}\ 64\ s^5} +)\left(s^{-13/2}\right)\right] \tag{15}$$

Each term of expansion (B14) is an inverse Laplace transform and is evaluated explicitly below.

$$-\frac{1}{2\pi j}\int_{\tau'} e^{|x|s} F(s)\, ds = \mathcal{L}^{-1}F(s) \tag{16}$$

where $\mathcal{L}^{-1}$ denotes the inverse Laplace transform. Therefore for arg Z=0, one finds

$$V_0(x) = 2\pi\, \mathcal{L}^{-1} \frac{w_2(js)}{w_2'(js)}$$

$$\sim -2\pi j \frac{e^{j\frac{\pi}{4}}}{\sqrt{\pi}\, x^{\frac{1}{2}}}\left(1 - \frac{\sqrt{j\pi}}{4} x^{3/2} + \frac{j7}{60} x^3 + \frac{7\sqrt{\pi}}{512\sqrt{j}} x^{9/2} + \ldots\right) \tag{17}$$

and for arg $Z = -\frac{\pi}{2}$, one obtains

$$V_0(x) = 2\pi\, e^{j\frac{\pi}{6}}\, \mathcal{L}^{-1} \frac{w_2\left(j e^{j\frac{\pi}{6}} s\right)}{w_2'\left(j e^{j\frac{\pi}{6}} s\right)}$$

$$\sim 2\pi\, e^{-j\frac{\pi}{12}}\left[e^{-j\frac{\pi}{12}} \frac{1}{\sqrt{\pi}\, |x|^{\frac{1}{2}}} - \frac{e^{-j\frac{\pi}{3}}\sqrt{j}}{4} |x| + 7j\, e^{-j\frac{7\pi}{12}} \frac{8|x|^{5/2}}{15\sqrt{\pi}}\right.$$

$$\left. + \frac{21\, e^{-j\frac{5\pi}{6}}}{\sqrt{j}\ 64} \frac{|x|^4}{24} + \ldots\right] \tag{18}$$

$$= -2\pi j \frac{e^{j\frac{\pi}{4}}}{\sqrt{\pi}\, x^{\frac{1}{2}}} \left(1 - \frac{\sqrt{j\pi}}{4} x^{3/2} + \frac{j7}{60} x^3 + \frac{7\sqrt{\pi}}{\sqrt{j}\,512} x^{9/2} + \ldots\right) \tag{18}$$

Note that (B17) and (B18) have the same form, but the former is valid for real x while the latter for x complex. In either case, if one defines $v_0(x)$ as the "power series" shown in the bracket of (B17) or (B18)

one has

$$v_0(x) = \begin{cases} 1 - \frac{\sqrt{j\pi}}{4} x^{3/2} + \frac{j7}{60} x^3 + \frac{7\sqrt{\pi}}{\sqrt{j}\,512} x^{9/2} + \ldots, & \text{for small } x \qquad (19) \\ \frac{\sqrt{\pi}\, x^{\frac{1}{2}}}{e^{j\frac{\pi}{4}}} \sum_{p=1}^{\infty} \frac{e^{-jx\bar{t}_p}}{\bar{t}_p}, & \text{for large } x \qquad (20) \end{cases}$$

and

$$V_0(x) = -2\pi j \frac{e^{j\frac{\pi}{4}}}{\sqrt{\pi}\, x^{\frac{1}{2}}} v_0(x) \tag{21}$$

The two series in (B20) and (B21) connect smoothly both in the amplitude and phase. If one considers ten residue terms and four power series terms, then at x = 0.6, the difference between the two series is about 0.0025 percent in amplitude and 0.012 degree in phase. Figure II-4 shows the cross-over for $v_o(x)$.

The derivatives of the curvature terms can be obtained by a direct differentiation of $V_0(x)$. Thus, for the first derivative of the hard curvature term, one has

$$V_0'(x) = -j \int_{\tau} e^{-jxt} t \frac{w_2(t)}{w_2'(t)}\, dt = -j\, V_1(x), \tag{22}$$

where

Defining $v_1(x)$ as

$$v_1(x) = \begin{cases} 1 + \frac{\sqrt{j\pi}}{2} x^{3/2} - \frac{j7}{12} x^3 - \frac{7\sqrt{\pi}}{\sqrt{j}\ 64} x^{9/2} + \dots , & \text{for small } x \quad (23) \\ \frac{2\sqrt{\pi}\, x^{3/2}}{e^{-j\frac{\pi}{4}}} \sum_{p=1}^{\infty} e^{-jx\bar{t}_p}, & \text{for large } x \quad (24) \end{cases}$$

$$\text{one has } V_1(x) = -2\pi j \frac{e^{-j\frac{\pi}{4}}}{2\sqrt{\pi}\, x^{3/2}} v_1(x) . \quad (25)$$

For ten residue terms and four power series terms, the difference between (B25) and (B26) at $x = 0.6$ is about 0.42 percent in the amplitude and 0.126 degree in the phase. Figure II-5 shows the cross-over for $v_1(x)$.

The second derivative of the hard curvature term is

$$V_0''(x) = -\int_{\tau} t^2 e^{-jxt} \frac{w_2(t)}{w_2'(t)} dt = -V_2(x) , \quad (26)$$

With

$$v_2(x) = \begin{cases} 1 + \frac{j7}{12} x^3 + \frac{7\sqrt{\pi}}{\sqrt{j}\ 32} x^{9/2} + \dots , & \text{for small } x \quad (27) \\ \frac{4}{3}\sqrt{\pi}\, e^{j\frac{\pi}{4}} x^{5/2} \sum_{p=1}^{\infty} \bar{t}_p\, e^{-jx\bar{t}_p} , & \text{for large } x \quad (28) \end{cases}$$

one has

$$V_2(x) = -\frac{3\sqrt{\pi}\, e^{-j\frac{\pi}{4}}}{2x^{5/2}} v_2(x) \quad (29)$$

The cross-over point is in the proximity of x = 0.6 where the difference between (B29) and (B30) is about 1.7 percent in the amplitude and 0.101 degree in phase.

b. The Soft Curvature Term

$$\int_{-\infty}^{\infty} e^{-j\nu\Phi} \frac{H_\nu^{(2)\prime}(Z)}{H_\nu^{(2)}(Z)} d\nu \sim - e^{-jZ\Phi} \int_{\tau} e^{-jxt} \frac{w_2'(t)}{w_2(t)} dt \tag{30}$$

where $x = f\Phi$, and τ is the same contour as shown in Figure B-1.

The soft curvature term $U_0(x)$ is defined by

$$U_0(x) = \int_{\tau} e^{-jxt} \frac{w_2'(t)}{w_2(t)} dt \tag{31}$$

In an analogous fashion, the residue series representation of $U_0(x)$ is

$$U_0(x) = - 2\pi j \sum_{p=1} e^{-jx t_p} \tag{32}$$

where $t_p = |t_p| e^{-j\frac{\pi}{3}}$, $Ai(- |t_p|) = 0$. This series (B34) converges rapidly for large x.

Similarly for small x, with t = js, one has (since arg $Z = -\frac{\pi}{2}$ will not generate a new function, we consider only the case arg Z=0 here)

$$\frac{w_2'(js)}{w_j(js)} \sim e^{j\frac{\pi}{4}} s \left[\frac{1}{s^{\frac{1}{2}}} + \frac{\sqrt{j}}{4s^2} - \frac{j5}{32 s^{7/2}} - \frac{15}{\sqrt{j}\, 64 s^2} + O\left(s^{-13/2}\right) \right] \tag{33}$$

Hence,

$$U_0(x) = 2\pi \mathcal{L}^{-1} \frac{w_2'(js)}{w_2(js)}$$

$$\sim 2\pi e^{j\frac{\pi}{4}} \left[\frac{d}{dx}\left(\frac{1}{\sqrt{\pi}x^{\frac{1}{2}}} + \frac{\sqrt{j}}{4}x - \frac{5j}{32}\frac{x^{5/2}8}{15\sqrt{\pi}} - \frac{16}{\sqrt{j}\,64}\frac{x^4}{24} + \ldots\right)\right]. \qquad (34)$$

Consequently,

$$U_0(x) \sim -2\pi j \frac{e^{-j\frac{\pi}{4}}}{2\sqrt{\pi}x^{3/2}}\left(1 - \frac{\sqrt{j\pi}}{2}x^{3/2} + \frac{j5}{12}x^3 + \frac{5\sqrt{\pi}}{\sqrt{j}\,64}x^{9/2} + \ldots\right). \qquad (35)$$

Defining $u_0(x)$ via

$$u_0(x) = \begin{cases} 1 - \frac{\sqrt{j\pi}}{2}x^{3/2} + \frac{j5}{12}x^3 + \frac{5\sqrt{\pi}}{\sqrt{j}\,64}x^{9/2} + \ldots, & \text{for small } x \qquad (36) \\ \frac{2\sqrt{\pi}\,x^{3/2}}{e^{-j\frac{\pi}{4}}} \sum_{p=1}^{\infty} e^{-jx t_p}, & \text{for large } x \qquad (37) \end{cases}$$

one has

$$U_0(x) = -2\pi j \frac{e^{-j\frac{\pi}{4}}}{2\sqrt{\pi}\,x^{3/2}} u_0(x) \; . \qquad (38)$$

The two series in (B38) and (B39) connect smoothly at $x = 0.6$, if one takes ten residue terms and four power series terms. The difference is 0.2 percent in the amplitude and 0.10 degree in the phase.

There is no need for the derivative of the soft curvature term, since it yields terms of higher order in $\frac{1}{ka}$ than considered here.

Appendix C. Asymptotic Series for Laplace Type Integrals

Derivation of the complete asymptotic series for the case of an isolated saddle point for the following canonical integral is reviewed below.

$$I(\Omega) = \int_{SDP} e^{\Omega q(\alpha)} F(\alpha)\, d\alpha \tag{1}$$

where $\Omega >> 1$, SDP denotes the steepest descent path while F and q are analytic functions of α.

If $q(\alpha)$ has a first order saddle point, i.e. $q'(\alpha_s) = 0$ but $q''(\alpha_s) \neq 0$. then one transforms $q(\alpha)$ into a simpler function $\tau(s)$ via

$$q(\alpha) = \tau(s) = - j - s^2 \tag{2}$$

With this transformation the saddle point α_s maps into the origin of the s-plane. Therefore

$$q(\alpha_s) = - j . \tag{3}$$

Consequently, the integral becomes

$$I(\Omega) = e^{\Omega q(\alpha_s)} \int_{-\infty}^{\infty} G(s)\, e^{-\Omega s^2} ds \quad , \tag{4}$$

where

$$G(s) = F(\alpha) \frac{d\alpha}{ds} . \tag{5}$$

The proper branch of $s = \sqrt{-j - q(\alpha)}$ is determined by the orientation of the SDP, i.e. by the phase angle of $\frac{d\alpha}{ds}$ at the saddle point. One then expands G(s) into a power series about s = 0, and evaluates the integral in (4) by carrying out the integration term by term. The radius of convergence of this power series will be determined by the numerical distance, or the distance from s = 0 to the nearest singularity of G(s). The numerical distance will determine the error of the asymptotic expansion. Thus,

$$I(\Omega) \sim e^{\Omega q(\alpha_s)} \int_{-\infty}^{\infty} \left[G(0) + s\,G'(0) + \frac{s^2}{2!}\,G''(0) + \ldots\right] e^{-\Omega s^2}\,ds$$

$$= e^{\Omega q(\alpha_s)} \sum_{n=0}^{\infty} \frac{G^{(2n)}(0)}{(2n)!}\,\frac{\Gamma\left(\frac{2n+1}{2}\right)}{\Omega^{\frac{2n+1}{2}}} \tag{6}$$

where $\Gamma(Z)$ denotes the Gamma function and $G^{(2n)}(s)$ the 2nth derivative of $G(s)$. Note, odd terms do not appear since

$$\int_{-\infty}^{\infty} s^n\, e^{-\Omega s^2} ds = 0 \text{ for } n \text{ odd.} \tag{7}$$

Appendix D. Vector Form of Planar Green's Function

The fields radiated by a z directed magnetic point current source $\underline{M} = \hat{z}\, M_z$ on an infinite ground plane which coincides with the yz plane of a Cartesian coordinate system, are

$$\underline{H}(\underline{r}, \underline{r}') = jM_z \frac{k^2 Y}{2\pi} \left[\hat{\theta} \left(\sin\theta - j \sin\theta \frac{1}{kr} - \sin\theta \frac{1}{(kr)^2} \right) - \hat{r} \left(j2 \cos\theta \frac{1}{kr} + 2 \cos\theta \frac{1}{(kr)^2} \right) \right] \frac{e^{-jkr}}{kr} \tag{1}$$

$$\underline{E}(\underline{r}, \underline{r}') = - jM_z \frac{k^2}{2\pi} \hat{\varphi} \sin\theta \left(1 - j \frac{1}{kr} \right) \frac{e^{-jkr}}{kr} \tag{2}$$

where r, θ and φ are the standard spherical coordinates.

Formulae (1) and (2) may be cast into a ray vector form. The ray trajectories are straight lines emanating radially from the source to the observation point. Let the unit vectors $\hat{t}$, $\hat{t}'$ and $\hat{b}$, $\hat{b}'$ denote the tangent (radial) and the binormal directions of the ray at the observation point and at the source point, respectively. Furthermore let $\hat{s}$ be the unit vector in the direction of the source and $\hat{n}$ the unit normal to the ground plane, so that

$$\hat{b} = \hat{t} \times \hat{n} \tag{3}$$

and

$$\hat{r} = \hat{t}\,. \tag{4}$$

Referring to Figure D-1, one has

$$\hat{\theta} \sin\theta = - \hat{s} \cdot \hat{b}'\, \hat{b} \tag{5}$$

$$\hat{\varphi} \sin\theta = \hat{s} \cdot \hat{b}'\, \hat{n} \tag{6}$$

$$\cos\theta = \hat{s} \cdot \hat{t}' \tag{7}$$

Therefore,

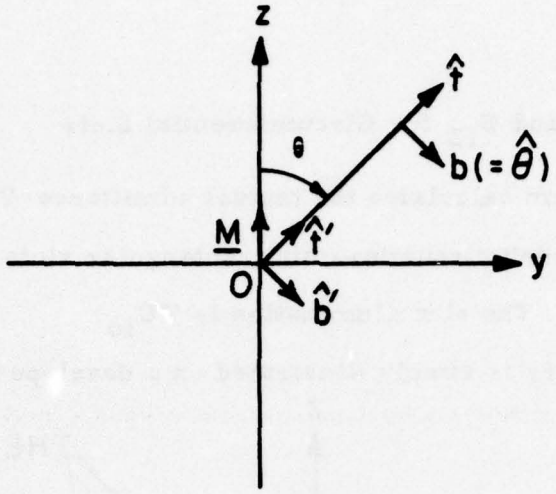

Figure D-1. Surface Ray on a Ground Plane

$$\underline{H}(\underline{r},\underline{r}') = -j\frac{k^2 Y}{2\pi}\underline{M}\cdot\left[\hat{b}'\hat{b}\left(1 - j\frac{1}{kD} - \frac{1}{(kD)^2}\right) + \hat{t}'\hat{t}\left(2j\frac{1}{kD} + 2\frac{1}{(kD)^2}\right)\right]\frac{e^{-jkD}}{kD} \tag{8}$$

and

$$\underline{E}(\underline{r},\underline{r}') = -j\frac{k^2}{2\pi}\underline{M}\cdot\hat{b}'\hat{n}\left(1 - j\frac{1}{kD}\right)\frac{e^{-jkD}}{kD} \tag{9}$$

Here $\underline{M}$ denotes an arbitrarily oriented magnetic point source and r has been replaced by D the distance between the source and the observation point.

Formulae (8) and (9) are in a vector form and are thus invariant to the choice of coordinate system.

Appendix E. Y_{12} and S_{12} for Circumferential Slots

This program calculates the mutual admittance Y_{12} (and S_{12}) between "single mode" circumferential rectangular slots on a Conducting Circular Cylinder. The slot illumination is TE_{10}.

The geometry is simply illustrated on a developed cylinder.

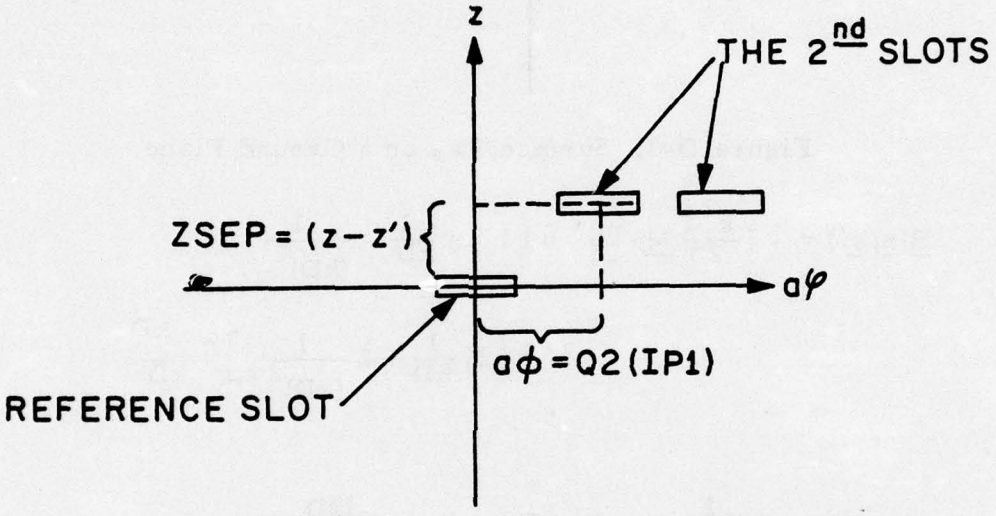

Figure E-1. Developed Cylinder-Circumferential Slots.

In Figure E-1 the center of the reference slot is fixed at r = a, $\varphi' = 0$, $z' = 0$ of a standard cylindrical coordinate system. Thus, the reference slot is located at

Q1 (1) = Radius of the cylinder,

Q1 (2) = $\varphi' = 0^{\circ}$,

Q1 (3) = $z' = 0$.

The locations of the centers of the other slots are generated by DO LOOP 56. Each step of increase in Φ_0 is 10° for R = 1.991" and 10.133° for R = 3.777". For different steps value the step size in DO LOOP 56 should be modified. The symbols are

Q2 (I) = radius of the cylinder

Q2 (Ip1) = $\Phi_o = \varphi_{center}$

Q2 (Ip2) = z_{center}

The long side of the slot is divided into N subdivisions and the short side M subdivisions. Thus, the total number of sub-areas in one aperture is M x N.

The Green's function of the surface magnetic field $\left(H_{\varphi}^{c}\right)$ is found in the subroutine "Fock", where

$$HTD = H_{\varphi}^{c} .$$

If ITT = 1, denotes Y_{12} (or S_{12}) calculated by the "variant" formula. If ITT $\neq$ 1, the "Full Formula" is used.

In the program:

Y_{11} is the self-admittance of the aperture in TE_{10} illumination,

Y_g - the characteristic admittance of the feeding waveguide,

ZSEP - the axial separation of the reference slot and the second slot,

WL - the wavelength.

The curvature terms $v_0(x)$, $v_1(x)$ and $u_0(x)$ are termed in the program VV, VV1 and UU, respectively. $X(= f_t\Phi)$ is called XX in subroutine "Fock".

Aperture size is a x b.

The program is composed by three parts; (1) the main part, (2) the subroutine SLOCA (which treats the locations of the subdivisions of the second slot.) and (3) the subroutine Fock.

```
V G LEVEL  21                    MAIN                    DATE = 76190          13/14/21

      C     MUTUAL ADMITTANCE OF CIRCUMFERETIAL SLOTS ON A CYLINDER
            COMPLEX HT,HR,YY(200),SM,Y1,CEXP
            DIMENSION Q2(200),Q1(3)
            REAL K,LQ
            COMMON /AREA1/ITT,N,M,PI,AA,BB,CC,K,WL,DEL,SX,SY
      C     Q1(1)=R, Q1(2)=PHI, Q1(3)=Z.
      C     IN THE INPUT WL IS IN CMS, ALL OTHERS ARE IN INCHES.
            READ(5,411)Q1(1),Q1(2),Q1(3),WL,ZSEP
            READ(5,412)YG,Y1
       411  FORMAT(5F10.5)
       412  FORMAT(3E15.5)
            ITT=1
      C     IF ITT=1 DENOTES THE FORMULA OF NO V1 AND DROPPING V0 FROM X<.3.
            R1=Q1(1)*2.54
            PI=3.14159
            TF=2.33811
            TFB=1.01879
            ND1=19*6
            ND2 =ND1*2
            ND3=ND1*3
      C     Y1=SELF ADMITTANCE, YG=CHARACTERISTIC ADMITTANCE
            Y1=Y1*YG
             YA=SQRT(REAL(Y1)**2+AIMAG(Y1)**2)
             YP=ATAN2(AIMAG(Y1),REAL(Y1))*180./PI
      C     WAVEGUIDE SIZE=AA"*BB", WL=WAVELENGTH IN CM.
            AA=.9*2.54
            BB=.4*2.54
            K=2.*PI/WL
            SSX=AA
            N=14
            M=2
            NNM=N*M
            WRITE(6,35) NNM
       35   FORMAT(1H1,1X,I3,1X,'POINTS IN THE APERTURE, CIRCUM. SLOTS')
      C     GENERATE THE ARRAY OF THE SECOND SLOTS.
            WRITE(6,2214)
       2214 FORMAT(20X,'K. CYL.',16X,'Z IN CM.', 3X,'PHI. IN DEG.')
            DO 56 I=1,ND1,3
            IP1=I+1
            IP2=I+2
            II=IP2/3
            Q2(I)=Q1(1)
            Q2(IP1)=10.*(IP2/3-1)*PI/180.
            Q2(IP2)=ZSEP*2.54
            IF(I.GT.ND1/2) Q2(IP1)=-2.*PI+Q2(IP1-ND1/2)
            QP=Q2(IP1)*180./PI
       56   WRITE(6,82)II,Q2(I),Q2(IP1),Q2(IP2),QP
            WRITE(6,81) (Q1(L),L=1,3)
            WRITE(6,83) N,M,AA,BB,WL
       81   FORMAT(1X,'R1=',F12.5,10X,'PH 1=',F12.5,10X,'TH 1=',F12.5)
       82   FORMAT(1X,I3,10X,4F12.5)
       83   FORMAT(1X,'N=',I3,10X,'M=',I3,/1X,'A=',F12.5,'CMS',10X,
           1'B=',F12.5,'CMS',10X,'WAVELENGTH=',F12.5,'CMS')
```

```
      WRITE(6,976) Y1,YA,YP,YG
  976 FORMAT(1X,'SELF-ADMIT=',2E20.6,10X,'MAG=',E15.5,10X,'PH=',F15.5,/
     11X,'CHAC. ADMIT.=',E20.5)
      PQ1=Q1(2)*PI/180.
      SX=AA/N
      SY=BB/M
      DEL=SX*SY
      WRITE(6,191)
  191 FORMAT(1H1,1X,'Y DENOTES MUTUAL ADMITTANCE, S ISOLATION')
C     NUMERICAL INTEGRATION BEGINS
      WRITE(6,547)
  547 FORMAT(1X,'PHI',11X,'REAL',18X,'IMA',14X,'MAG',16X,'PHASE',15X,
     1'DB')
      DO 50 I2=1,ND1,3
      IJK=(I2-1)/3+1
      YY(IJK)=(1.,1.)
      IF(IJK.GT.18.AND.IJK.LT.31)GO TO 50
      IF(IJK.GT.36)GO TO 50
      IP1=I2+1
      IP2=I2+2
      XQ2=Q2(IP1)*R1
      YQ2=Q2(IP2)
      HT=(0.,0.)
      HR=(0.,0.)
      IF(YQ2.NE.0.0)GO TO 1074
      IF(IP2/3.LT.4)GO TO 50
 1074 CONTINUE
      DO 41 I=1,N
      SNX=(FLOAT(N+1)/2.-FLOAT(I))*SX
      E2=COS(PI*SNX/(SX*N))
      XQ2C=XQ2+SNX
      DO 41 J=1,M
      SMY=(FLOAT(M+1)/2.- FLOAT(J))*SY
      YQ2C=YQ2-SMY
   41 CALL SLOCA(E2,R1,XQ2C,YQ2C,HT,HR)
      YY(IJK )=-HT*2./(AA*BB)
      IF(IJK.GT.12)GO TO 50
      IJ=10*(IJK-1)
      TYY=SQRT(REAL(YY(IJK ))**2+AIMAG(YY(IJK ))**2)
      TYP=ATAN2(AIMAG(YY(IJK )),REAL(YY(IJK )))*180./PI
      TYL=20.*ALOG10(TYY/ YA)
      WRITE(6,958)IJ ,  YY(IJK ),TYY,TYP,TYL
      SM=-2.*YG*YY(IJK)/((YG+Y1+YY(IJK))*(YG+Y1-YY(IJK)))
      SA=SQRT(REAL(SM)**2+AIMAG(SM)**2)
      SP=ATAN2(AIMAG(SM),REAL(SM))*180./PI
      SL=20.*ALOG10(SA)
      WRITE(6,959)SM,SA,SP,SL
   50 CONTINUE
      NN=ND1/6
      DO 31 IJ=1,NN
      IF(IJ.LT.13)GO TO 31
      IJK=10*(IJ-1)
      YY(IJ)=YY(IJ)+YY(IJ+NN )
```

```
      SM=-2.*YG*YY(IJ)/((YG+Y1+YY(IJ))*(YG+Y1-YY(IJ)))
      SA=SQRT(REAL(SM)**2+AIMAG(SM)**2)
      SP=ATAN2(AIMAG(SM),REAL(SM))*180./PI
      SL=20.*ALOG10(SA)
      YAM=SQRT(AIMAG(YY(IJ))**2+REAL(YY(IJ))**2)
      YAMM=YAM/YG
      YAR=ATAN2(AIMAG(YY(IJ)),REAL(YY(IJ)))*180./PI
      YARR=-360.+YAR
      TYL=20.*ALOG10(YAM/ YA)
      TYPD=YAR- YP
      DISK=1.0
      TYPDD=TYPD-DISK
      TYDDC=YAR-DISK
      WRITE(6,958)IJK,YY(IJ),YAM,YAR,TYL
      WRITE(6,959)SM,SA,SP,SL
   31 CONTINUE
   63 FORMAT(1X,'S=',2E14.5,5X,'AMP=',E14.5,5X,'PHA=',E14.5,5X,
     1'DB-S=',E14.5)
  337 FORMAT(3X,'YO',I3,'=',2E20.6,10X,'MAG=',E15.5,10X,'PH=',F15.5,
     13X,F7.2)
  827 FORMAT(1X,'DB-Y=',E20.6,10X,'PH-DIF=',3F15.5)
   33 FORMAT(1X,'YO',I2,'=',2E20.6,/)
  958 FORMAT(1X,I3,5X,'Y=',2E15.5,5X,E15.5,5X,F15.5,5X,E15.5)
  959 FORMAT( 9X,'S=',2E15.5,5X,E15.5,5X,F15.5,5X,E15.5,/)
      STOP
      END
```

```
      SUBROUTINE SLOCA(E2,R1,XC2C,YQ2C,HT,HR)
      COMPLEX HHT,HTD,HTS,HT,HR
      REAL K,LQ
      COMMON /AREA1/ITT,N,M,PI,AA,BB,CC,K,WL,DEL,SX,SY
      DEL=SX*SY
      DO 11 I=1,N
      SNX=(FLOAT(N+1)/2.-FLOAT(I))*SX
      EC=COS(PI*SNX/(SX*N))
      XD=XQ2C-SNX
      DO 11 J=1,M
      SMY=(FLOAT(M+1)/2.- FLOAT(J))*SY
C     SMY=(J-2)*SY
      YD=YQ2C+SMY
      IF(XD.EQ.0.0)GO TO 21
      TCL=ATAN2(YD,XD)
      GO TO 23
 21   TCL=PI/2.
C     IF(YD.LT.0.)TCL=-PI/2.
 23   LQ=R1/(COS(TCL)**2)
      FF=EXP(ALOG(K*R1*ABS(COS(TCL))/2.)/3.)
      ANG=XD/R1
      XX=FF*ABS(ANG)
      SOK=SQRT(XD**2+YD**2)
      CALL FOCK(ITT,K,R1,CC,XX,PI,FF,LQ,SOK,TCL,HTD,HTS)
      HHT=HTD+HTS
      HT=HHT*EC*E2*DEL**2+HT
      HR=(0.,0.)
 11   CONTINUE
      RETURN
      END
```

```
      SUBROUTINE FOCK(III,K,R1,CC,XX,PI,EE,LQ,DIS,I  ,HTD,HTS)
      COMPLEX H4,H5
      COMPLEX VV,UU,VVD,VP,CEXP,HTD,HTS,H3,H1,VV1,VV2
      COMPLEX'KKDTP,B3B,AA1,AA2,TTO,YYZZ,KKDT,KKD,TTOP,CONJG
      REAL K,LQ
      DIMENSION TFB(10),TF(10)
C     TFB ARE THE ROOTS OF THE AIRY FCT DERIVATIVE, TF THE ROOTS OF AIRY FCT.
      DATA TFB/1.01879,3.24819,4.82010,6.16331,7.37218,8.48849,
     19.53545,10.5277,11.4751,12.3848/
      DATA TF/2.33811,4.08795,5.52056,6.78671,7.94413,
     19.02265,10.0402,11.0085,11.9360,12.8288/
      PI=3.14159
      PRO=SQRT(PI)/2.
C     ALG=R1/COS(T)**2
C     TLG=R1/SIN(T)**2
      H5=CEXP((0.,1.)*PI/4.)
      H8=SQRT(PI)
      Y=1./377.
      YYY=K*DIS/(2.*EXP(ALOG(K*R1/2.)*2./3.))
      IF (XX.LT.0.8000  ) GO TO 53
      VVD=(0.,1.)*PI/3.
      VP=(0.,-1.)*XX*CEXP((0.,-1.)*PI/3.)
      VV=(0.,0.)
      VV1=VV
      VV2=VV
      UU=VV
C     RESIDUE SERIES
      DO 37 I=1,10
      VV=CEXP(VP*TFB(I)      +VVD)/TFB(I)+VV
      VV1=CEXP(VP*TFB(I)      )+VV1
      VV2=TFB(I)*CEXP(VP*TFB(I)-VVD)+VV2
 37   UU=CEXP(VP*TF(I)      )+UU
      VV=VV*SQRT(PI*XX)*CEXP((0.,-1.)*PI/4.)
      VV1=VV1*2.*SQRT(PI*XX**3)*CEXP((0.,1.)*PI/4.)
      VV2=VV2*4.*(0.,1.)*CEXP((0.,1.)*PI/4.)*SQRT(PI*XX**5)/3.
      UU=UU*2.*SQRT(PI*XX**3)*CEXP((0.,1.)*PI/4.)
      GO TO 54
C     POWER SERIES
 53   VV=(1.-CEXP((0.,1.)*PI/4.)*SQRT(PI*XX**3)/4.
     1+7.*(0.,1.)*XX**3/60.+7.*SQRT(PI*XX**9)*CEXP((0.,-1.)*PI/4.)/512.)
      VV1=1.+CEXP((0.,1.)*PI/4.)*SQRT(PI*XX**3)/2.-7.*(0.,1.)
     1*XX**3/12.-7.*CEXP((0.,-1.)*PI/4.)*SQRT(PI*XX**9)/64.
      VV2=1.+7.*(0.,1.)*XX**3/12.+7.*CEXP((0.,-1.)*PI/4.)*SQRT(PI*XX**9)
     1/32.
      UU=(1.-CEXP((0.,1.)*PI/4.)*SQRT(PI*XX**3)/2.
     1+5.*(0.,1.)*XX**3/12.+CEXP((0.,-1.)*PI/4.)*5.*
     1SQRT(PI*XX**9)/64.)
C     H4=1.-(1.+SIN(T)**2)*H5*SQRT(PI*YYY**3)/2.+(5.+7.*SIN(T)**2)
C    1*(0.,1.)*YYY**3*COS(T)**2/12.+(5.+7.*SIN(T)**2)*SQRT(PI*YYY
C    1**9)*COS(T)**4/(64.*H5)
 54   CONTINUE
      H1=(K**2*Y/(2.*PI))*CEXP((0.,-1.)*K*DIS)/(K*DIS)
      HTD=(0.,-1.)*VV*(SIN(T)**2-2*SIN(T)**2*(0.,1.)/(K*DIS)+COS(T)**2
```

amplitude and phase angle are printed out.

DB in Y denotes $20 \log_{10} \left| Y_{12}/Y_{11} \right|$

DB in S is $20 \log_{10} \left| S_{12} \right|$.

```
IV G LEVEL  21                    MAIN                    DATE = 76182          11/32/41

      C     MUTUAL COUPLING OF AXIAL SLOTS ON A   CYLINDER
            COMPLEX HT,HR,YY(200),SM,Y1,CMPLX
            DIMENSION C2(200),Q1(3)
            REAL K,LQ
            COMMCN /AREA1/N,M,PI,AA,EB,CC,K,WL,DEL,SX,SY
      C     IN THE INPUT WL IS IN CMS, ALL OTHERS ARE IN INCHES.
      C     Q1(1)=R, Q1(2)=PHI, Q1(3)=Z.
            READ(5,411)Q1(1),Q1(2),Q1(3),WL,ZSEP
            READ(5,412)YG,Y1
       411  FORMAT(5F10.5)
       412  FORMAT(3E15.5)
            R1=Q1(1)*2.54
            PI=3.14159
            ND1=19*6
            ND2 =ND1*2
            ND3=ND1*3
            Y1=Y1*YG
             YA=SQRT(REAL(Y1)**2+AIMAG(Y1)**2)
             YP=ATAN2(AIMAG(Y1),REAL(Y1))*180./PI
      C     APERTURE SIZE=AA"*BB"
            AA=.4*2.54
            BB=.9*2.54
            K=2.*PI/WL
            SSX=AA
            N=2
            M=10
            NNM=N*M
            WRITE(6,35) NNM
       35   FORMAT(1H1,1X,I3,1X,'POINTS IN THE APERTURE, AXIAL SLOTS')
      C     GENERATE THE ARRAY OF THE SECOND SLOTS.
            WRITE(6,2214)
       2214 FORMAT(20X,'R. CYL.',16X,'Z IN CM.', 3X,'PHI. IN DEG.')
            DO 56 I=1,ND1,3
            IP1=I+1
            IP2=I+2
            II=IP2/3
            Q2(I)=Q1(1)
            Q2(IP1)=10.*(IP2/3-1)*PI/180.
            Q2(IP2)=ZSEP*2.54
            IF(I.GT.ND1/2) C2(IP1)=-2.*PI+Q2(IP1-ND1/2)
            QP=Q2(IP1)*180./PI
       56   WRITE(6,82)II,Q2(I),Q2(IP1),Q2(IP2),QP
            WRITE(6,81) (Q1(L),L=1,3)
            WRITE(6,83) N,M,AA,BB,WL
      C
       81   FORMAT(1X,'R1=',F12.5,10X,'PH 1=',F12.5,10X,'TH 1=',F12.5)
       82   FORMAT(1X,I3,10X,4F12.5)
       83   FORMAT(1X,'N=',I3,10X,'M=',I3,/1X,'A=',F12.5,'CMS',10X,
           1'B=',F12.5,'CMS',10X,'WAVELENGTH=',F12.5,'CMS')
            WRITE(6,976) Y1,YA,YP,YG
       976  FORMAT(1X,'SELF-ADMIT=',2E20.6,10X,'MAG=',E15.5,10X,'PH=',F15.5,/
           11X,'CHAR.-ADMIT.=',E20.5)
            FQ1=Q1(2)*PI/180.
```

```
      SX=AA/N
      SY=BB/M
      DEL=SX*SY
      WRITE(6,191)
  191 FORMAT(1H1,1X,'Y DENOTES MUTUAL ADMITTANCE, S ISOLATION')
C     NUMERICAL INTEGRATION BEGINS
      WRITE(6,547)
  547 FORMAT(1X,'PHI',11X,'REAL',18X,'IMA',14X,'MAG',16X,'PHASE',15X,
     1'DB')
      DO 50 I2=1,ND1,3
      IJK=(I2-1)/3+1
      YY(IJK)=(1.,1.)
      IF(IJK.LT.3.AND.ZSEP.EQ.0.)GO TO 50
      IF(IJK.GT.19.AND.IJK.LT.31)GO TO 50
      IP1=I2+1
      IP2=I2+2
      XQ2=Q2(IP1)*R1
      YQ2=Q2(IP2)
      HT=(0.,0.)
      HR=(0.,0.)
      DO 41 I=1,N
      SNX=(FLOAT(N+1)/2.-FLOAT(I))*SX
      XQ2C=XQ2+SNX
      DO 41 J=1,M
      SMY=(FLOAT(M+1)/2.- FLOAT(J))*SY
      E2=COS(PI*SMY/(SY*M))
      YQ2C=YQ2-SMY
C     SLOCA TREATS THE SUBDIVISIONS OF THE 2ND APERTURE.
   41 CALL SLOCA(E2,R1,XQ2C,YQ2C,HT,HR)
      YY(IJK )=-HT*2./(AA*BB)
      IF(IJK.GT.12)GO TO 50
      TYY=SQRT(REAL(YY(IJK ))**2+AIMAG(YY(IJK ))**2)
      TYP=ATAN2(AIMAG(YY(IJK )),REAL(YY(IJK )))*180./PI
      TYL=20.*ALOG10(TYY/ YA)
      IJ=10*(IJK-1)
      WRITE(6,958)IJ ,  YY(IJK ),TYY,TYP,TYL
      SM=-2.*YG*YY(IJK)/((YG+Y1+YY(IJK))*(YG+Y1-YY(IJK)))
      SA=SQRT(REAL(SM)**2+AIMAG(SM)**2)
      SP=ATAN2(AIMAG(SM),REAL(SM))*180./PI
      SL=20.*ALOG10(SA)
      WRITE(6,959)SM,SA,SP,SL
   50 CONTINUE
      NN=ND1/6
      DO 31 IJ=1,NN
      IF(IJ.LT.13)GO TO 31
      IJK=10*(IJ-1)
      YY(IJ)=YY(IJ)+YY(IJ+NN )
      YAM=SQRT(AIMAG(YY(IJ))**2+REAL(YY(IJ))**2)
      YAR=ATAN2(AIMAG(YY(IJ)),REAL(YY(IJ)))*180./PI
      TYL=20.*ALOG10(YAM/ YA)
      SM=-2.*YG*YY(IJ)/((YG+Y1+YY(IJ))*(YG+Y1-YY(IJ)))
      SA=SQRT(REAL(SM)**2+AIMAG(SM)**2)
      SP=ATAN2(AIMAG(SM),REAL(SM))*180./PI
```

```
IV G LEVEL  21                    MAIN                    DATE = 76182          11/32/41

            SL=20.*ALOG10(SA)
            WRITE(6,958)IJK,YY(IJ),YAM,YAR,TYL
            WRITE(6,959)SM,SA,SP,SL
      31    CONTINUE
     958    FORMAT(1X,I3,5X,'Y=',2E15.5,5X,E15.5,5X,F15.5,5X,E15.5)
     959    FORMAT( 9X,'S=',2E15.5,5X,E15.5,5X,F15.5,5X,E15.5,/)
            STOP
            END
```

```
      SUBROUTINE SLOCA(E2,R1,XC2C,YC2C,HT,HR)
      COMPLEX HHT,HTD,HTS,HT,HR
      REAL K,LQ
      COMMON /AREA1/N,M,PI,AA,EB,CC,K,WL,DEL,SX,SY
      DEL=SX*SY
      DO 11 I=1,N
      SNX=(FLOAT(N+1)/2.-FLOAT(I))*SX
      XD=XC2C-SNX
      DO 11 J=1,M
      SMY=(FLOAT(M+1)/2.- FLOAT(J))*SY
      EC=COS(PI*SMY/(SY*M))
      YD=YC2C+SMY
      IF(YC.EQ.0.0)GO TO 21
      TCL=ATAN2(YD,XD)
      GO TO 23
   21 TCL=0.0
      IF(XC.LT.0.)TCL=PI
   23 LQ=R1/(COS(TCL)**2)
      FF=EXP(ALOG(K*R1*ABS(COS(TCL))/2.)/3.)
      ANG=XD/R1
      XX=FF*ABS(ANG)
      SOK=SQRT(XC**2+YD**2)
C     FOCK TREATS THE CURVATURE TERMS AND THE GREEN'S FUNCTION.
      CALL FOCK(K,R1,CC,XX,PI,FF,LQ,SOK,TCL,HTD,HTS)
      HHT=HTD+HTS
      HT=HHT*EC*E2*DEL**2+HT
      HR=(0.,0.)
   11 CONTINUE
      RETURN
      END
```

```
      SUBROUTINE FOCK(K,R1,CC,XX,PI,FF,LQ,DIS,T  ,HTD,HTS)
      COMPLEX VV,UU,VVD,VP,CEXP,HTD,HTS,H3,H1,VV1,VV2,H4,H5
      REAL K
      DIMENSION TFB(10),TF(10)
C     TFB ARE THE ROOTS OF THE AIRY FCT DERIVATIVE, TF THE ROOTS OF AIRY FCT.
      DATA TFB/1.01879,3.24819,4.82010,6.16331,7.37218,8.48849,
     19.53545,10.5277,11.4751,12.3848/
      DATA TF/2.33811,4.08795,5.52056,6.78671,7.94413,
     19.02265,10.0402,11.0085,11.9360,12.8288/
      PI=3.14159
      H5=CEXP((0.,1.)*PI/4.)
      H8=SQRT(PI)
      Y=1./377.
      YYY=K*DIS/(2.*EXP(ALOG(K*R1/2.)*2./3.))
      IF (XX.LT.0.8000  ) GO TO 53
      VVD=(0.,1.)*PI/3.
      VP=(0.,-1.)*XX*CEXP((0.,-1.)*PI/3.)
      VV=(0.,0.)
      VV1=VV
      VV2=VV
      UU=VV
C     RESIDUE SERIES
      DO 37 I=1,10
      VV=CEXP(VP*TFB(I)+VVD)/TFB(I)+VV
      VV1=CEXP(VP*TFB(I))+VV1
   37 VV2=TFB(I)*CEXP(VP*TFB(I)-VVD)+VV2
      VV=VV*SQRT(PI*XX)*CEXP((0.,-1.)*PI/4.)
      VV1=VV1*2.*SQRT(PI*XX**3)*CEXP((0.,1.)*PI/4.)
      VV2=VV2*4.*(0.,1.)*CEXP((0.,1.)*PI/4.)*SQRT(PI*XX**5)/3.
      GO TO 54
C     POWER SERIES
   53 VV=(1.-CEXP((0.,1.)*PI/4.)*SQRT(PI*XX**3)/4.
     1+7.*(0.,1.)*XX**3/60.+7.*SQRT(PI*XX**9)*CEXP((0.,-1.)*PI/4.)/512.)
      VV1=1.+CEXP((0.,1.)*PI/4.)*SQRT(PI*XX**3)/2.-7.*(0.,1.)
     1*XX**3/12.-7.*CEXP((0.,-1.)*PI/4.)*SQRT(PI*XX**9)/64.
      VV2=1.+7.*(0.,1.)*XX**3/12.+7.*CEXP((0.,-1.)*PI/4.)*SQRT(PI*XX**9)
     1/32.
   54 CONTINUE
      H1=(K**2*Y/(2.*PI))*CEXP((0.,-1.)*K*DIS)/(K*DIS)
C     THE GREEN'S FUNCTION
      HTD=H1*(((0.,-1.)*COS(T)**2+(20.*SIN(T)**2/9.-29.*COS(T)**2/24.)/
     1(K*DIS))*VV)
      HTS=(0.,0.)
      RETURN
      END
```

Input data
E-6

20 POINTS IN THE APERTURE, AXIAL SLOTS

	R. CYL.		Z IN CM.	PHI, IN DEG.
1	1.99100	0.0	3.81000	0.0
2	1.99100	0.17453	3.81000	9.99999
3	1.99100	0.34907	3.81000	19.99998
4	1.99100	0.52360	3.81000	29.99998
5	1.99100	0.69813	3.81000	39.99998
6	1.99100	0.87266	3.81000	49.99998
7	1.99100	1.04720	3.81000	59.99994
8	1.99100	1.22173	3.81000	69.99994
9	1.99100	1.39626	3.81000	79.99995
10	1.99100	1.57079	3.81000	89.99988
11	1.99100	1.74533	3.81000	99.99985
12	1.99100	1.91986	3.81000	109.99988
13	1.99100	2.09439	3.81000	119.99985
14	1.99100	2.26892	3.81000	129.99988
15	1.99100	2.44346	3.81000	139.99985
16	1.99100	2.61799	3.81000	149.99988
17	1.99100	2.79252	3.81000	159.99985
18	1.99100	2.96706	3.81000	169.99989
19	1.99100	3.14159	3.81000	179.99985
20	1.99100	-6.28318	3.81000	-359.99976
21	1.99100	-6.10865	3.81000	-349.99976
22	1.99100	-5.93411	3.81000	-339.99976
23	1.99100	-5.75958	3.81000	-329.99976
24	1.99100	-5.58505	3.81000	-319.99976
25	1.99100	-5.41051	3.81000	-309.99976
26	1.99100	-5.23598	3.81000	-300.00000
27	1.99100	-5.06145	3.81000	-289.99976
28	1.99100	-4.88692	3.81000	-280.00000
29	1.99100	-4.71239	3.81000	-270.00000
30	1.99100	-4.53785	3.81000	-260.00000
31	1.99100	-4.36332	3.81000	-250.00005
32	1.99100	-4.18879	3.81000	-240.00009
33	1.99100	-4.01425	3.81000	-229.99997
34	1.99100	-3.83972	3.81000	-220.00008
35	1.99100	-3.66519	3.81000	-210.00005
36	1.99100	-3.49066	3.81000	-200.00000
37	1.99100	-3.31612	3.81000	-190.00005
38	1.99100	-3.14159	3.81000	-180.00008

R1= 1.99100 PH 1= 0.0 TH 1= 0.0

N= 2 M= 10

A= 1.01600CMS B= 2.28600CMS WAVELENGTH= 3.33333CMS

SELF-ADMIT= 0.135792E-02 0.787883E-03 MAG= 0.15699E-02 PH= 30.1225

CHAR.-ADMIT.= 0.18154E-02

Output data

E-7

Y DENOTES MUTUAL ADMITTANCE, S ISOLATION

PHI		REAL	IMA	MAG	PHASE	DB
0	Y=	-0.47427E-04	0.17953E-04	0.50711E-04	159.26601	-0.29816E 02
	S=	0.11383E-01	-0.12927E-01	0.17224E-01	-48.63435	-0.35277E 02
10	Y=	-0.30573E-04	0.35392E-04	0.46768E-04	130.82185	-0.30519E 02
	S=	0.35523E-02	-0.15479E-01	0.15882E-01	-77.07510	-0.35982E 02
20	Y=	0.24174E-04	0.39336E-04	0.46170E-04	58.42708	-0.30630E 02
	S=	-0.13504E-01	-0.79705E-02	0.15680E-01	-149.44890	-0.36093E 02
30	Y=	0.48343E-04	-0.22501E-04	0.53323E-04	-24.95874	-0.29379E 02
	S=	-0.10934E-01	0.14437E-01	0.18111E-01	127.13921	-0.34841E 02
40	Y=	-0.18018E-04	-0.54904E-04	0.57785E-04	-108.16835	-0.28681E 02
	S=	0.14124E-01	0.13621E-01	0.19622E-01	43.96063	-0.34145E 02
50	Y=	-0.54674E-04	0.12849E-04	0.56164E-04	166.77483	-0.28928E 02
	S=	0.14371E-01	-0.12548E-01	0.19078E-01	-41.12636	-0.34389E 02
60	Y=	0.96467E-05	0.49334E-04	0.50268E-04	78.93602	-0.29892E 02
	S=	-0.10728E-01	-0.13277E-01	0.17069E-01	-128.94098	-0.35356E 02
70	Y=	0.41705E-04	-0.85217E-05	0.42567E-04	-11.54849	-0.31336E 02
	S=	-0.11165E-01	0.91854E-02	0.14458E-01	140.55673	-0.36798E 02
80	Y=	-0.85606E-05	-0.33677E-04	0.34748E-04	-104.26260	-0.33099E 02
	S=	0.79181E-02	0.87495E-02	0.11800E-01	47.85564	-0.38562E 02
90	Y=	-0.26208E-04	0.89118E-05	0.27681E-04	161.21977	-0.35074E 02
	S=	0.64512E-02	-0.68389E-02	0.94015E-02	-46.67137	-0.40536E 02
100	Y=	0.90806E-05	0.19702E-04	0.21694E-04	65.25497	-0.37191E 02
	S=	-0.58553E-02	-0.44718E-02	0.73676E-02	-142.62994	-0.42653E 02
110	Y=	0.14280E-04	-0.88776E-05	0.16814E-04	-31.86893	-0.39404E 02
	S=	-0.28762E-02	0.49333E-02	0.57105E-02	120.24239	-0.44866E 02